Damage Development

Under Compression-Compression Fatigue Loading

In a Stitched Uniwoven Graphite/Epoxy

Composite Material

by

Nancy Vandermey

Thesis submitted to the Faculty of the

Virginia Polytechnic Institute and State University

in partial fulfillment of the requirements for the degree of

Master of Science

in

Engineering Mechanics

APPROVED:

Don H. Morris, Chairman

O. Hayden Griffin

Wayne W. Stinchcomb

April, 1991

Blacksburg, Virginia

c2

LD
5655
V355
1991
V367
c.2

Damage Development

Under Compression-Compression Fatigue Loading

in a Stitched Uniwoven Graphite/Epoxy

Composite Material

by

Nancy Vandermey

Don H. Morris, Chairman

Engineering Mechanics

(ABSTRACT)

Damage initiation and growth under compression-compression fatigue loading were investigated for a stitched uniweave material system with an underlying AS4/3501-6 quasi-isotropic layup. Performance of unnotched specimens having stitch rows at either 0° or 90° to the loading direction was compared. Special attention was given to the effects of stitching-related manufacturing defects. Damage evaluation techniques included edge replication, stiffness monitoring, X-ray radiography, residual compressive strength, and laminate sectioning. It was found that the manufacturing defect of inclined stitches had the greatest adverse effect on material performance. 0° and 90° specimen performances were generally the same. While the stitches were the source of damage initiation, they also slowed damage propagation both along the length and across the width and affected through the thickness damage growth. A pinched layer zone formed by the stitches particularly affected damage initiation and growth. The compression failure mode was transverse shear for all specimens, both in static compression and fatigue cycling tests. Specimens without stitches were not available for for comparison.

ACKNOWLEDGEMENTS

The author would like to express her appreciation for their help, support, relief, or otherwise that the following provided:

- Dr. Don Morris, for his role as committee chairperson, and his encouraging attitude towards thesis-writing;
- Buddy Poe, for serving as my mentor at NASA-Langley and supporting my research there;
- John Masters, Marc Portanova, and the rest of the gang at NASA-Langley, for all their help with my experiments, the analysis thereof, fixing my car, etc.;
- Drs. Griffin and Stinchcomb, for serving on my committee and helping to review this document;
- Everyone at Virginia Tech who helped with my questions and problems, especially all the great people in the NASA-Virginia Tech Composites Program
- The Montgomery County Humane Society, for providing a pleasant escape from campus (KITTENS!!! CATS!!! PUPPIES!!! DOGS!!! for information, call 552-6546);
- And all my friends, human and otherwise, for interesting extracurricular activities

Table of Contents

List of Illustrations

List of Tables

I. INTRODUCTION

The aerospace industry has been using laminated composite materials in place of more traditional engineering materials for over 20 years, largely due to the considerable savings in weight composites provide. New material systems and manufacturing techniques result in more and more applications for composites every day. Larger and more complex structures are now being made out of composites with near net shape manufacturing. This results in even more cost savings. However, it is not the conventional laminated composites, such as tape or prepreg, which are being used in these new applications. These composites are limited by their tendency to delaminate, resulting in low damage tolerance. The new trend is to use composites which are reinforced in one or two directions, to inhibit delamination and improve impact and damage tolerance. These new composites, referred to as either advanced fiber composites or textile composites, encompass a variety of reinforcement techniques, including weaving, stitching, braiding, and knitting.

These new textile composites are not without their limitations. In general, composites reinforced by these techniques show an improvement in impact and damage tolerance at the cost of

reducing in-plane properties such as strength. However, Palmer and Curzio [1], in their identification of the major factors limiting increased composite material usage, show that any improvement in damage tolerance will more than compensate for a loss in strength. Consequently, textile composites are getting more and more attention as their potential applications continue to expand.

The NASA-Langley Research Center is currently involved in a program to characterize several textile composite material systems. Work with stitched uniweaves, stitched and unstitched knits, 3-D braids, and 3-D weaves is either presently being performed or is planned. To date, the most extensive work has been with stitched uniweaves [2-7], which are described later. In the present investigation, a material similar to that used by Portanova [7] was tested in compression-compression fatigue to determine modes of damage, including damage initiation and propagation.

Literature review

This section contains a brief review of laminated composite reinforcement techniques aimed at suppressing delamination, a more detailed review of work done with the specific material system tested for this report, and a discussion of damage mechanisms and development in composites, especially three-dimensionally-reinforced laminates.

Delamination Resistance

Conventional composite materials have a high tendency to delaminate, causing brittle compressive fracture and low impact tolerance, and prompting extensive research into new material systems aimed at suppressing delamination. Several different methods to suppress

delamination have been investigated, broadly divided into those that affect the resin and those that affect the fibers. Resin alterations have included using a toughened matrix resin [8], or using an interleaf resin between layers which is tougher than the matrix resin [9]. Fiber alterations include the new textile techniques, tufting [10] or stitching [11-16] third-direction fibers through the thickness, or incorporating a buffer strip [17] into the laminas. All of these methods have been shown to improve delamination resistance and damage tolerance in composite materials. The newest textile materials, such as 3-D weaves, braids, and knits, often have their fibers interlocked in such a way that conventional delamination is no longer possible. These materials, such as stitched uniweaves [2-7, 18], 3-D braids [19], and interlock weaves [20], fail in a transverse shear mode under compressive loading.

Now that it is known that delamination resistance can be improved by a variety of advanced fiber techniques, further research is being conducted to determine the advantages and disadvantages of each method. Factors to be considered include cost of materials and processing, ease of manufacturing, and whether the strength and stiffness of these materials meet design requirements. Taking these factors into account, Palmer and Curzio [1] advocate a woven/stitched material (also referred to as a stitched uniweave) as having the best potential for large applications when compared to materials having similar properties. Its advantages over conventional composite materials include improved resistance to crack propagation, increased interlaminar fracture toughness, better compression after impact properties, improved resistance to delamination, labor savings over individual ply layups, and damage-tolerant, cost-effective structural parts [1]. These advantages have encouraged industry and researchers to take a closer look at stitched uniweaves.

Stitched Uniweaves

Stitched uniweaves are formed in three steps. First, unidirectional tows are held together by woven fill fibers (2% of total fiber weight) to form a lamina. Next, these lamina are stacked together and stitched through the thickness to form a laminate (see figure 1). Finally, the laminates are infiltrated with resin.

The fill fibers and stitch fibers usually differ from each other in weight and/or material. The stitch fibers have three parameters besides material and weight: direction, spacing, and pitch (see figure 1). Direction refers to the angle between the stitch direction and the loading direction. Stitch spacing is the distance between adjacent rows of stitches. Stitch pitch is the number of stitches per inch within a row of stitches. Together, stitch spacing and pitch determine the number of penetrations per inch that the material experiences.

The laminates are usually impregnated using a resin transfer molding process, which requires a low viscosity resin. The graphite tows forming the laminae and the resin system used varied from study to study.

Work done to date with stitched uniweaves has investigated various combinations of stitch parameters and materials to evaluate the resultant material properties. A review of this work follows.

The earliest work with a stitched uniweave material system, performed at NASA-Langley in 1985, was done by Funk, Dexter, and Lubowinski [2]. They investigated three stitch configurations and performed several types of tests. The stitching direction was 0° only, and the stitch fibers were either polyester or Kevlar. They found that while the different stitch configurations had similar static properties, they exhibited significant differences under impact and open hole compression

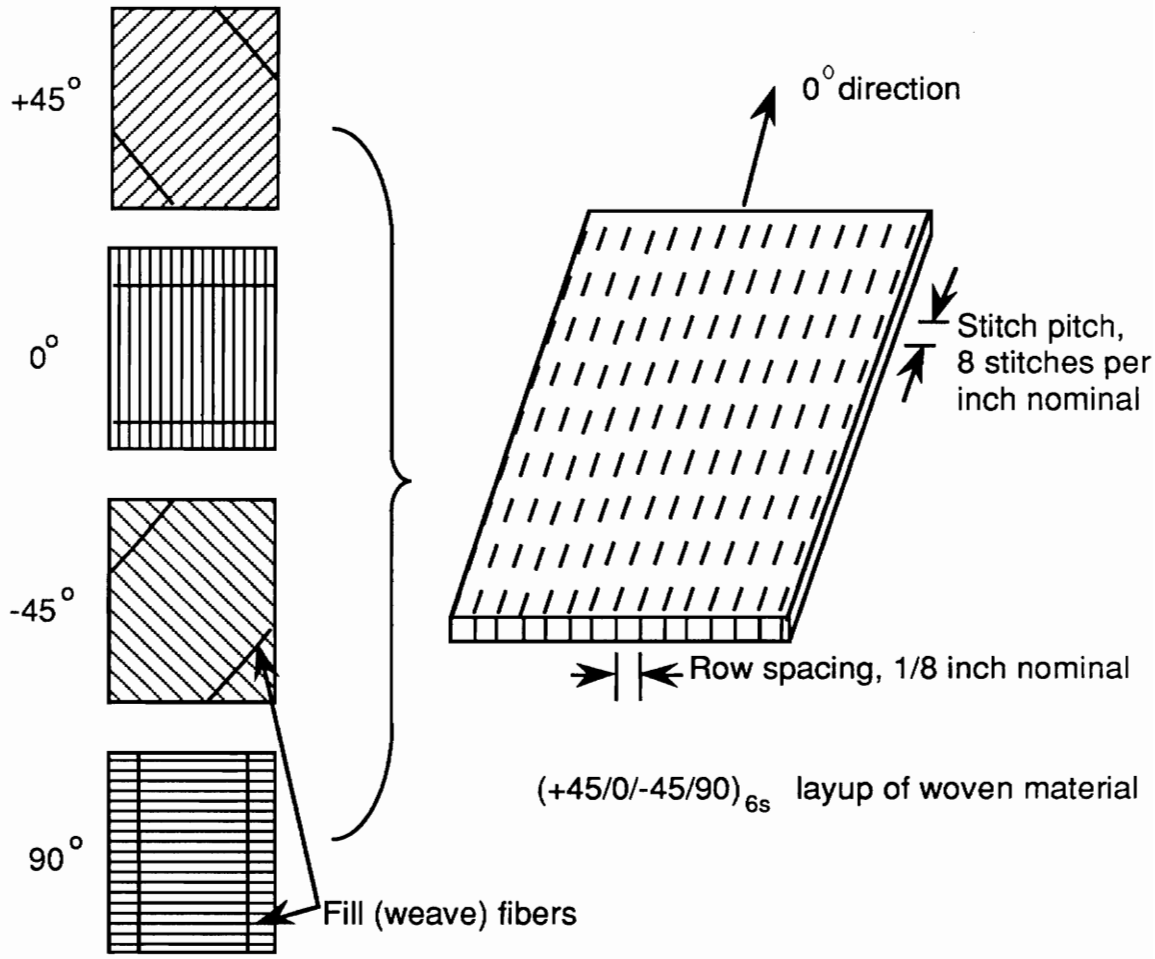

Figure 1. Stitching Nomenclature (after [2])

testing. In comparing the stitched material to a similar unstitched material system, they noted improvements in compression after impact performance, lower impact damage area, and higher interlaminar fracture toughness.

Dexter and Funk [3] expanded on this work in 1986, this time investigating five stitch configurations. In this study the effects of stitch pitch and spacing were investigated. Findings included: increasing the number of stitches reduced tension strength but increased compression strength, stitch pitch significantly affected damage resistance and interlaminar fracture toughness, and the material with the most stitch penetrations per inch was the most effective in suppressing impact damage and improving interlaminar fracture toughness.

The next study of this material system performed at NASA-Langley was published by Lubowinski and Poe [4] in 1987. They used extra material left over from the 1985 study [2], this time performing fatigue testing and looking at damage progression in the stitched material. Stiffness loss and delamination onset were recorded, and radiographs were taken to monitor damage progression. They found that while the stitched materials had lower static strengths and earlier delamination onset than a similar unstitched material, all the stitch configurations resulted in longer fatigue lives than the unstitched material, and that fatigue performance improved as the number of stitches increased.

Also in 1987, Ogo [18] performed a study at the University of Delaware on stitched uniweaves. He investigated various stitch configurations and their effects on in-plane and interlaminar properties. As in previous studies, he found that the static tensile and compressive strengths decreased due to stitching, while interlaminar fracture toughness increased.

The Palmer and Curzio report [1] was published in 1988. In addition to advocating the woven/stitched textile manufacturing process and citing its advantages, they discuss the fabrication of a three-blade stiffened panel preform and the vacuum impregnation process used to transfer resin into the preform. By their estimates, a cost reduction of over 48 percent could be achieved by using this manufacturing process with stitched uniweave composites for large stiffened panels.

Dow, Smith, and Lubowinski [5] also published a report in 1988 dealing with stitched uniweaves. They placed stitches in both the 0° and 90° directions and used a variety of stitch spacings and pitches. They also used a heavier fill yarn than was used in the earlier studies. In addition, they looked at fiberglass and carbon stitch fibers at deniers that gave similar knot breaking strengths to the Kevlar being used. They also tried two different fabric/resin systems, one of which was a high performance system which performs much better than the other one in the unstitched state (and also costs much more). Findings included: the two fabric/resin systems performed comparably in the stitched states, all three stitch threads provided similar performances, and performance improved as stitches became more closely spaced (more penetrations per inch).

Dow and Smith published again in 1989 [6], a continuation of their earlier work. Twelve stitch configurations, varying all three parameters (stitch spacing, pitch, and direction), were investigated. Further findings indicated that a stitch pitch of eight stitches per inch gave the best performance, and that stitching in one direction only gave as good a performance as stitching in two perpendicular directions. They also noted that stitching did not degrade open hole compression strength from the unstitched state, and that thermal cycling did not result in a loss of compression strength. Three-blade stiffeners, manufactured as described in [1], were tested, and they performed excellently in post impact compression.

The most recent Langley study of this material was performed by Portanova, Poe, and Whitcomb [7], published in 1990. Based on results from the earlier studies, they focused on just one stitch configuration: stitch pitch of eight stitches per inch, row spacing of one-eighth of an inch apart, stitch direction 0°, and S-2 fiberglass stitch thread. The layup of the woven material was quasi-isotropic, $[+45/0/-45/90]_{6S}$. The fatigue performance of this material was compared to an unstitched toughened resin tape composite designed to resist delamination. The stitched uniweave was found to be much more damage tolerant, but it suffered a weight penalty because it was 20% thicker than the tape composite due to the stitch and fill fibers. Fatigue damage progression was monitored in open hole compression testing, and it was found the that stitches changed the compressive failure mode from matrix cracking and delaminations to a transverse shear/fiber buckling mode.

In conjunction with NASA-Langley, Douglas Aircraft Company has been performing stitch parameter evaluations of stitched uniweaves. In their progress report of April 1990 [21], they present a comparison of properties of composites made with different stitch threads but the same stitch configuration. These studies resulted in the material system shown in figure 1. It was essentially the same woven material system as that tested in [7] except that the fill fiber percentage was decreased from 5% to 2% (by weight). This resulted in an improved performance in several areas, including compression after impact, impact damage area, and strain at failure. Some changes in static properties were noticed (in compression, a lower ultimate strength and higher modulus; in tension, both a higher ultimate strength and modulus). The authors had two recommendations. First, due to a poor performance in transverse testing, they said that the stitch direction for structures should be the same as the major loading direction. However, the layup of their material was non-quasi-isotropic, which probably contributed to the performance deficiencies. Secondly, like Portanova [7], they noted that the increased thickness

due to the stitches and fill fibers added a large weight penalty and needed to be controlled.

To date, analysis and/or modelling of stitched materials has been limited. Mignery, et. al. [14] used a 2-D finite element model to compare interlaminar normal stresses and strain energy release rates between stitched and unstitched materials. Pelstring and Madan [15] developed semi-empirical relations based on stitch parameters. Su [16] constructed a fracture model to simulate delamination in a stitched material. However, no works have yet been published dealing with the modelling or analysis of stitched uniweaves.

Damage Development

Damage mechanisms and development in conventional laminated composites have been the topic of many studies. Charewicz and Daniel [22], in their study, reviewed the different types of studies done to monitor damage in composites and performed their own tests to develop a cumulative damage model. Their damage evaluation methods included x-radiographs, residual stiffness, and residual strength. In addition to these methods, edge replication [23] has proven useful in documenting the initiation and growth of edge damage. Stalnaker and Stinchcomb [24] successfully employed this method to track edge damage of a quasi-isotropic tape laminate during fatigue loading.

Many studies have employed stiffness loss monitoring to assess the degree of damage present in a composite fatigue specimen. Most of these studies tested specimens in either tension-tension (T-T) or tension-compression (T-C) fatigue. In both tension fatigue stiffness loss and compression fatigue stiffness loss, it was found that tape composites generally follow a three stage pattern of stiffness loss [25, 26]. The three stages are: a sharp stiffness drop in the first 5-

10% of life, a gradual linear decline in the next 80-90% of life, and a very sharp decrease in the final 5-10% of life. In woven composites, it was found that in tension fatigue stiffness loss the first stage is less pronounced, and often runs into a middle stage which is not as linear as in tape composites [27]. In addition, the gross tension cycle stiffness loss before failure was higher for woven than for tape composites. In T-C fatigue, Bakis [26] found that for tape laminates compression cycle stiffness loss was more severe than tension cycle stiffness loss, with final specimen failure being controlled by compression. Bakis also found that by normalizing both stiffness loss and specimen fatigue life, a single master curve of stiffness loss for all fatigue stress levels could be postulated. While not much work has been done with compression-compression (C-C) stiffness loss, it follows from Bakis's T-C results that it should be a reliable method for estimating the stage of life for C-C fatigue specimens. However, the pattern of compression fatigue stiffness loss for stitched uniweaves would be expected to be more like the pattern seen for woven composites than for tape composites.

Damage development in composites subjected to compression-compression fatigue loading (the loading conditions studied in this report) was examined extensively by Ryder and Walker ([28],[29]). They worked with prepreg tape graphite/epoxy laminates of various lay-ups and geometries. They found a generally applicable compression fatigue damage process which changed very little for different lay-ups, loading conditions, and specimen geometries. The general pattern was: microcracks initiate (or are present initially), grow, and saturate; delaminations become the dominant damage event and extend; fibers fracture in many regions; fracture occurs at a "worst site" of damage ([28], p. 236). It was hoped that a similar general damage process could be established for stitched uniweave compression-compression damage growth.

Damage development in composites reinforced through the thickness has been examined in several studies. In an early work, Robinson and Francis [30] tested a 3-D woven material and used acoustic emission monitoring to record damage events. They also used scanning electron micrographs to more closely examine sites of damage. Other authors have looked at deformation and failure mechanisms in nonwoven stitched composites. Cholakara, et. al. [11] observed that the compressive failure mode changes from being predominantly delamination in 2D composites to modes such as fiber buckling and matrix cracking in stitched laminates. They also noted that a combination of failure modes in the stitched composites led to a gradual failure process, as opposed to a sudden failure process as seen in 2D composites. Chung, et. al. [12] used optical and scanning electron microscopes to look at failure mechanisms in stitched and unstitched composites. They found that third-direction fibers suppressed free edge delamination and slowed delamination propagation. They further noted that the stitched composite's failure mode was fiber-dominated, including fiber buckling, breakage, and pull-outs, as well as interfacial debonding. Mignery, et. al. [14] used enhanced x-radiographs to monitor delamination progression in stitched composites, and found that the stitching effectively arrested delamination propagation.

Two of the previously mentioned works dealing with stitched uniweaves also included a look at damage development. Radiographs were used by Lubowinski and Poe [4] to monitor damage propagation through the thickness of a stitched uniweave. Under both tension-compression and compression-compression fatigue loading, they found that damage progressed slowly until just a few thousand cycles before failure, when damage began to spread rapidly. They also monitored compression cycle stiffness loss during fatigue loading, and found that stiffness loss in stitched uniweaves started earlier but progressed more slowly than in unstitched composites, allowing the stitched composites to experience more damage before failing. The final value of stiffness loss

was quite high compared to unstitched laminates, and similar to that found in woven materials.

Portanova, et. al. [7] used edge replicas to monitor fatigue damage progression in open-hole compression-compression specimens. They also found that damage in stitched uniweaves progressed more slowly than in unstitched specimens, and delaminations were less predominant. They speculated that the stitching arrested delamination growth by reducing the opening or peel stresses, thus prolonging the fatigue life of these specimens.

The variety of methods used to monitor damage development reflects both the goals of the authors and the equipment available to them. Both destructive (laminate sectioning, residual strength testing) and nondestructive (X-rays, C-scans, edge replicas, stiffness loss) testing provide valuable information concerning the state of damage present in a composite specimen at different stages in its life. Through a combination of these evaluation methods, a more complete characterization of a material's damage modes can be achieved.

Summary

Stitched uniweaves show great promise as a damage-tolerant composite material which is easily fabricated into large net-shape parts and structures, and is much less costly than other damage-tolerant systems such as toughened matrix composites. Work to date with stitched uniweaves has included evaluations of static properties and damage tolerance, as measured by impact resistance, compression after impact, and delamination propagation. Stitch parameter studies have investigated various combinations of stitch material, weight, direction, spacing, and pitch. From these studies a particular stitch configuration was chosen and further studies were made, such as investigating open hole and post impact compression fatigue behavior. Some preliminary

work was done with fatigue damage initiation and propagation. A more thorough examination of damage initiation and modes is needed.

There have been two major concerns noted pertaining to the performance of this material system. The first is that the increase in laminate thickness due to stitch and fill fibers causes a weight penalty [7] and should be minimized. This was overcome by decreasing the weight percentage of fill fibers [21]. The second concern is that the material performed poorly when the loading and stitching directions did not coincide; however, this occurred for a thin, non-quasi-isotropic layup [21], as opposed to the thicker quasi-isotropic layup tested in [7]. In this study, a quasi-isotropic layup with the decreased fill fiber percentage was tested, thereby addressing both performance concerns.

Problem Statement

The primary objectives of the present study were to investigate damage initiation and propagation in a graphite/epoxy stitched uniweave material. The stitch configuration for this material was chosen based on the results from previous studies. Special attention was given to stitching-related material defects, and the effects these defects may or may not have on material properties and response. Specimens were tested in compression-compression fatigue because compression is usually the limiting factor in composite material usage. Damage was monitored on both a global (laminate) and local (ply) level using a variety of destructive and nondestructive test methods. The effect of damage states on the laminate were monitored by stiffness loss and residual strength, while damage on a local level was monitored using edge replicas and x-ray radiographs.

II. EXPERIMENTAL PROCEDURES

Material and Specimens

The specifications for the material system used for this study were chosen based on results from previous studies. The dry fabric, consisting of individually woven laminae laid up quasi-isotropically and then stitched together, was made by Textile Technologies, Inc. The stitching process used is known as the modified lock stitch (see figure 2). The advantage of modified lock stitching over standard lock stitching is that the knots formed by the needle and bobbin threads are placed at the outer surface of the laminate, minimizing lamina fiber damage [5].

Referring to figures 1 and 2 for nomenclature, table 1 lists the raw materials used to manufacture the specimens for this study. AS4 graphite fibers are commonly used for lamina warp tows. The sole function of the weave fibers was to hold the lamina tows in place during stitching, therefore they were a low-denier fiber and only comprised 2% of the total dry fabric weight (denier is a textiles term meaning weight in grams per 9000 meters of yarn length). Next, the woven laminae were stacked in a quasi-isotropic 48-ply layup ($[+45/0/-45/90]_{6S}$) prior to stitching. Modified lock

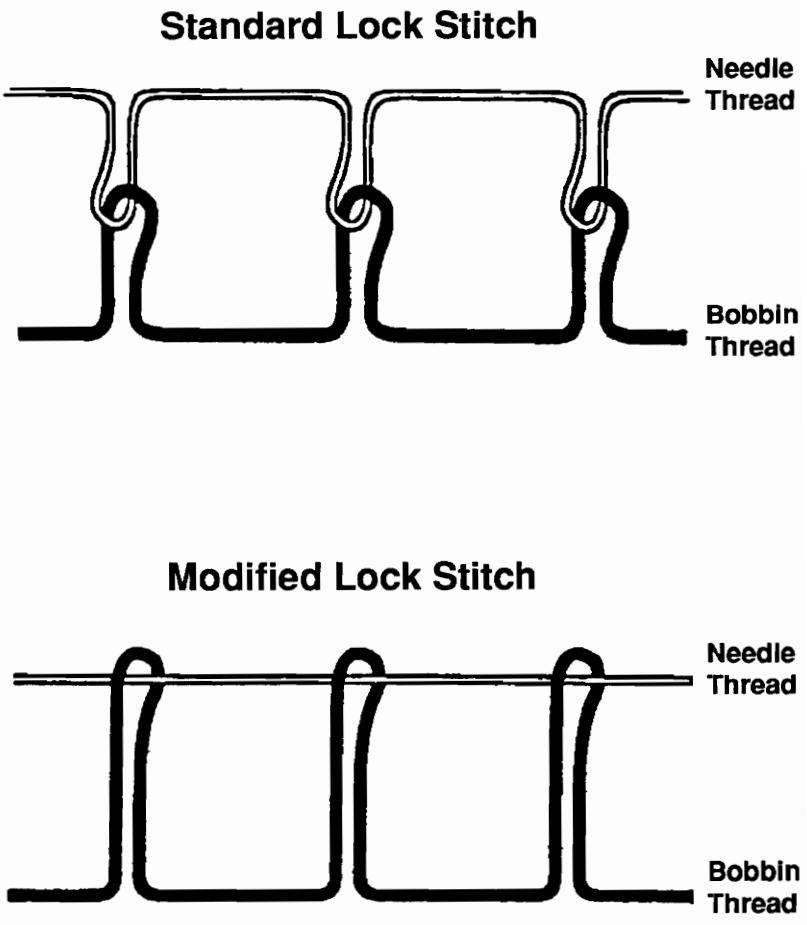

Figure 2. Lock Stitching [5]

Table 1. Composite raw material information

Laminae		AS4 graphite tows
Fill (weave) fibers		225 denier 1/0 glass untwisted, plain weave pattern
Stitch fibers	needle thread	200 denier Kevlar 29 2-end twisted
	bobbin thread	3678 denier S-2 glass 449-1250 untwisted
Matrix		3501-6 neat resin

stitching was then performed in one direction only, at one-eighth inch row spacing and a pitch of eight stitches per inch. The two different fibers used in the modified lock stitching process have similar knot breaking strengths, but the S-2 fiberglass threads are much more flexible than the Kevlar threads. Therefore, S-2 fibers were used as the bobbin thread, which was generally crimped much more than the needle thread (see figure 2). The dry fabric preforms were then impregnated by Douglas Aircraft Company using their resin transfer molding (RTM) process known as vacuum impregnated molding (VIM). This process required a low viscosity resin, for which 3501-6 was chosen.

Four plates (designated K, L, M, and N) were received from Douglas Aircraft Company. Their average dimensions were 12.05 inches long by 7.00 inches wide by 0.300 inches thick. Each plate was ultrasonically C-scanned to detect major defects; all plates were determined to be of similar quality. Manufacturing uniformity was also checked by performing acid digestion tests on scraps from each plate. This test determines the relative weight and volume percentages of fibers and matrix. Results for fiber percentages, reported in table 2, include all fibers; that is, tow (AS4 graphite), stitch (3678 denier S-2), and fill (225 denier S-2) fibers together comprise a weight fraction of about 66%, which compares quite favorably with fiber weight fractions achieved in high-quality unstitched laminates (typically 65-70%). For comparison, the similar stitched uniweave material tested in [7] had only 56% weight fraction fibers, although that material had a higher weight percentage of fill fibers. This difference alone should account for a significant increase in specimen static strength.

The plates were machined at NASA-Langley Research Center. The machining pattern is shown in figure 3. Each plate yielded ten specimens with the stitches running in the longitudinal (0°) direction, and seven specimens with the stitches running in the transverse (90°) direction. The six

Table 2. Plate content information

Plate	Density, gm/mm^3	Fiber weight percentage
K	1.60	66.6
L	1.59	64.4
M	1.59	66.1
N	1.58	66.7

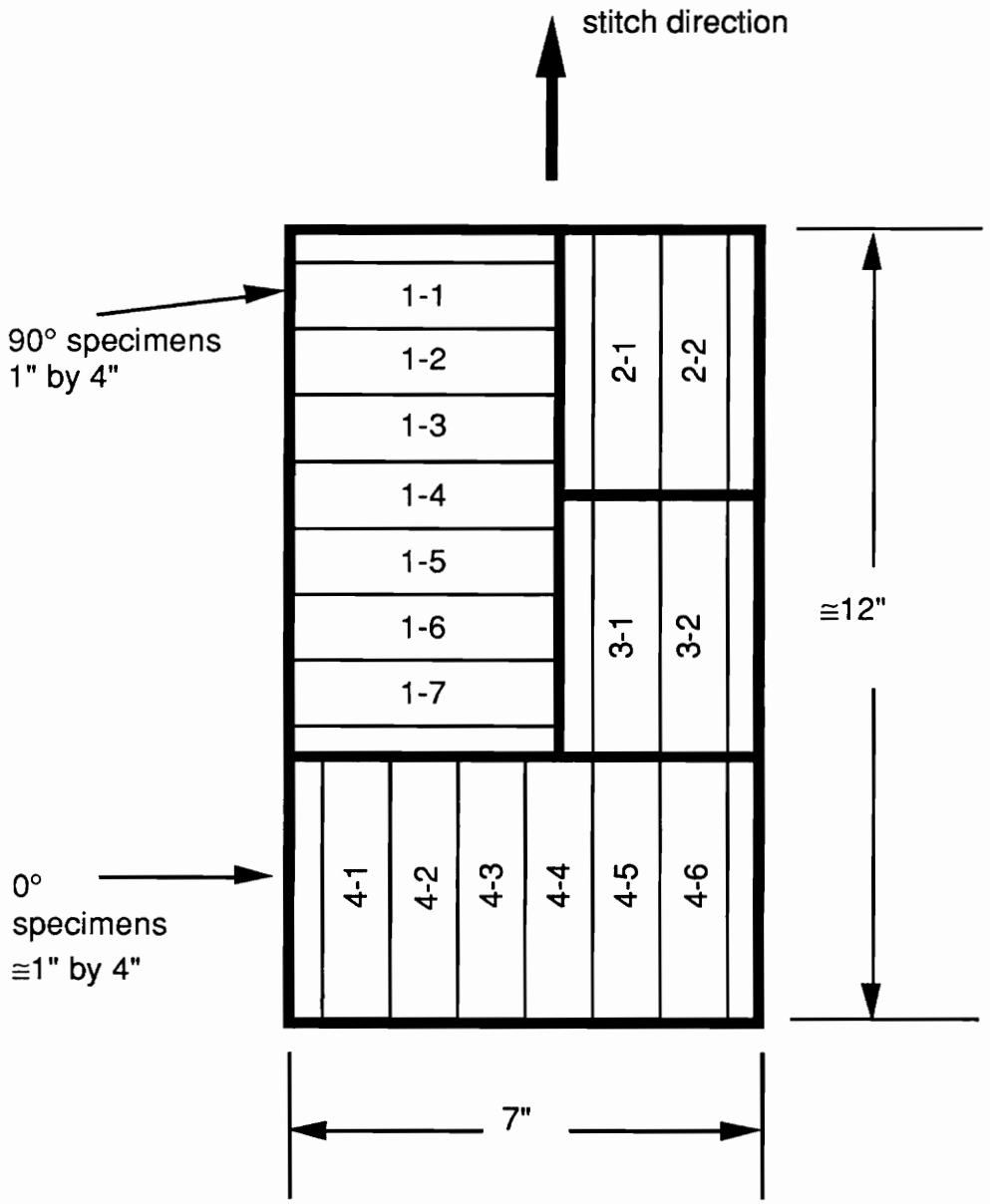

Figure 3. Plate Machining Scheme and Specimen Nomenclature

0° and two 90° scraps left over from each plate were used for static compression tests. The 0° specimens from the last two plates machined were specified to be cut along stitch lines on both edges, and therefore were not exactly one inch wide.

Stitch-Related Defects

A schematic drawing of what the edge of a stitched uniweave should look like when cut along a stitch line is shown in figure 4, while a collage of photomicrographs of the edge of a "good" specimen is shown in figure 5. Visible in both are individual layers, weave fibers, and stitch fibers. Even a perfectly manufactured plate will have some "defects" which are a product of the stitching process itself. For instance, the domes formed by the stitch fibers create both a resin pocket and a zone of pinched layers. This zone has a reduced load-carrying capacity due to deformed layers [31], and also has residual strains due to the bending of the stitch fiber [32] and residual thermal stresses introduced during the resin infiltration process due to different material thermal expansion coefficients. This zone would be expected to both lower the material strength and provide a damage-initiation zone. An imperfectly manufactured plate will introduce even more defects. Some of the major stitching-related defects are cataloged below.

As the stitches punch through the woven layers, the lamina and weave fibers are misplaced slightly in-plane and often crimped or fractured, as shown in figure 6 (a photomicrograph of a pyrolyzed specimen). Previous authors have concluded that this has no serious effect on the material's performance [7]. However, in addition to in-plane misalignment, the stitch fibers also cause out-of-plane misalignment. That is, a 0° layer is no longer aligned in the 0° direction in the vicinity of the stitch fibers, and often layers are deformed quite dramatically near the stitches, as shown in figures 7 and 8. It is expected that this is a major reason that stitched uniweaves have

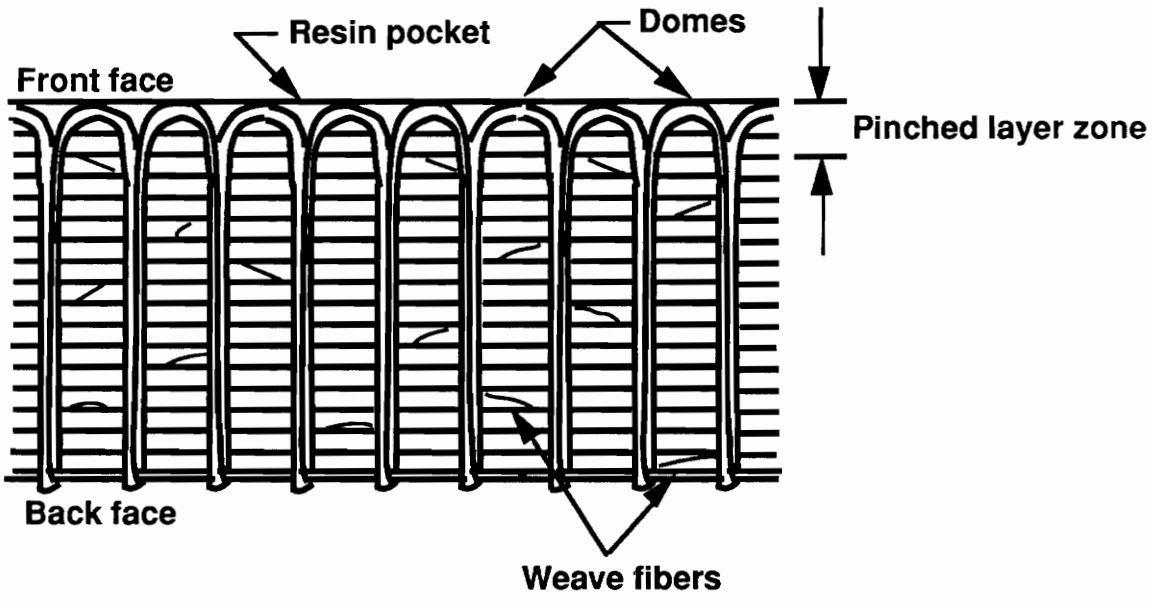

Figure 4. Schematic of Edge View of a Specimen

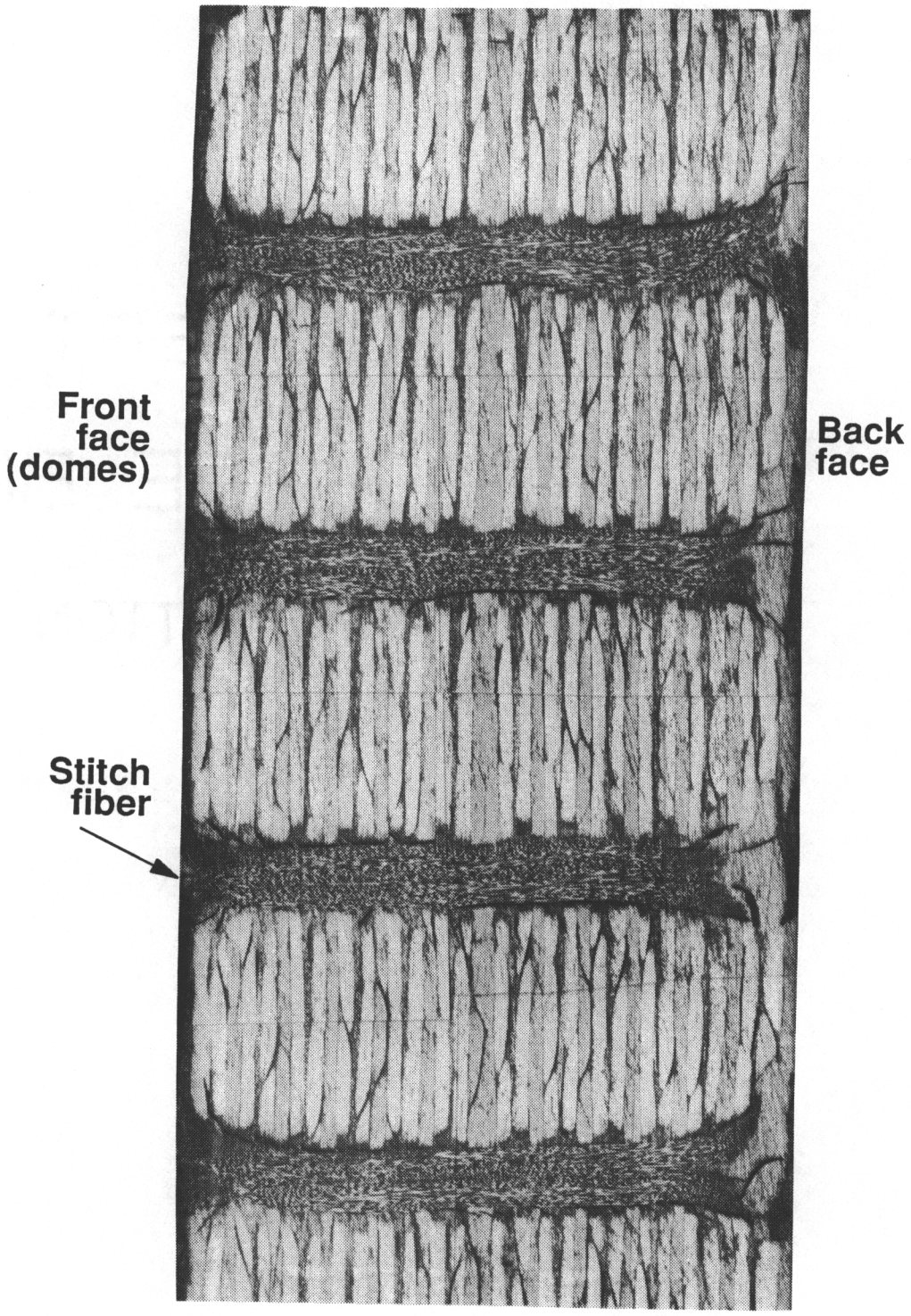

Figure 5. Edge of 0° Specimen M 4-6

Figure 6. Stitch Puncture Site

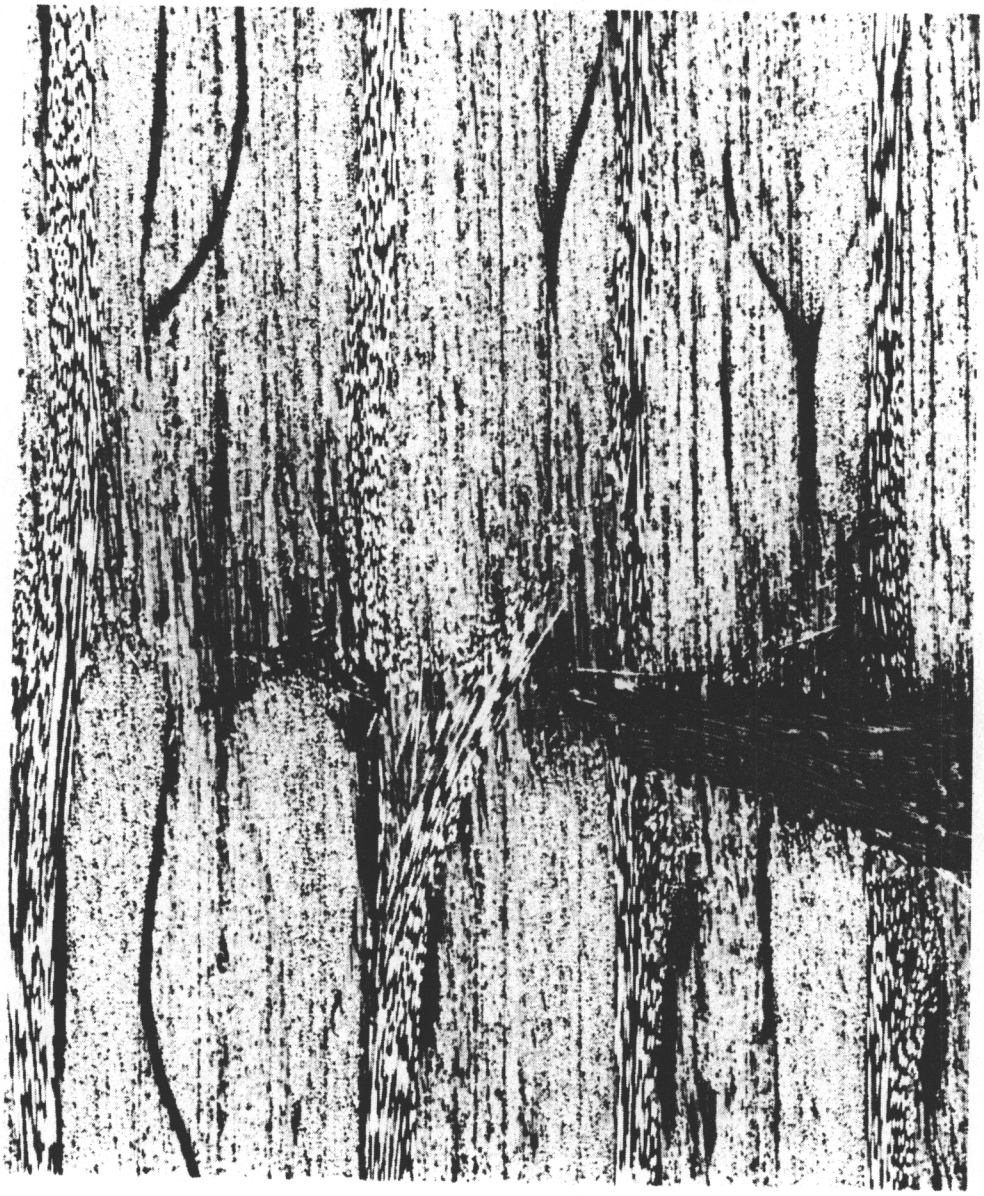

Figure 7. Layers Pulled Out-Of-Plane: 0° Specimen

Figure 8. Layers Pulled Out-Of-Plane: 90° Specimen

lower strengths than unstitched uniweaves, as the load-carrying 0° layers are directly affected.

Another frequently observed occurrence in these stitched materials is microcracks and voids, mostly in the vicinity of the stitch fiber, and especially near the specimen's edge at the dome created by the stitch fibers. Examples of microcracks and voids can be seen in figures 9 and 10. Whether or not these microcracks propagate and contribute to specimen failure will be discussed in the next chapter.

Nominally, the stitch configuration for this material was eight stitches per inch pitch and one-eighth inch row spacing. However, the material received did not have uniform stitch spacing or row spacing. A computer-scanned image of a 7" by 4" portion of plate L was used to count the actual values of stitch spacing and row spacing present in that plate. Histograms shown in figure 11 depict the distributions of row spacing and stitch spacing (pitch), which both should have nominally been 0.125", but were actually an average of 0.127" and 0.147", respectively. Uneven stitch spacing is also exhibited in figure 12, which is a collage of photomicrographs from the edge of a "bad" specimen. This figure is further discussed below.

Comparing figure 12 to figure 5, it is apparent that the stitches are inclined by approximately 10° in the "bad" specimen. This defect was noted in two of the four plates (K and L had inclined stitches, while M and N had relatively straight stitches). It was speculated that the inclination came about during the resin transfer molding process as a result of transverse movement between the top and bottom surfaces of a plate. Also visible in figure 12 are other examples of defective positioning of the bobbin and needle threads.

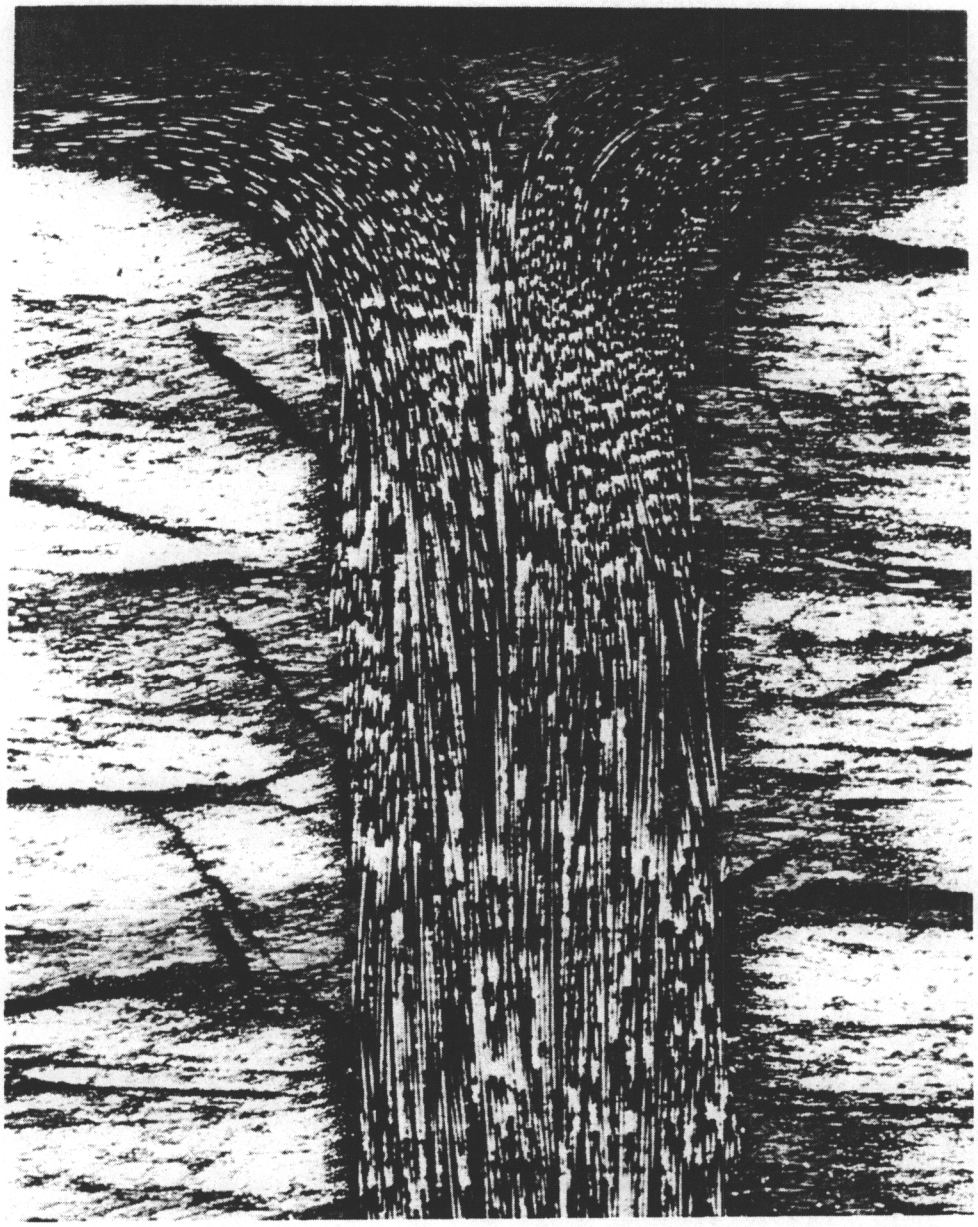

Figure 9. Microcracks Near the Edge of a Specimen

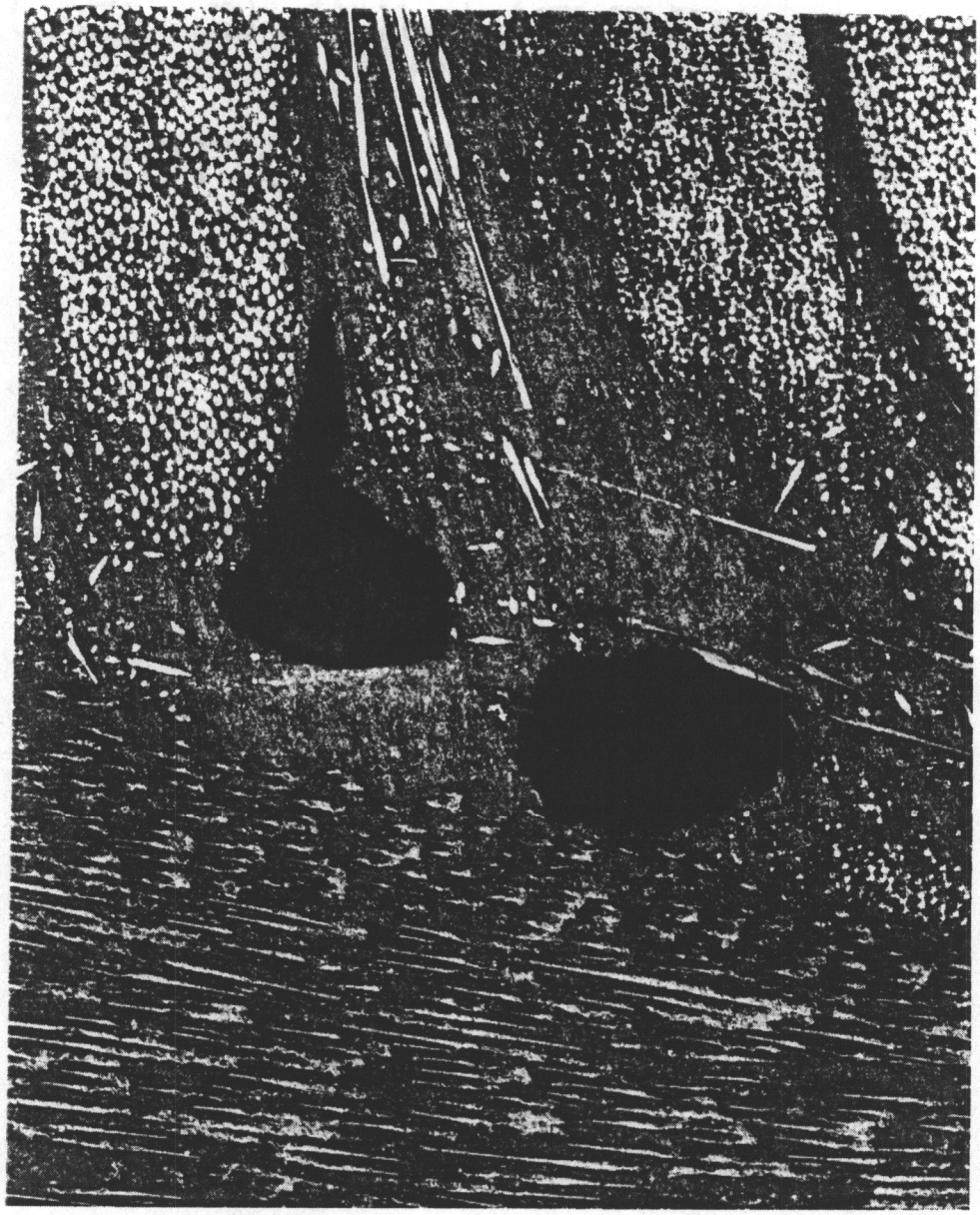

Figure 10. Voids Near a Stitch Fiber

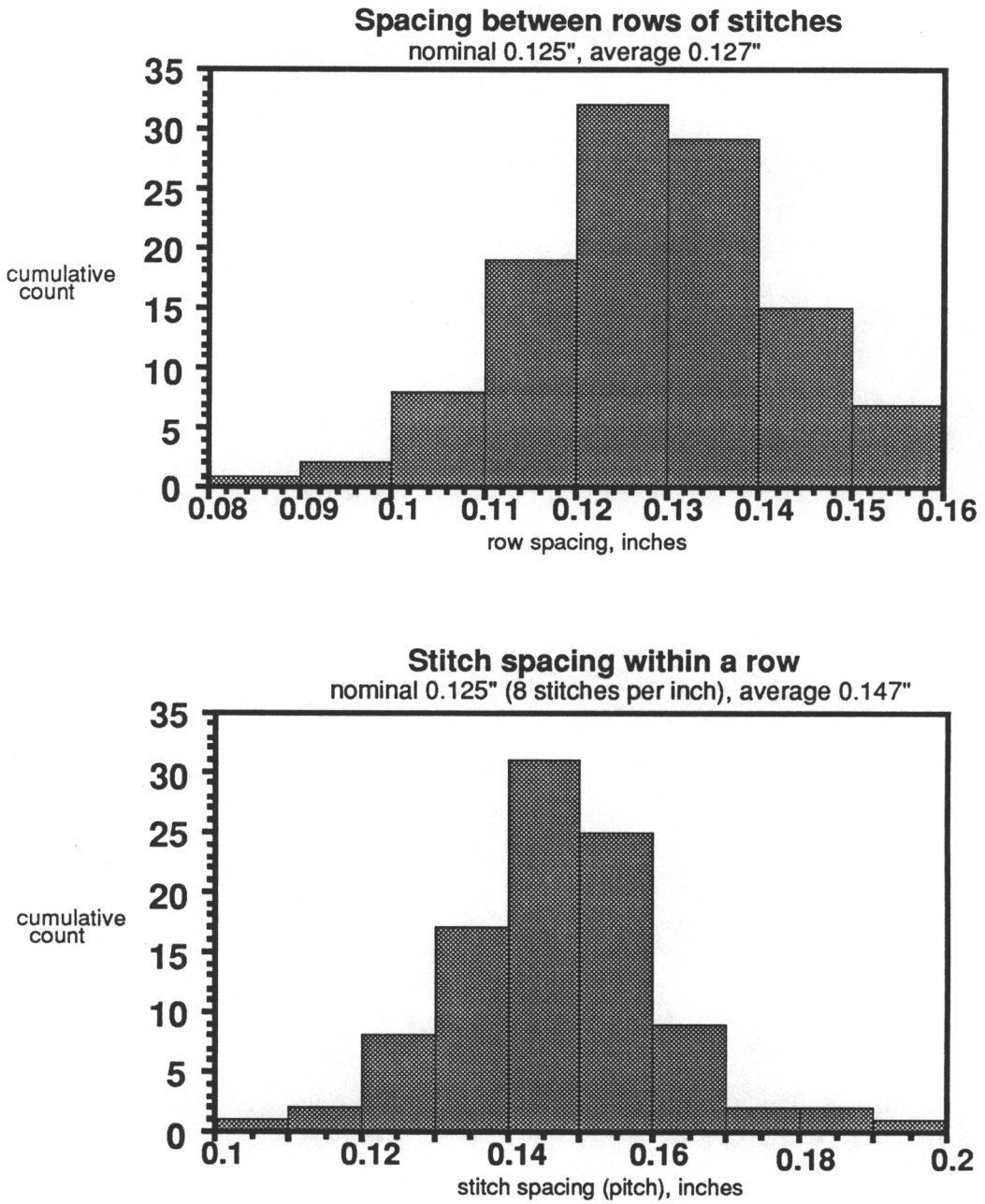

Figure 11. Row Spacing and Stitch Spacing (pitch) Histograms

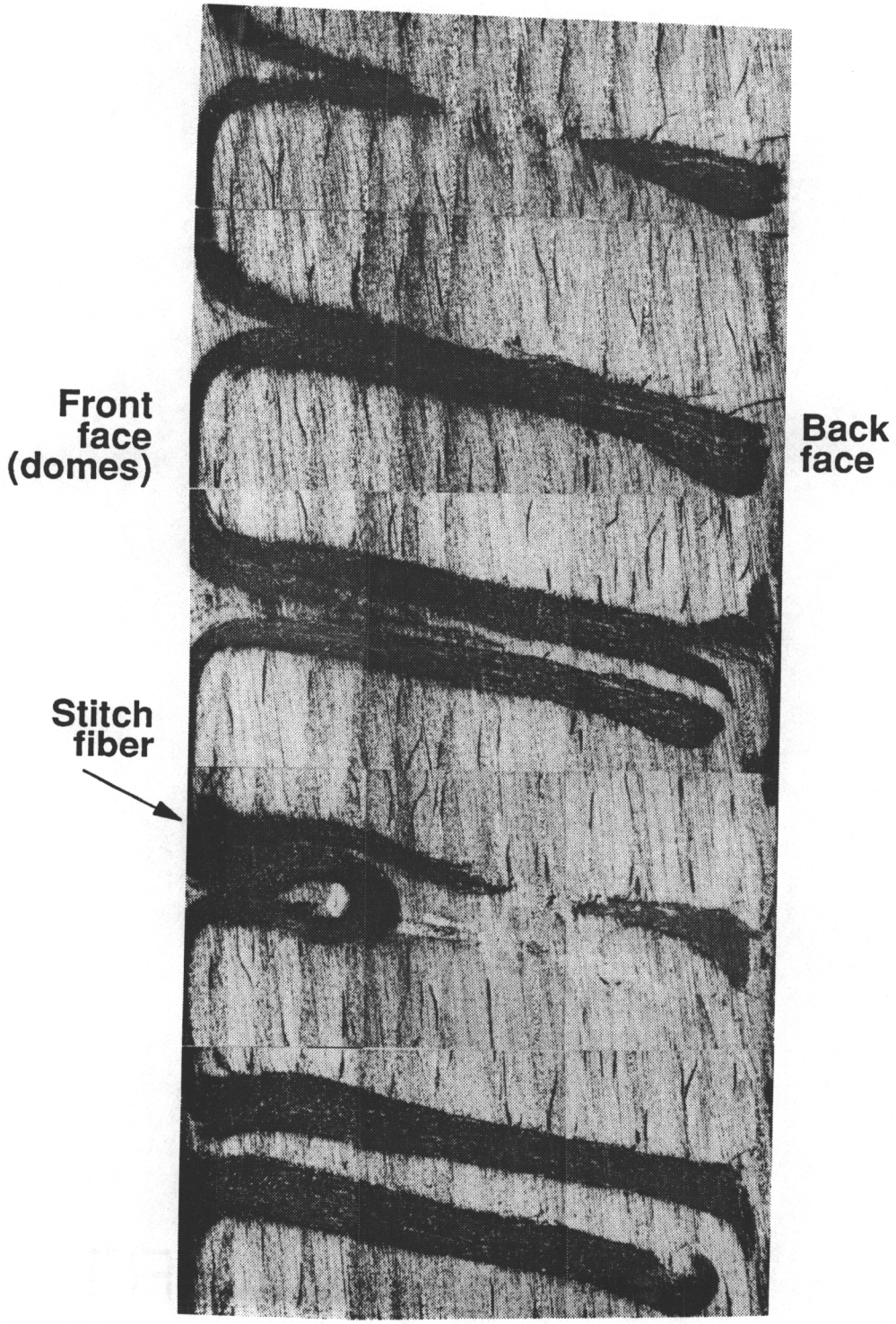

Figure 12. Edge of 0° Specimen K 4-4

Figure 13 is a schematic illustration of inclined stitches and several of the other stitching-related defects. The domed areas are more pronounced in the inclined-stitch specimens, causing a larger pinched-layer zone. Also illustrated in figure 13 is the fact that the bottom Kevlar thread, which is supposed to lie in a straight line along the bottom of a specimen, is occasionally pulled up too far by the bobbin thread. This creates a resin pocket and deforms layers much as in the dome area at the top of a specimen. Possible effects of stitch defects on material performance are discussed in the next chapter.

Mechanical Tests

Mechanical tests were performed at the NASA-Langley Research Center. All fatigue (cyclic) tests were performed in a special fixture designed for compression testing [33], shown in figure 14. The fixture has alignment rods running on linear bearings to ensure that the upper and lower grip remain in line during compression testing. There are also end stops in both the upper and lower grip upon which the specimen rests. The purpose of the end stops is to eliminate slipping of the specimen. In this study, end stops of thickness 0.280 inches were used, since the average specimen thickness was 0.300 inches. The four inner bolts of the grips were torqued to 100 ft-lbs, while the four outer bolts were just torqued snug (approximately 20 ft-lbs). Thus, the specimens were held firmly between the lightly serrated grip faces while resting on the end stops. This set-up helped reduce premature failure by ensuring the specimen was loaded in true axial compression.

These grips were mounted in a test stand as shown in figure 15. Because the stand had only a 20 kip load cell, not all static compression tests could be performed on this machine, due to the

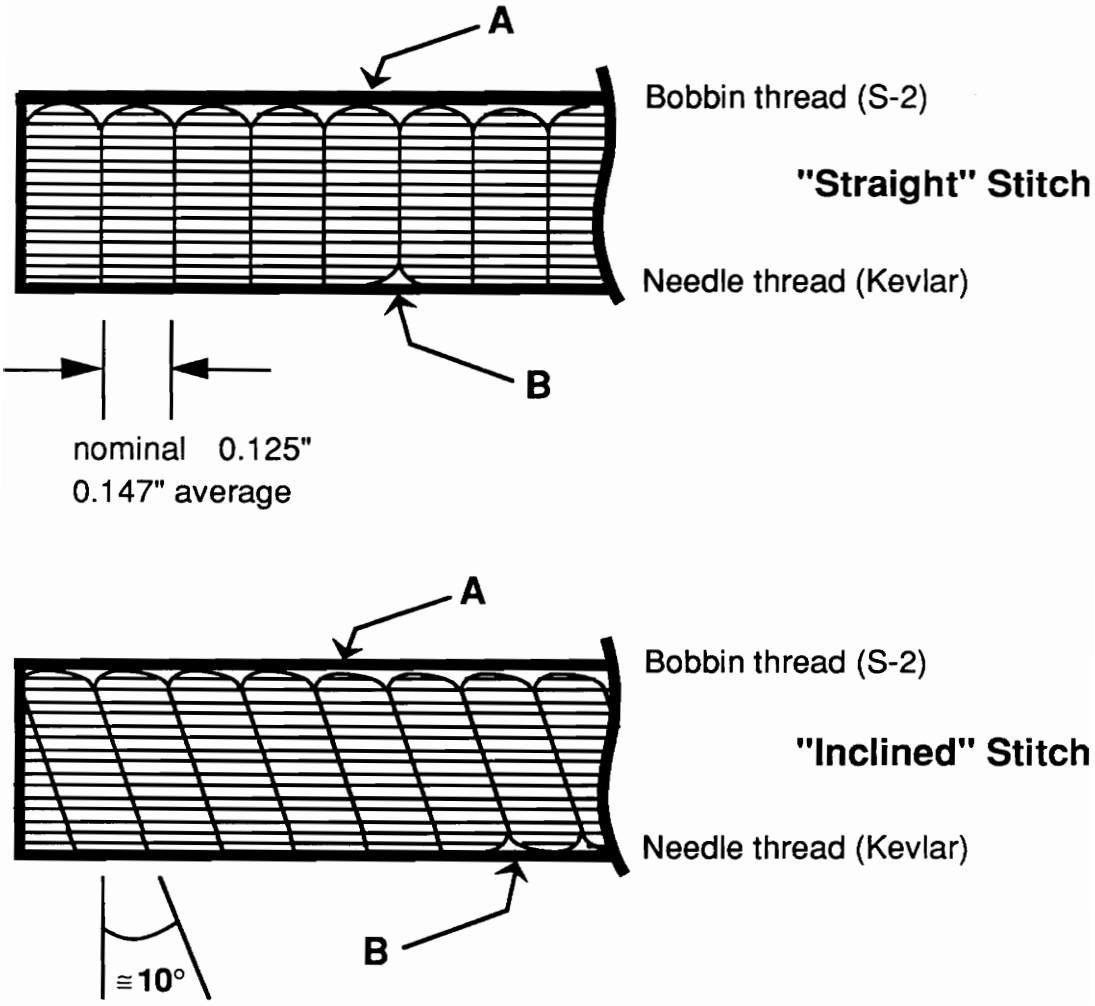

A: dome made by bobbin thread: creates resin pocket, pinches top layers

B: needle thread pulled up by bobbin thread, creating resin pocket

Figure 13. Edge View Schematic Showing Stitching-Related Defects

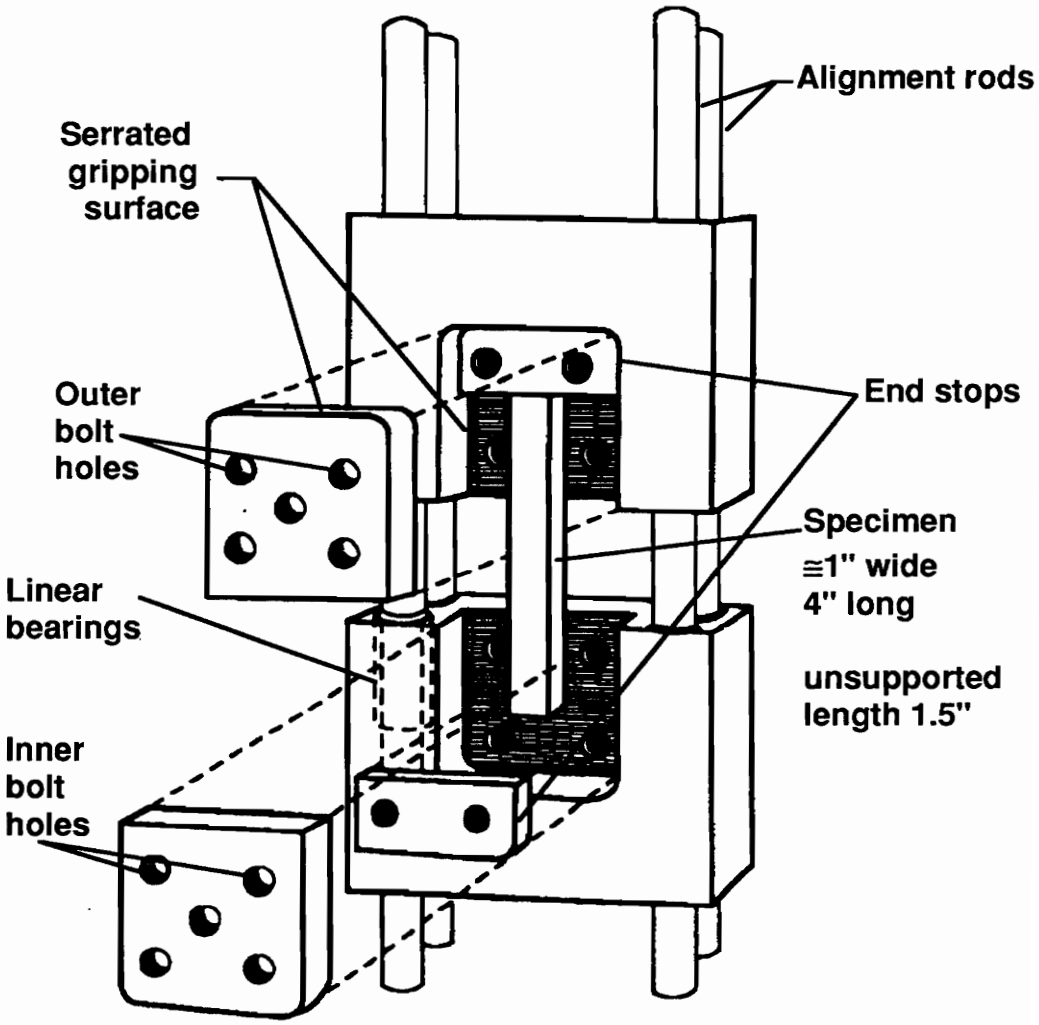

Figure 14. Mechanical Compression Fixure (after [4])

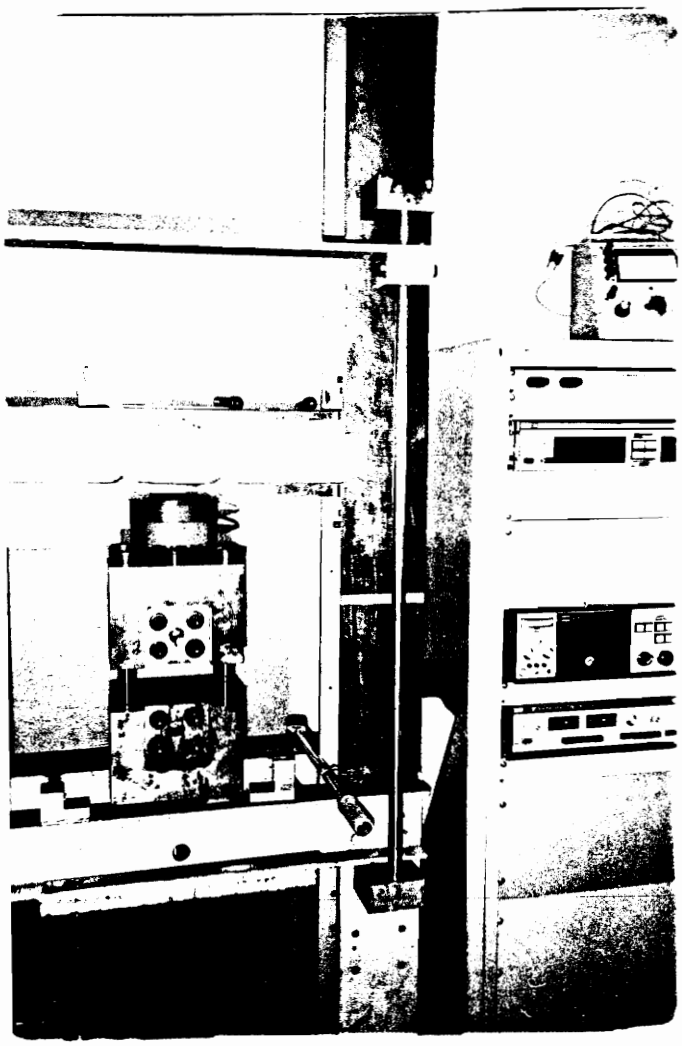

Figure 15. Test Stand with Mechanical Compression Fixure

strength of the material. Some tests on full-size specimens were run on a 50 kip machine, which had hydraulic grips. This is further discussed below. In the results section, the machine and grip type which were used are noted when discussing static compressive strengths.

Monotonic Loading Tests

Static compression tests were run on both 0° and 90° specimens to determine initial properties. First, a full size (1 inch wide by 4 inches long) specimen cut from the first plate was loaded at a rate of 1000 pounds per minute to 20,000 pounds (machine maximum) in the mechanical grips without failing. Subsequent static tests on full size specimens were performed on a 50 kip machine which had hydraulic grips. A grip pressure of 2000 psi was found to be sufficient if end stops similar to those used in the mechanical grips were inserted into the hydraulic grips. However, scraps from each plate, ranging from 0.183 to 0.618 inches wide, were compressively loaded to failure successfully in the mechanical grips.

A different static compression test known as a short block compression test was also performed on several 1 inch wide by 1 3/4 inches long specimens. The test fixture for short block compression tests is shown in figure 16. This test commonly gives static strengths 10-14% higher than those obtained by the regular compression tests described above [5, 34]. Presumably, this is due to both the specimen geometry and the grips. As one of the branches at NASA-Langley commonly reports strengths obtained from this test method, this type of test was run in order to be able to compare the performance of this material to the performance of other materials.

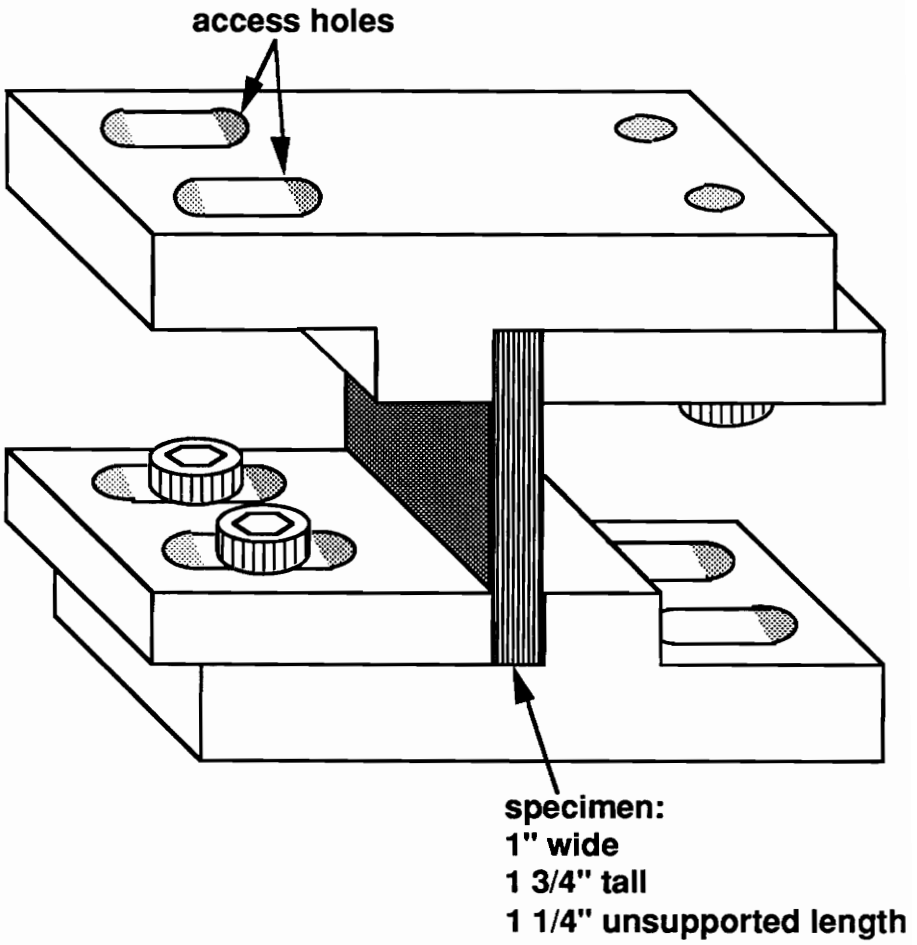

Figure 16. Short Block Compression Fixure

Cyclic Loading Tests

All cyclic tests were performed in the mechanical fixure previously discussed and shown in figure 14. It was important that all tests be run in the same fixure because in compression loading, especially compression-compression fatigue, the gripping and specimen support used can have a large effect on the test results.

Tests were performed under load control. The ratio of maximum to minimum stress (absolute values), R, was 10 for all tests. In some cases, the first five or ten cycles were applied manually for damage evaluation purposes. The rest of the cycles were run at a frequency of 10 Hz using a sine wave function generator. All tests were stopped at various numbers of cycles to perform different damage evaluation tests. Many specimens were cycled until failure, while others were stopped before failure for destructive damage evaluation of the specimen. In all cases, metal blocks were placed between the upper and lower grips to prevent post-failure crushing of the specimen.

Damage Evaluation

A variety of experimental methods was used to evaluate the state of damage in a specimen at different stages in its life, both before, during, and after loading. These methods were employed both at NASA-Langley and at Virginia Tech. Some of the methods were nondestructive to the specimen (ultrasonic C-scans, edge replication, stiffness loss, X-ray radiography), while some were destructive (residual strength testing, laminate sectioning and deply). A brief discussion of each method follows.

Nondestructive Evaluation

Nondestructive evaluation (NDE) of materials, especially composites, is a growing field. This field broadly encompasses any damage evaluation technique which does not affect the strength, stiffness, or life of the material being evaluated. Using these methods, damage initiation and propagation in a single specimen can be monitored. In addition to the methods described below, visual observation was found to be useful in tracking damage growth across the face of a specimen.

Ultrasonic C-Scan

The four plates of material received seemed to be of similar quality, except for the matter of stitch inclination discussed previously. To check if the interiors of the plates were of similar quality and relatively void-free, an ultrasonic C-scan was performed on each plate. This process involves placing the material to be scanned in a tank of a loss-dampening medium such as water, and passing a low-frequency ultrasonic transducer over the material. The signal reflected through the material is compared to the signal reflected if no material is in the tank. Some sections of the material will show a higher loss (attenuation) than other sections. These higher losses are associated with damage, including delaminations, voids, and inclusions. C-scans are extensively used to assess the degree of damage present in a composite material. However, since the information received is a total loss signal, the individual type of damage and its location through the thickness can not be determined with a C-scan. A-scans and B-scans, which process the complete signal received and provide more information about the damage, are being developed at NASA-Langley, but this technique was not available at the time of this study. Therefore, C-scans were only used to assess the relative quality of the four plates.

A portion of a typical C-scan of this material is shown in figure 17. This is the C-scan of plate M, before machining. The four dark spots are the support rods the plate rested on in the tank of water. The striped patterns of light and dark correspond to the stitches. The several darker areas within the plate could correspond to plate compositional differences, or it could just be random signal attrition. Since all four plates had similar C-scans, it was assumed that none had a higher proportion of internal defects than the others (plate L, which had a lower fiber weight percentage as determined in acid digestion tests, had a C-scan essentially similar to those of the other 3 plates).

Edge Replication

As mentioned previously, edge replication is a method for reproducing the edge of a specimen. These replicas are very detailed and pick up the smallest of damage events. Replicas are extremely useful because they can be done while the specimen is under load, thus minimizing the effects of test interruptions and also preserving compression-induced damage which might be less visible in an unloaded state.

To obtain a better replica, all specimens were first polished on the edges. Polishing was performed at NASA-Langley on an automatic rotating-wheel polisher. Most specimens needed only two grades of sandpaper (600 and 800 grit) to achieve a glossy finish. The specimen in figure 5 is an example of a polished specimen edge. Many features, including damage events, were much clearer on replications made on a polished edge.

Edge replication is a very simple technique. The materials needed are cellulose acetate replicating film (acetyl cellulose) and reagent grade acetone (or ethyl acetate). The cellulose

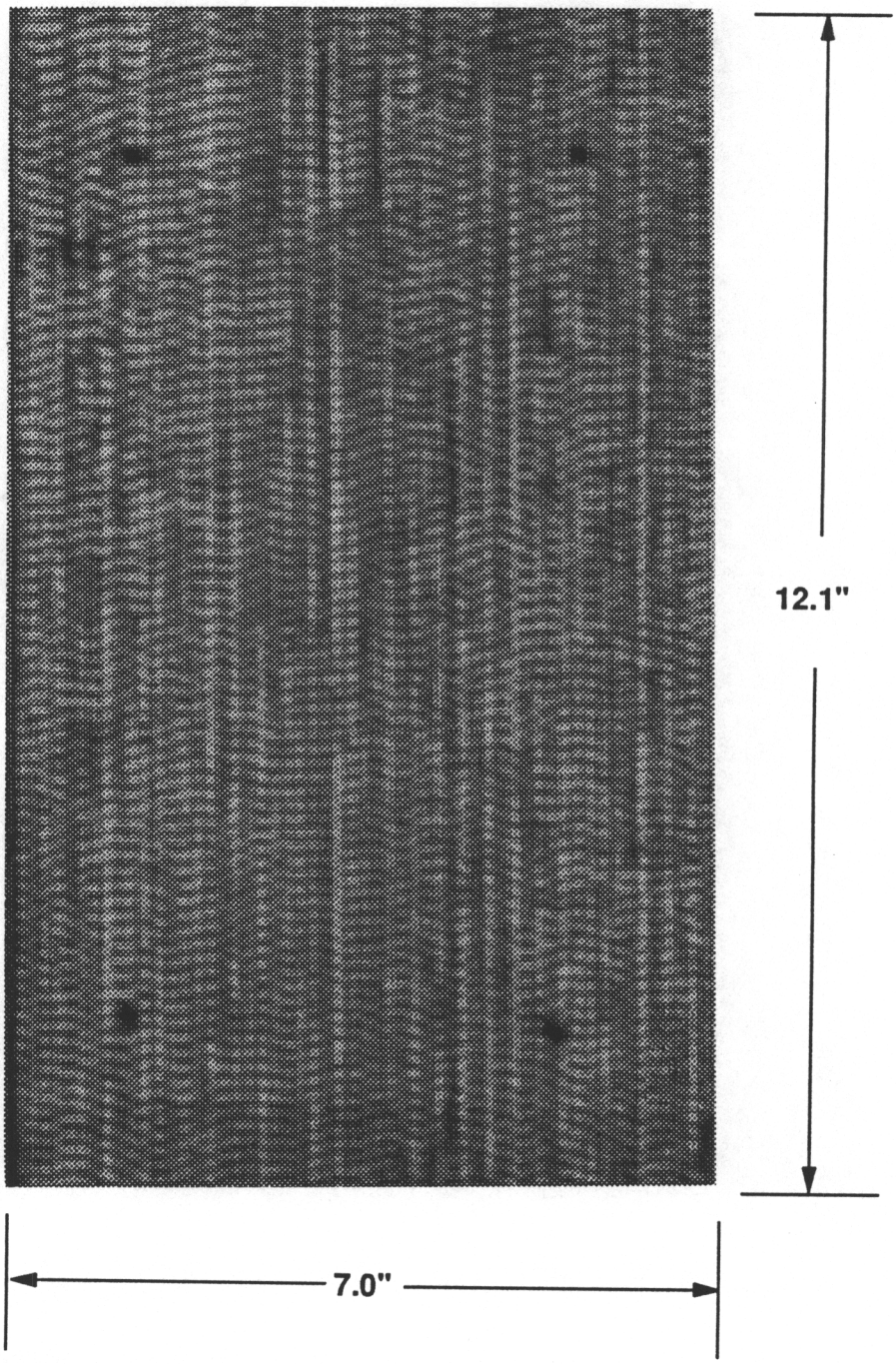

Figure 17. Ultrasonic C-Scan of Plate M

acetate film is available from several manufactures in a variety of thicknesses; for this study, a medium weight (0.034 mm) film was used. Most replicas were made while the specimen was in the mechanical grips under load; in this case, the film was pre-cut to 1 1/2 inches (specimen gage length). Best results were achieved when the film was held in place at the bottom of the specimen (at the grips) by a piece of tape, then acetone was applied at the top of the specimen with a hypodermic needle. When the acetone had run down the edge of the specimen from the top to the bottom, finger pressure was applied to the film from the bottom up to ensure even adhesion of the film to the specimen. The acetone softens the film, which then adheres to the specimen edge and flows into any surface features. The acetone evaporates in a few minutes, and the film can then be removed and viewed either quickly in a standard microfiche reader, or under higher magnification with a light microscope. These films give a permanent record of edge damage. Done properly, this technique picked up all edge damage (cracks, delaminations) quickly and accurately. Problems encountered included bubbles in the replicas due to an excess of acetone, and difficulty in obtaining a good replica when there was a large amount of edge damage (because fibers started to break and bulge from the edge, making an uneven surface to try to replicate). In spite of these difficulties, this method is the best available for quickly obtaining a permanent record of damage at a given stage in the life of a specimen, and it was extensively used in this study to monitor damage progression in fatigue specimens.

Stiffness Monitoring

Stiffness loss monitoring was performed for two reasons: first, to see if a single normalized master curve could be established for compression stiffness loss in stitched uniweaves, regardless of the applied cyclic stress level, and secondly as a damage evaluation parameter used to stop residual strength specimens before failure at a specific stage of life.

Stiffness loss was monitored using a one inch MTS extensometer to record strains. The extensometer was placed on the specimen using rubber bands because the springs provided for attachment were too small. The extensometer knife edges were centered in V-notched aluminum tabs cemented to the specimens. This setup is illustrated in figure 18. This setup generally worked well, except that the rubber bands occasionally broke during long life fatigue tests. It was found that any disturbance to the rubber bands (trying to replace a broken one, trying to remove and replace the extensometer during testing, or moving the rubber bands to check if damage was initiating under them) had a significant effect on the strain reading that was impossible to adjust for. Therefore, stiffness monitoring tests were performed without removing or disturbing the extensometer.

When the extensometer was first placed on a new specimen, a small load was ramped up and down manually to settle the knife edges in the aluminum tabs and then the strain reading was zeroed. Then the load was manually ramped to one volt (2,000 pounds) and then to the maximum cyclic stress level, taking strain readings each time. When the load was returned to zero, the strain zero was checked. Since the strain zero never shifted by more than 15 microstrain, this offset value was subtracted from the strain reading. The one volt strain reading gave an initial elastic modulus, as stress-strain curves plotted on an X-Y plotter generally remained linear for the first 2,000 pounds. The strain reading at the maximum cyclic stress level gave a secant stiffness, which is the quantity generally monitored in stiffness loss testing. The first ten cycles were applied to specimens manually to obtain initial stiffness loss data. Subsequent readings were taken by interrupting the cycling, resetting the load to zero, re-zeroing the strain reading (which usually shifted during cyclic loading), and then ramping the load manually to the maximum cyclic stress level. In most cases, the extensometer was removed from

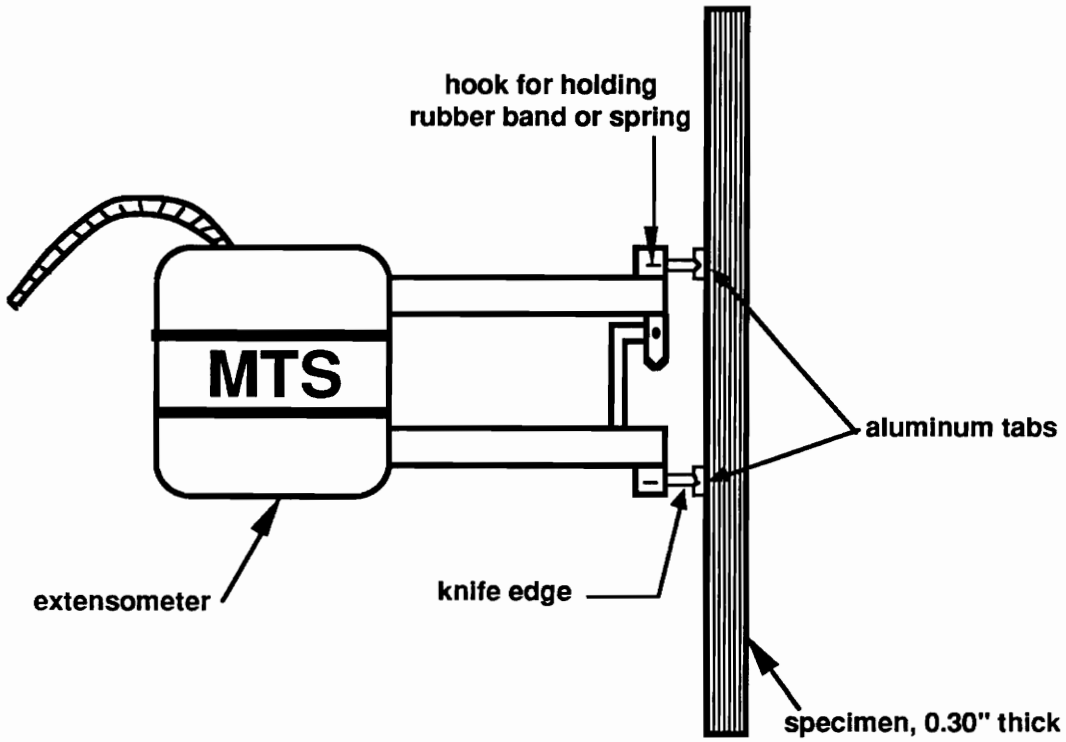

Figure 18. Extensometer Set-Up

the specimen just before failure; however, in three cases the specimen broke with the extensometer still attached. The metal blocks placed between the grip heads saved the extensometer from destruction, and maximum output readings indicated that the extensometer had not been compressed greater than its capacity of five volts (corresponding to 0.15 inches).

X-Ray Radiography

Most nondestructive evaluation techniques do not provide information about the internal state of damage in a composite specimen. One technique which does is penetrant-enhanced X-ray radiography. By taking both face and edge X-rays and comparing them to known surface damage features, the extent of internal damage can be postulated. This technique is widely used to track damage in composite specimens. The penetrant used in this study consisted of:

- 10 ml water
- 10 ml Kodak Photo-Flo 200
- 10 ml isopropyl alcohol
- 60 grams zinc iodide (ZnI_2)

The Photo-Flo helps the solution evenly wet the surface of the specimen, while the alcohol is a carrier which enhances penetration of the solution into the interior of the composite specimen through cracks and delaminations. These areas then become opaque to X-rays. For X-rays taken while the specimen was still in the grips and under load, the penetrant was allowed to soak into the specimen for 15-30 minutes before taking the X-ray. Specimens X-rayed out of the grips were soaked overnight in the penetrant. It is believed that the amount of time the penetrant is left on affects the amount of damage picked up in the X-ray [27]. However, the X-rays taken while the specimen was in the grips were generally of poor quality because the photographic film had to be folded to fit in the grips next to the specimen; therefore, all X-ray radiographs discussed in the

next chapter were taken while the specimen was out of the grips. Thus, all specimens were soaked overnight in the penetrant solution and the time-dependance should not be a factor. A Baltograph II X-ray machine was used at NASA-Langley for all X-rays. The settings which gave the best results were found by trial and error, and are presented in table 3.

Destructive Evaluation

A destructive evaluation technique is one which can only be performed once in a specimen's life because the test destroys the specimen. Specimens which were tested destructively were first evaluated nondestructively in several ways to determine how far advanced in damage they were. Three types of destructive damage evaluation testing were employed in this study.

Residual Strength

Several specimens of both stitch orientations were cycled at the same stress level until a certain amount of stiffness loss was recorded. These specimens were then removed from the grips, X-rayed, and tested in monotonic compression to failure. This residual compressive strength was then compared to the virgin compressive strength.

It has been reported that for woven composite materials, the residual compressive strength remains fairly constant over a large amount of fatigue cycles, unlike tape laminates [35], indicating good damage tolerance properties. It was postulated that stitched uniweaves would behave similarly to woven materials in residual compressive strength testing. This would be a good quality for stitched uniweaves to have. No previous studies on stitched uniweaves tested the residual compressive strength of this material system.

Table 3. Baltograph X-ray settings

	Face View[1]	Edge View[2]
amperage, mA	10	9-10
penetration, kV	20	30-32
time, seconds	30	30
distance from specimen, in.	12	14-16

[1] thickness to penetrate = 0.30"
[2] thickness to penetrate = 0.81 to 1.08"

Laminate Sectioning and Deply

Three sets of similar cyclic tests were run on 0°/90° specimen pairs from the same plate, and then these six specimens were X-rayed and sectioned down the middle lengthwise. The inner edges were then examined to see if damage was confined to one area, or dispersed along the length. This was done to see if the outer edges or the stitches were a more important factor in controlling damage initiation.

These sectioned specimens were then deplied to examine the extent and pattern of fiber fracture. To deply a specimen, it is first pyrolized by being placed in an oven set at approximately 500° C for 5 hours to burn off the matrix material. The stitches must then be removed so that the lamina layers can be deplied. Since the Kevlar needle thread melted during the pyrolization process, the remaining fiberglass stitch threads could be pulled out of the laminate row by row. Individual layers could then be pulled apart from one another; however, the top layers in the pinched zone often fell apart as the stitches were removed. In addition, the removal of the stitch fibers caused additional damage and displacement of the fiber bundles in the layers. Because of these difficulties encountered in removing the stitch fibers without disturbing the damage stat[illegible] deply results are presented.

III. EXPERIMENTAL RESULTS AND DISCUSSION

Monotonic Material Properties

Static Compressive Strength

As mentioned previously, full-size specimens could not be failed in static compression in the mechanical grips due to that test stand having only a 20 kip load cell. When further static tests on full size specimens were run on a 50 kip machine, not only did the grip type change, but the unsupported (gage) length of the specimens was sometimes also different. Results presented in table 4 indicate that this gage length variation did not have a significant effect on the test results. Also in table 4 are results from tests performed in the mechanical grips on thin scraps left over from machining the first plate. These results show that the small width of the scraps does not affect the resulting compressive strength, even when the width of the scrap (0.183") is less than the thickness of the specimen (≅0.30"). Therefore, scraps from the other plates (average width 0.344") were tested in static compression to give compression strengths for those plates. These results are presented in table 5. In addition to comparing the compression strengths between the

Table 4. Compressive Strength / Effects of specimen geometry

Stitch Direction	Specimen	Unsupported Length, in. [3]	Width, in.	Strength, ksi
	K 2-1	1.22	1.025	66.5
	K 2-2	1.50	0.933	68.9
0°	K 4-2	1.50	1.054	67.7
	K 4-5	1.21	1.087	68.3
	K scrap[1]	1.50	0.618	70.4
	K scrap[1]	1.50	0.183	69.3
average				**68.5**
std. deviation				**1.23**
	K 1-2	1.22	1.002	74.0
90°	K 1-5	1.50	1.002	65 + [2]
	K 1-6	1.50	1.003	63.9
	K scrap[1]	1.50	0.589	72.0
average				**70.0**
std. deviation				**4.37**

[1] End loaded in 20 kip machine; other specimens tested with hydraulic grips in 50 kip machine

[2] Loaded to machine maximum 20 kips (65 ksi) without breaking in 20 kip machine; broke at 17.1 kips (56.6 ksi) in 50 kip machine

[3] Total specimen length was 4.0 inches

Table 5. Compressive Strength / Effects of stitch inclination and direction

Plate	Stitch Direction	Number of Specimens	Average Strength, ksi
K [1]	0°	6	68.5
	90°	3	70.0
L [2]	0°	6	65.9
	90°	2	64.9
M [2]	0°	6	71.2
	90°	2	68.3
N [2]	0°	5	69.1
	90°	2	68.4
averages	0°	23	**68.7 (2.18)**
(std. deviations)	90°	9	**67.9 (2.14)**
	all	32	**68.3 (2.04)**

[1] average of strengths in table 4; both mechanical and hydraulic grips; average specimen width 0.85", length 4.0"

[2] average of tests on scraps; mechanical grips only; average specimen width 0.344", length 4.0"

four plates, table 5 also compares the strengths of specimens with their stitches along the loading axis (0° specimens) to the strength of specimens with their stitches transverse to the load (90° specimens). In comparing the four plates, the only one whose compression strength is significantly lower than the others is plate L. This is a reasonable result, based on the lower fiber weight percentage of this plate (table 2). The higher the fiber weight percentage, the stronger a composite should be, as the results for this material indicate. As for 0° vs. 90° compression strength, the maximum difference was less than two ksi, and that plate had an unusually high 0° specimen average strength. It was expected that on the average, the 0° and 90° compressive strengths for this material should be equal as the laminate layup was quasi-isotropic, and the stitches should have a similar effect on compressive strength no matter what direction they are relative to the axis of loading. It is expected that an unstitched uniweave of the same material and layup would have a higher compressive strength, because of damage associated with the stitching process (discussed earlier). While no unstitched material of this uniweave could be obtained, a previous study [7] has shown this to be true. This issue is further discussed below.

Presented in table 6 are the results of the short block compression tests, and a comparison to results obtained from the regular compression tests. The specimen size for these short block tests was 1 inch wide by 1 3/4 inches long. It can be seen that the short block compression test gives higher compression strengths, which must be due to the specimen size and gripping method.

Three short block compression strengths are compared in table 7. Material 1 is from this study, material 2 is the stitched uniweave from [7], and material 3 is an unstitched uniweave which was the base material for material 2. Unfortunately, no unstitched specimens of the uniweave tested for this study were available. Material 1 had a 12.3% higher strength than material 2, which was

Table 6. Compressive Strength / Short block compression

Specimen	Short Block Compression Strength, ksi [1]	Regular Compression Strength, ksi [2]	Percent Difference
L 0°	75.2[3]	65.9[4]	14.1
M 0°	79.8[3]	71.2[4]	12.1
M 90°	75.65[3]	68.3[3]	10.8
average	**76.9**	**68.5**	**12.3**

[1] specimen size: 1.0" wide, 1.75" long: unsupported length 1.25": special fixure (figure 16)

[2] specimen size: average 0.344" wide, 4.0" long: unsupported length 1.5": mechanical fixure (figure 14)

[3] average of 2 specimens

[4] average of 6 specimens

Table 7. Compressive Strength / Comparison between three materials

Material	Short Block Compression Strength, ksi
1 (this study')	76.9
2 (unnotched stitched uniweave from [7])	68.5
3 (unstitched uniweave from [7])	85.0

identical except for fill fiber weight percentage. However, this difference is probably not due only to the difference in fill fibers, because the manufacturing quality of material 2 was poor. Due to this, the plates of material 2 were 17% thicker than the plates of material 1, even though material 2 had the same layup. There was a 24% degradation in compression strength between the unstitched and stitched versions of material 2. It is expected that material 1 would not exhibit such a large drop-off in strength from the unstitched state, because the manufacturing quality of the stitched plates was higher. No unstitched version of material 1 was available.

Comparison to an Unstitched Tape Laminate

It was desired to compare the properties of the material of this study to those of a similar unstitched tape laminate. While no material of this type was available, its properties could be calculated theoretically. The longitudinal and transverse layer properties for an AS4/3501-6 lamina were obtained from a Hercules publication [36]. Then, a commercial computer program [37] was used to form a $[45/0/-45/90]_{6S}$ laminate with a total thickness of 0.30 inches (which corresponded to a lamina thickness of 0.0625 inches). Using basic laminate theory, the program calculated the laminate material properties and a compression strength (using the maximum normal stress criterion). Results for the theoretical compression strength and elastic modulus of the unstitched laminate are compared to the measured values for the stitched uniweave of this study in table 8. The results show a strength degradation of only 15.5%, and a modulus degradation of 25.3%. However, there are difficulties in comparing these results directly - both quantities for the stitched uniweave in table 8 are "worst case" values (the difference would be only 4.8% if the short block compression strength were used, and the elastic modulus may be low because of the measurement method). However, it does seem that the degradation in material

Table 8. Comparison of material properties with an unstitched tape laminate

Material	Strength, ksi	Elastic Modulus, Msi
This study[1] (stitched uniweave)	68.3	6.14
Tape laminate[2] (unstitched)	80.8	8.22
Percent difference	15.5	25.3

[1] experimental values: regular compression strength; elastic modulus assumes linear elastic behavior to 2,000 pounds load

[2] theoretical values

properties going from the unstitched to the stitched state is less severe for this material than for the similar material from [7].

Failure Patterns and Modes

Illustrated in figure 19 are the failure patterns observed in static compression failure tests of full-size specimens tested in hydraulic grips. Represented are the gage length portions of the left and right edges and front and back faces. Three out of seven specimens failed at the grip on one side of the specimen, and the other four failed near the grip. All specimens exhibited a transverse shear failure mode resulting in failure planes at an approximately 45° angle through the thickness of the specimen. All 90° specimens had surface failure lines which lay in between two rows of stitches. The surface failure lines of 0° specimens were ragged, connecting stitches in adjacent rows which seldom lined up stitch-for-stitch. This is illustrated in figure 20, which is two portions of a computer-scanned image of the front surface of plate L. Sample failure lines have been added. Failure patterns in short block compression specimens were similar to those observed in the full size specimens, also being near the grips and exhibiting similar edge and surface failure patterns. The small width scraps from each plate tested in the mechanical grips had similar edge and surface failure patterns to the full-size specimens, but were more likely to fail in the center of the gage length away from the grips, due to the specially-designed compression grips.

Fatigue Test Results

Fatigue Life Data

Stress-life data for compression-compression fatigue tests performed on full-size specimens from each plate are summarized in table 9 for both 0° and 90° specimens. The one cycle to failure

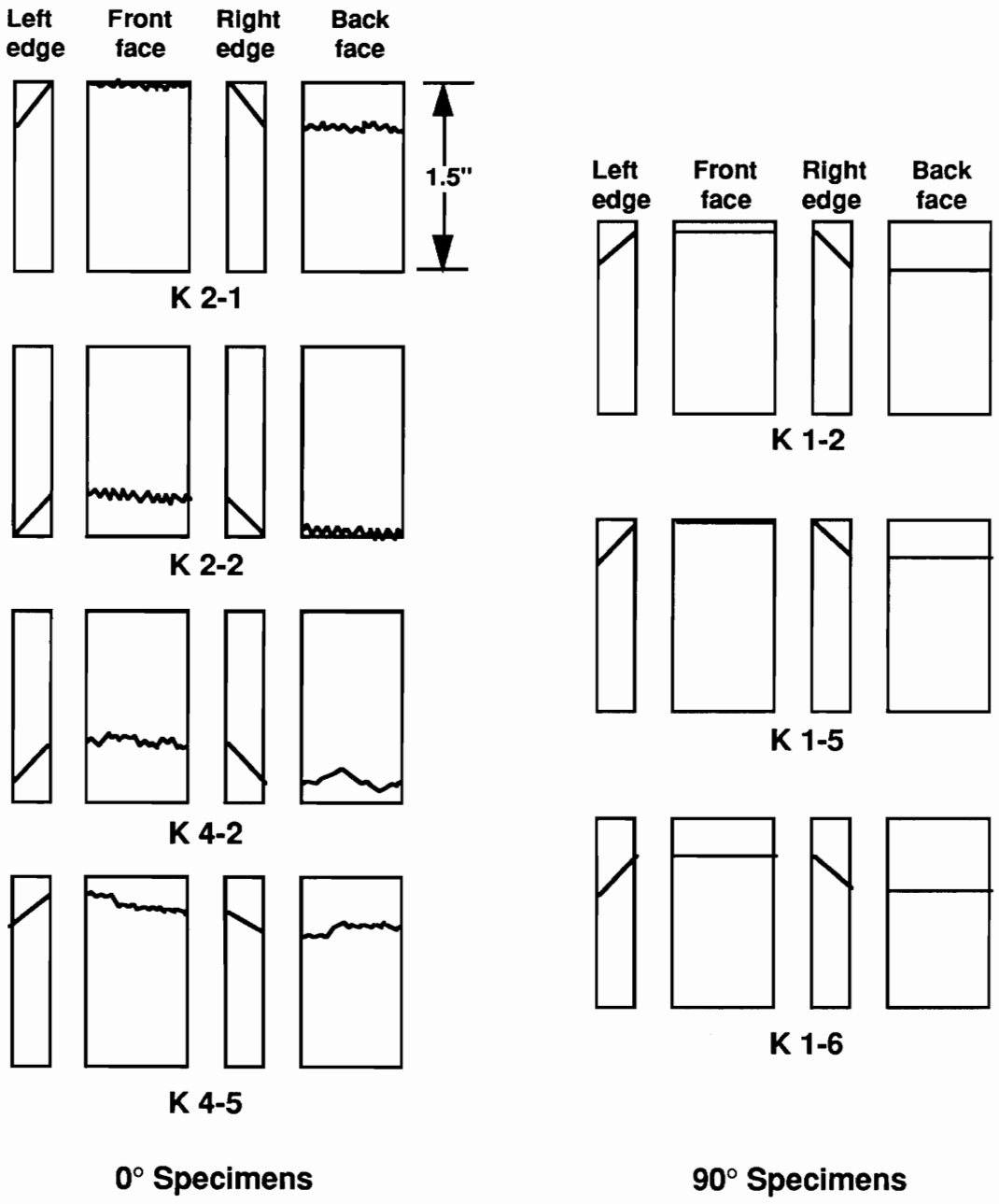

Figure 19. Static Compression Failure Patterns Observed in the Gage Length Portions of Full-Size Specimens

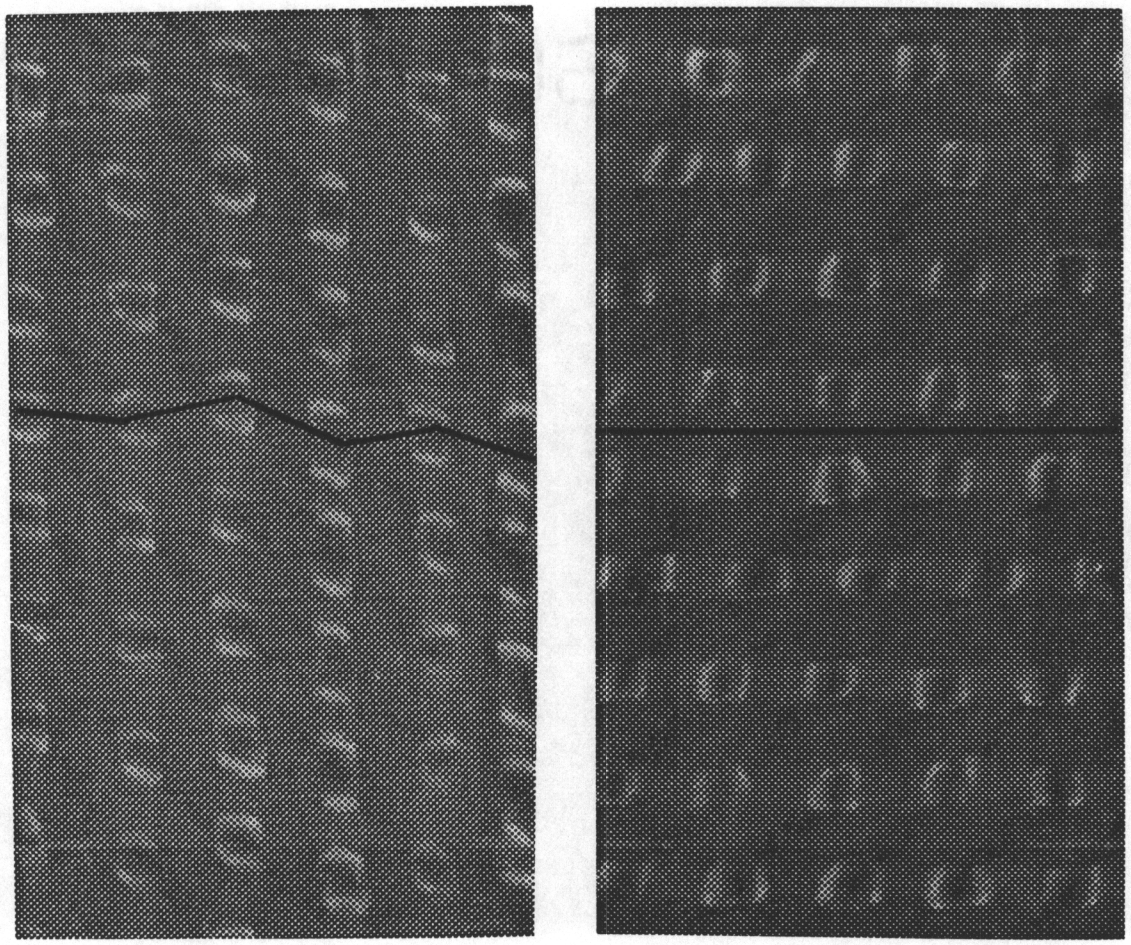

0° Image

90° Image

Figure 20. Portions of the Scanned Image of Plate L showing the Front Surface of 0° and 90° Specimens with Sample Failure Lines

Table 9. Stress-life data / Material 1 (this study)

Cycles to Failure	Stress Level (ksi)	Specimen
0° Specimens		
1	68.7	reg. compressive strength
1	77.5	short block comp. strength
1900	56.0	K 4-1
73840	52.1	K 3-1
77280	48.0	K 4-6
228260	45.2	K 4-4
398100	46.3	K 4-3
2970000	44.5	K 3-2
3310	55.4	L 2-1
19790	52.0	L 4-6
320	64.0	M 4-1
780	63.0	M 3-2
11460	55.0	M 2-2
55480	50.0	M 3-1
101,910	50.0	M 2-1
720	61.6	N 2-2
1730	60.0	N 4-6
4461	62.5	N 4-1
5800	59.0	N 4-2
13923	58.0	N 3-1
28860	53.4	N 4-5
32760	53.0	N 3-2
65521	51.0	N 2-1
476000	48.0	N 4-3
90° Specimens		
1	67.9	reg. compressive str[illegible]
1	75.6	short block comp. strength
5300	55.0	K 1-1
46810	51.5	K 1-3
246960	48.1	K 1-4
75000	49.0	L 1-6
255250	49.0	L 1-7
380	63.2	M 1-1
176530	49.0	M 1-5
2000000+	45.0	M 1-2
1690	62.9	N 1-1
3590	61.0	N 1-7
12010	55.0	N 1-5
16651	56.3	N 1-2
21590	54.3	N 1-6
56048	53.0	N 1-3
734920	46.0	N 1-4

stress levels are the average compression strengths from the regular compression tests and the short block compression tests, respectively.

Figure 21 is the stress-life curve for all of the data in table 9 illustrating the effect of stitch orientation (0° vs. 90°) on fatigue performance. The vertical axis is the maximum compressive stress the specimen experienced. The horizontal axis is the number of fatigue cycles until the specimen failed (or was stopped cycling). The 10^0 (1) cycle to failure stress levels are the static compression strengths from the regular compression tests and short block compression tests. Note that the 0° (open circle) and 90° (filled square) fatigue data points are evenly interspersed, indicating no difference in fatigue performance between 0° and 90° specimens of this material. The two lines plotted are least squares logarithmic curve fits using all the fatigue data points and either the regular compression strength or the short block compression strength. The curve fit using the short block compression strength (solid line) has a correlation coefficient of 0.932, while the curve fit using the regular compression strength (dashed line) has a correlation coefficient of 0.969.

To compare the performances of specimens from the four different plates, the data in table 9 was plotted in a different way. In figure 22, stress-life data is presented as a function of which plate a specimen came from. The regular compression strength obtained from scraps from each plate was used as the one cycle stress level. 0° and 90° specimens from the same plate are represented by the same symbol. The lower fiber weight percentage and compression strength of plate L do not seem to have affected fatigue performance. However, as indicated in figure 22, stitch inclination has an effect on fatigue performance. The specimens with straight stitches (plates M and N, filled symbols) exhibited a superior performance to specimens with inclined stitches (plates K and L, open symbols), at least under high stress/low life conditions. This

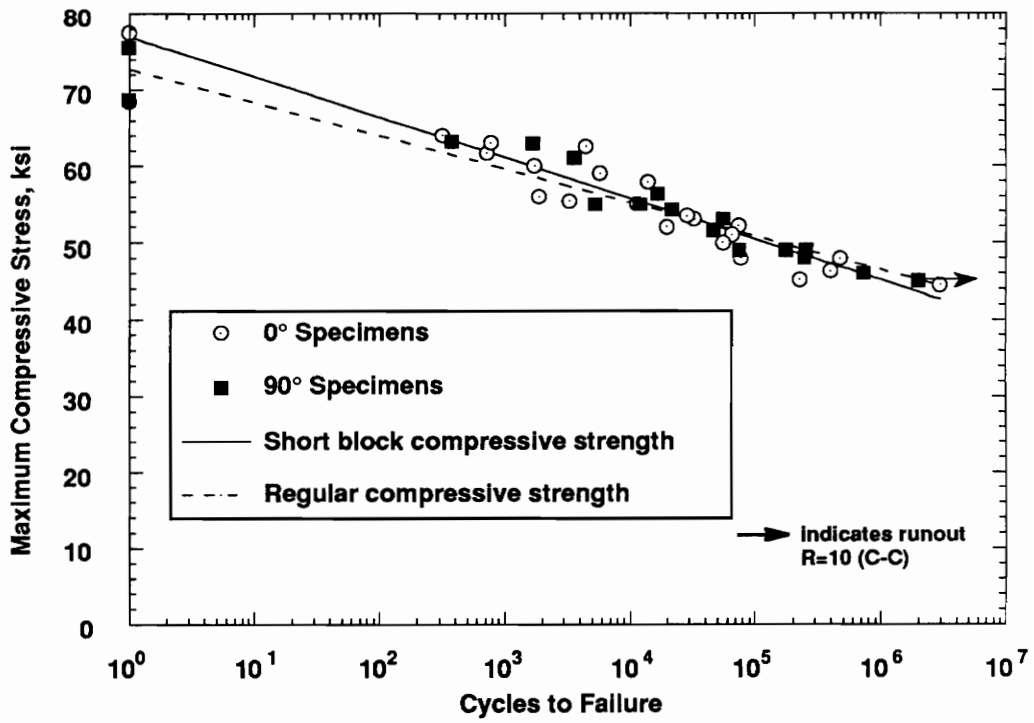

Figure 21. Stress-Life Curve / Effects of stitch orientation

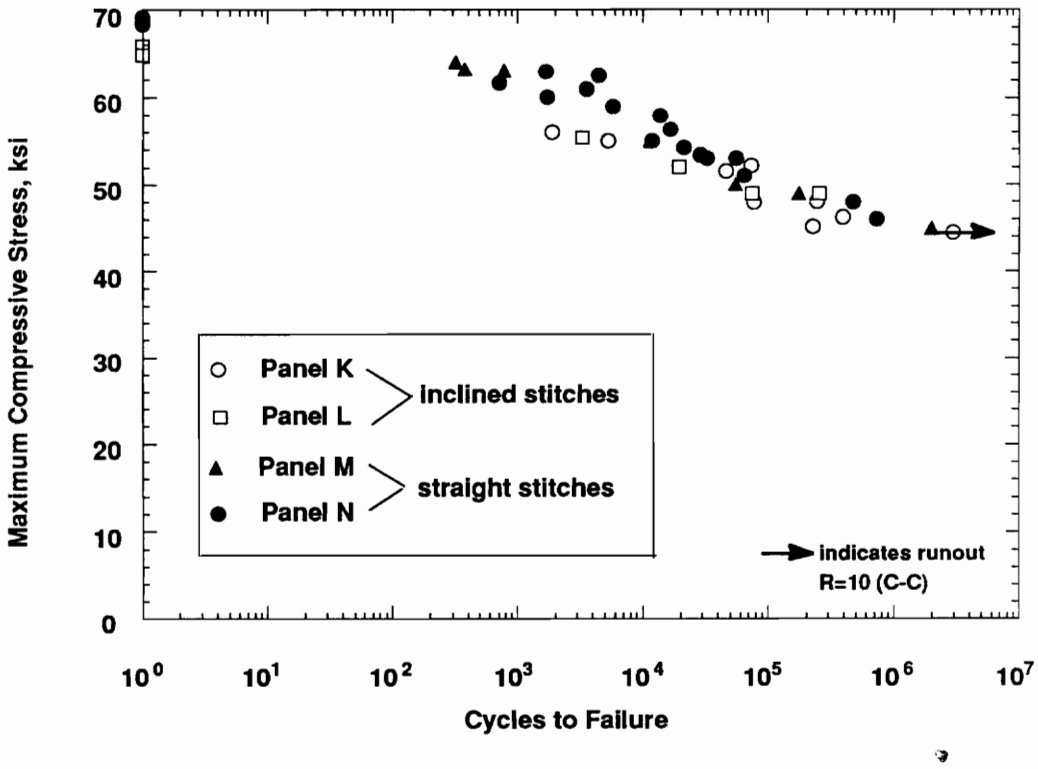

Figure 22. Stress-Life Curve / Effects of stitch inclination

performance disparity seems to end at a stress level of approximately 53 ksi. Below this stress level (long life specimens), the effects of stitch inclination appeared to diminish, and specimens from all plates performed similarly. This performance difference was blamed on stitch inclination because it is the only thing plates K and L have in common that is different from plates M and N. Why stitch inclination has this effect on fatigue performance is discussed in a later section of this chapter.

Figure 23 is a comparison in stress-life performance of the three materials discussed earlier whose strengths were compared in table 7. The data for materials 2 and 3 graphed in figure 23 is presented in table 10. Material 2, as tested in [7] by Portanova, was notched; therefore, the extra material left over from that study was tested in unnotched form to generate the data in table 10. The data for material 3 was previously presented in [5]. All fatigue tests for all three materials were run in the same mechanical grips. All one cycle stress levels are short block compression strengths. As shown in figure 23, the reduced fill fiber weight percentage and higher stitched-plate manufacturing quality has improved the performance of material 1 over that of material 2, and made the fatigue performance of material 1 comparable to that of material 3 despite the lower static strength.

Failure Patterns and Modes

Failure patterns observed in specimens failing in fatigue were generally similar to those observed in static compression tests. Figure 24 shows four photographs depicting the front face and one edge of two 0° fatigue specimens, with arrows denoting the path of face surface damage. The top one, N 2-1, failed after 65,521 cycles at 51 ksi. The bottom one, N 3-1, failed after 55,480 cycles at 50 ksi. All 22 0° fatigue specimens had similar surface failure patterns. Six failed at the

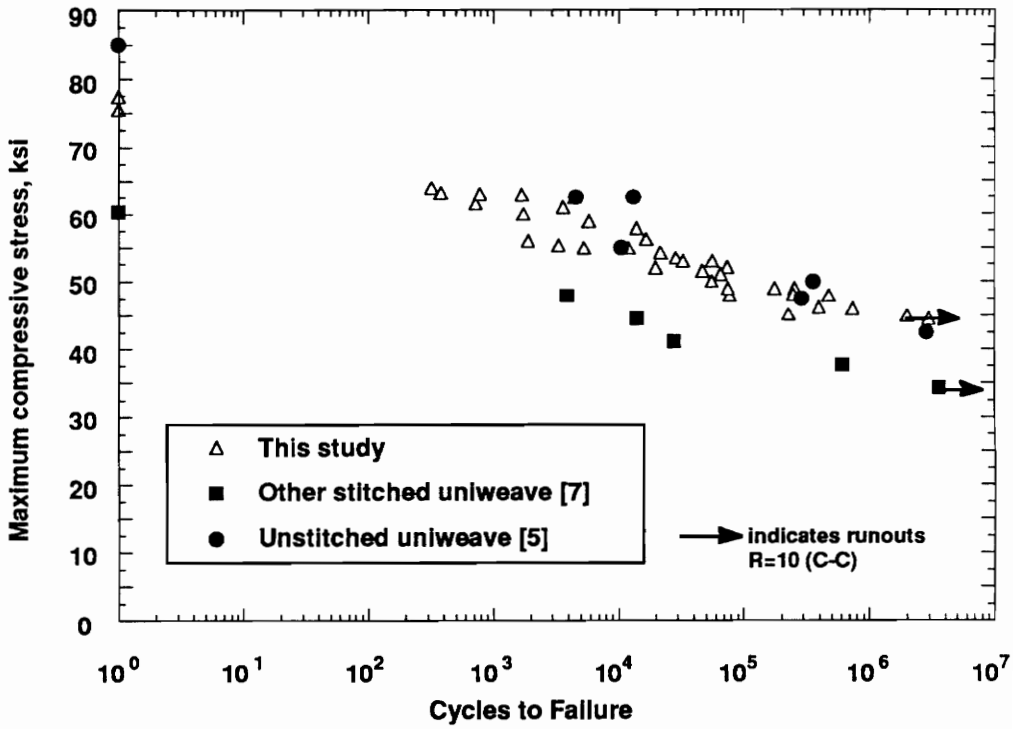

Figure 23. Stress-Life Curves / Comparison with other materials

Table 10. Stress-life data / other materials

Material 2: stitched uniweave unnotched [1]	
Cycles to failure	**Stress level, ksi**
1	68.5
3900	48.0
14020	44.5
28000	41.1
612000	37.7
3600000 +	34.2

[1] unnotched coupons taken from specimens tested in [7]

Material 3: unstitched uniweave base for material 2	
Cycles to failure	**Stress level, ksi**
1	85.0
4563	62.5
10560	55.0
13250	62.5
291100	47.5
355510	50.0
2836900	42.5

(from [5])

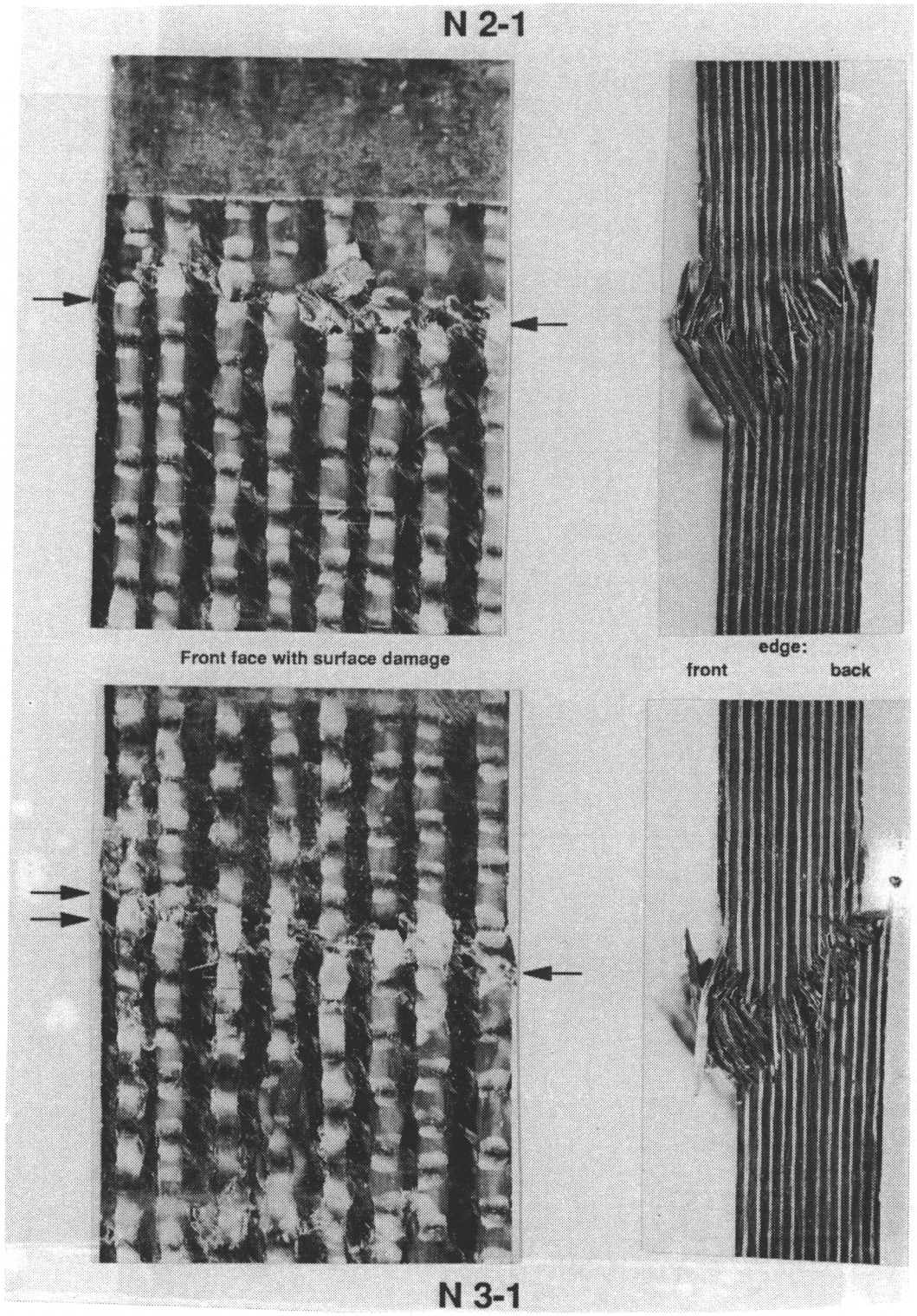

Figure 24. Fatigue Failure Patterns with Surface Damage Marked by Arrows (0° Specimens)

grips on one face, while another four failed near the grips (like 2-1) and the remaining twelve failed more in the center of the gage length (like N 3-1). This is similar to the percentage of grip failures for static compression tests on the scraps tested in the mechanical grips, again indicating that it was the hydraulic grips which caused the grip area failures observed in full-size static compression specimens. The failure mode for fatigue specimens was again transverse shear for all specimens; sixteen fatigue failure specimens (72.7%) had the same 45° single plane edge failure pattern as seen in the static compression specimens and in N 3-1 in figure 24, while six (27.3%) had a more V-shaped failure pattern on one or both edges, as seen in N 2-1 in figure 24. No correlations were seen between grip failures or V-shaped edge failures and loading conditions (high stress-short life vs. low stress-long life). However, all V-shaped edge failures occurred in specimens with straight stitches, as opposed to inclined stitches.

Shown in figure 25 are the failure patterns of two 90° specimens. Specimen N 1-3 failed after 56,048 cycles at 53 ksi, while N 1-4 failed after 734,920 cycles at 46 ksi. The face failure pattern was again always between two stitch lines, as was the case for the static compression specimens. Three of 14 specimens (21.4%) had a V-shaped failure pattern on one or both edges as described above, also only occurring in specimens with straight stitches. Ten of 14 specimens (71.4%) failed at or near the grips (like N 1-4). A higher percentage of 90° specimens (71.4%) failed at or near the grips than 0° specimens (45.5%); this is probably due to the relation between stitch pattern and failure pattern discussed earlier (see figure 20).

Damage Development under Fatigue Loading

Damage development was monitored using both nondestructive and destructive evaluation techniques, employed on both a global (laminate) level and a local (lamina) level. In this section,

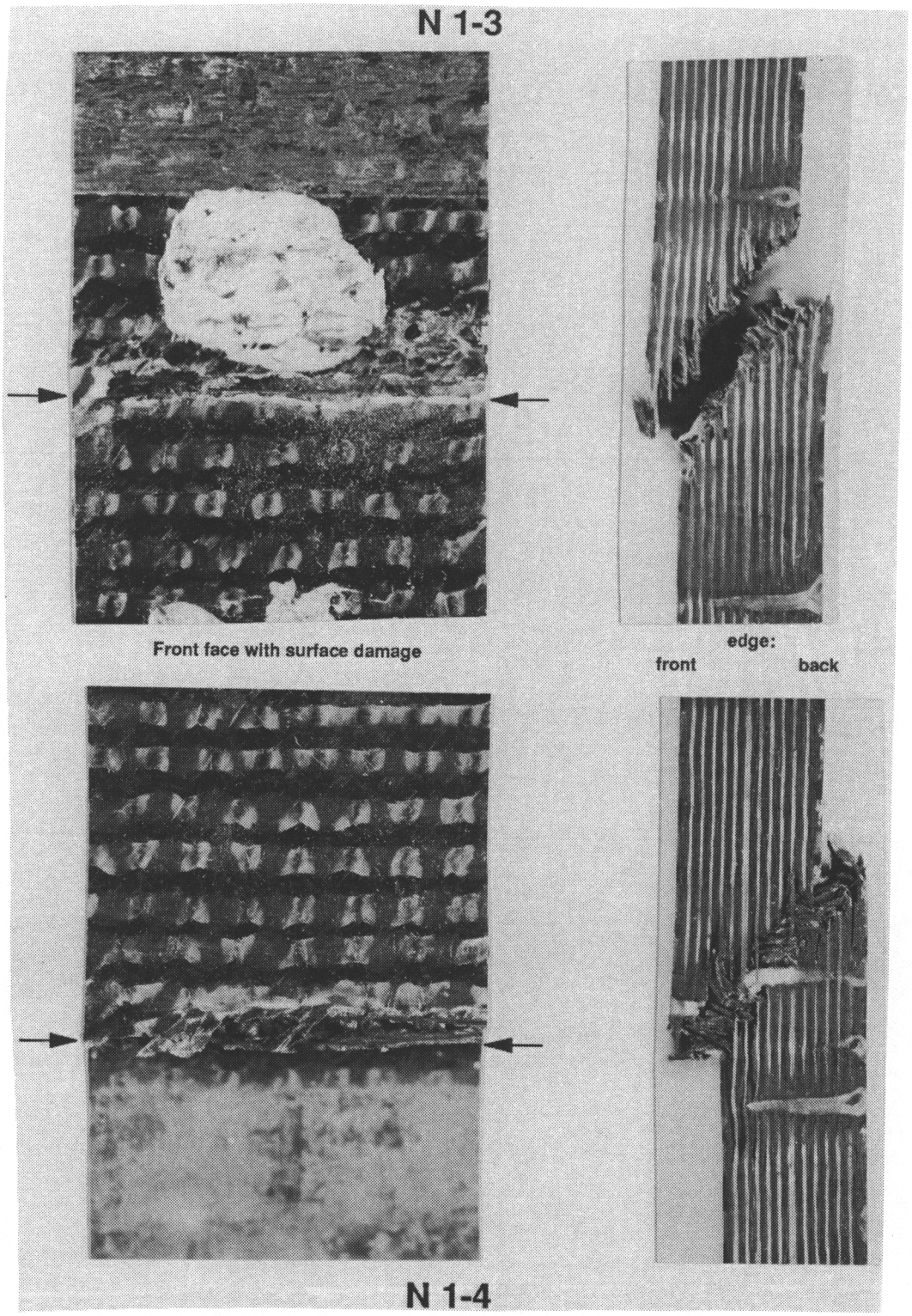

Figure 25. Fatigue Failure Patterns with Surface Damage Marked by Arrows (90° Specimens)

first global damage results are discussed (stiffness loss, hysteresis, and residual strength), followed by local damage results (edge replicas, X-rays, and laminate sectioning).

Stiffness Loss

The first specimen for which stiffness loss was monitored, K 4-4, had aluminum tabs on both the front face (the face where the domes formed by the bobbin threads are) and back face (the face where the needle thread lies) of the specimen. The extensometer was moved from the front to the back face during the first ten cycles to check if the readings were equivalent. They were, and subsequent readings taken during fatigue testing were taken with the extensometer mounted on the front face. This specimen then exhibited a very drastic loss in stiffness over its fatigue life. Visible surface damage was much more pronounced on the front face of the specimen than on the back face. Therefore, it was decided to run all subsequent stiffness loss tests with the extensometer mounted on the back face of the specimen to minimize the effects of surface damage. In addition, it was found that if the extensometer was removed from the specimen during testing and then replaced, the strain readings showed a large jump. This was probably due to the placement of the rubber bands, which had a large effect on the strain reading. Therefore, in all subsequent tests the extensometer was never removed from the specimen during cycling.

Results for all tests in which stiffness loss was monitored up until just before specimen failure are summarized in table 11. A variety of fatigue lives from 720 to 734,921 cycles are represented. Some specimens had initial stiffness readings taken at one volt (2,000 pounds) for elastic modulus determination, while others did not. The final stiffness loss before failure ranged from 5.4% of initial stiffness to 50.6% (for specimens with the extensometer mounted on the back

Table 11. Stiffness loss data

Specimen	Elastic modulus, Msi	Cycles to failure	% stiffness loss (fraction of life)[1]
N 1-2		16,651	34.1 (.999)
N 1-3		56,048	30.2 (.998)
N 1-4	5.93	734,921	5.4 (.992)
N 1-7 [2]	5.98	3,590	22.6 (.997)
N 2-1	6.31	65,521	11.0 (.977)
N 2-2	6.21	720	25.8 (.972)
N 3-1	6.19	13,923	26.6 (.992)
N 3-2		32,760	21.7 (.999)
N 4-1	6.12	4,461	17.9 (.999)
N 4-3		476,000	20.3 (.926)
M 2-1	6.22	101,910	50.6 (.999)
K 4-4		228,264	55.5 (.999)
average	**6.14**		**26.1**

[1] Column 4 represents the ratio of final secant stiffness to initial (1 cycle) secant stiffness, and the fraction of life at which the final reading was taken. The average reported is for the eight specimens whose last stiffness reading was taken after at least 99% of life had passed. Specimen K 4-4 is not included in this average because it had the stiffness measuring device mounted on the front face instead of the back face.

[2] This specimen failed at the grip on the back face; all other specimens failed either in the gage length of the extensometer or underneath the aluminum tabs

face). The average final stiffness loss was 26.1% of the initial stiffness for specimens in which the final stiffness reading was taken after at least 99.0% of life.

The average elastic modulus was 6.14×10^6 psi (as measured at 1 volt, approximately 6.7 ksi, assuming linear behavior to this point, since stress-strain curves were not monitored for all specimens). As discussed in relation to table 8, this value may actually be too low. It appears that 90° specimens had a lower elastic modulus than 0° specimens; however, the difference was only 7.5%, and the number of specimens tested was too low to be statistically significant.

Stiffness loss curves are presented in figures 26 and 27. In order to compare specimens of different initial secant stiffnesses and different lives, both axes are normalized. The vertical axis is measured secant stiffness normalized by the initial secant stiffness of that specimen. The horizontal axis is fraction of life (cycles normalized by cycles to failure for that specimen). By graphing stiffness loss data in this way, stiffness loss curves for different specimens can be compared.

Figure 26 shows the normalized stiffness loss curves of six specimens, two 0° and four 90°. All six followed a similar pattern, despite the variety of cyclic stress levels (46-62.5 ksi) and cycles to failure (3,590-734,921). These specimens exhibited a more or less two stage stiffness loss pattern, which was more similar to the pattern seen in woven composites than the pattern seen for tape composites. No sharp initial stiffness loss was seen in the first 5-10% of life, as was the case for tape laminates. Instead, these six specimens experienced a gradual stiffness decline in the first 90% of life, followed by an elbow in the curve and a sharp stiffness decline in the final 10% of life. Stitch orientation and applied stress level did not have a very significant effect on the shape of the stiffness loss curves for these six specimens. Therefore, an average "master curve"

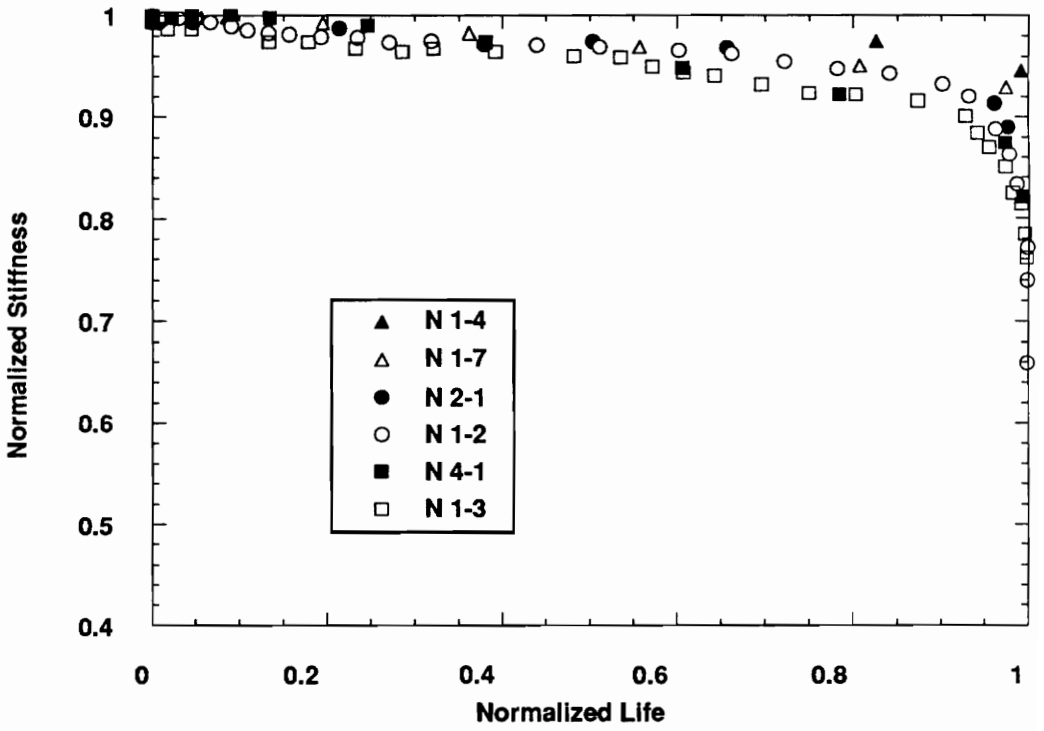

Figure 26. Stiffness Loss Curves / Two stage

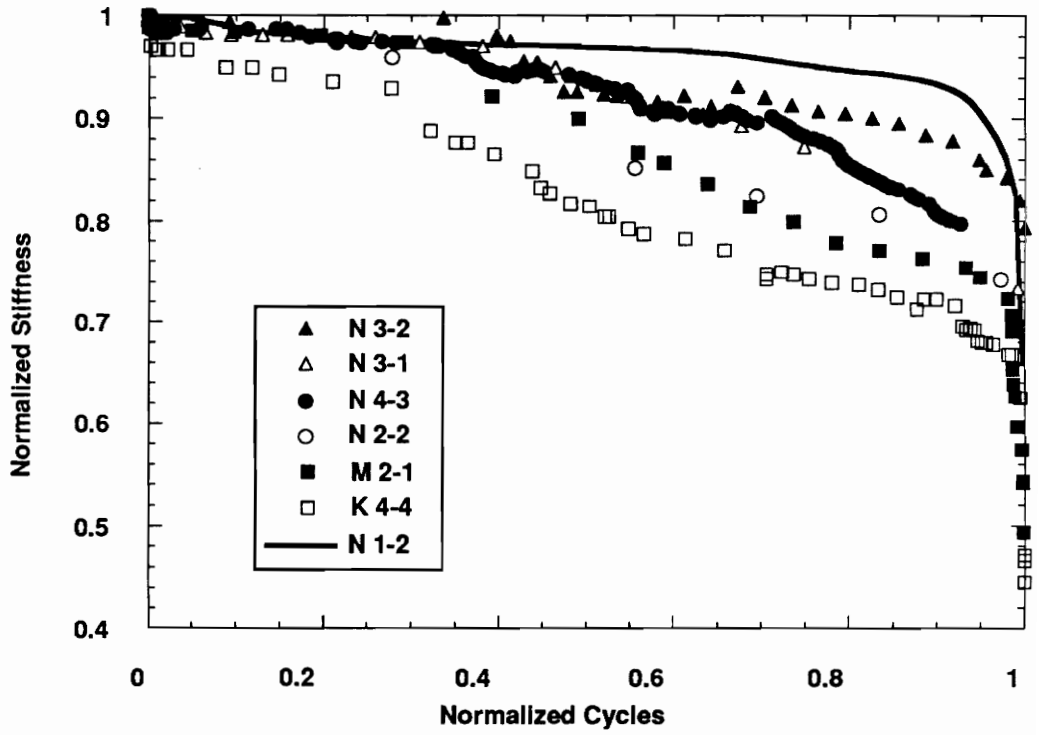

Figure 27. Stiffness Loss Curves / Nonlinear

can be postulated from these results. For simplicity, the curve of N 1-2 will be assumed to be the master curve.

However, there were six other specimens whose curves did not follow this master curve. One of these was K 4-4, the specimen which had the extensometer mounted on the front face. This specimen also had the extensometer removed and replaced during testing, which caused jumps in the strain readings. The other specimens did not have the extensometer, which was mounted on the back face, removed during testing. A normalized stiffness loss curve for these six specimens is presented in figure 27. All of these were 0° specimens, one from plate K, one from plate M, and four from plate N. Cyclic stress levels ranged from 45.2 to 61.7 ksi, with life ranges of 720 to 476,000 cycles. All of these stiffness loss curves fall below the master curve (solid line). The lowest curve is that of K 4-4. The other five lie in between this curve and the master curve. These six specimens exhibit a more nonlinear mid-life stiffness loss and a less steep final drop, except for M 2-1 which did have a steep drop at the end. However, this specimen exhibited visible back-face damage which would explain why its curve was the closest one to that of K 4-4, which had visible front face damage. The other four specimens in figure 27 may also have been experiencing back-face damage, although the face damage was not closely monitored. Face damage may explain why these curves differ from the master curve. Note that all of these specimens are 0°; all 90° specimens approximately followed the master curve.

Hysteresis

For one 0° specimen (M 2-1), secant stiffness readings were recorded on an X-Y plotter. Shown in figure 28 are the complete output curves for this specimen, including both the loading and unloading portions of each cycle. The number of fatigue cycles at which a reading was taken is

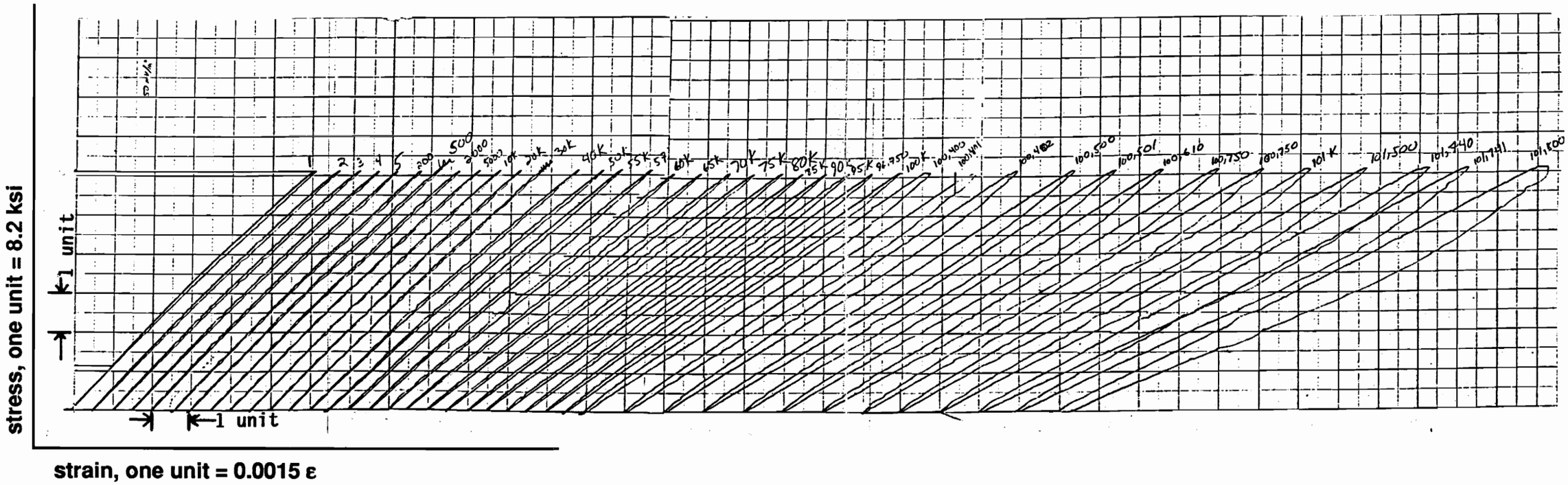

Figure 28. Hysteresis during Fatigue Loading of Specimen M 2-1

shown above each curve; this specimen failed after 101,910 cycles. The axes are scaled to show stress vs. strain, as calculated from the load transducer and extensometer outputs. The nonlinearity of the curve was observed to begin at approximately 1.1 volt (9.0 ksi) on the first cycle and at increasingly lower stress levels on subsequent readings. Also observed was increasing hysteresis with increasing fatigue cycles. Hysteresis is anelastic behavior of a material where the strain is out of phase with respect to the stress [38]. As shown in figure 28, the hysteresis loop between the loading and unloading portions of each cycle becomes increasingly larger with increasing number of fatigue cycles. The area within the hysteresis loop represents energy lost during that cycle. In the last reading, taken just 110 cycles before specimen failure, the loading and unloading curves do not meet at the zero load level, indicating inelastic hysteresis and permanent deformation in the material. It should be noted that this specimen was experiencing surface damage under the extensometer, as discussed in relation to figure 27, which may account for some of the hysteresis behavior.

Residual Strength

Six 0° and six 90° specimens were chosen for residual strength testing. Each was cy[illegible] at the same maximum stress level (50 ksi for 0° specimens, and 49 ksi for 90° specimens). Stiffness loss was monitored for all specimens, and cycling was stopped when a certain amount of stiffness loss was recorded. These specimens were then X-rayed and tested in static compression in a hydraulic grip machine. The X-rays confirmed the degree of damage (stage of life) indicated by the stiffness loss. The data for these specimens is summarized in table 12. The last 90° specimen broke while cycling; a replacement specimen also broke in fatigue. To be statistically significant, at least two (and preferably three) specimens of each stitch configuration should have been run to each stiffness loss level; however, this was not possible due to the limited number of

Table 12. Residual strength data

Specimen	Fatigue cycles	Stiffness loss, %	Residual strength, ksi	Strength loss, %
0° Specimens - cycled at 50 ksi, average regular strength 68.7 ksi				
L 4-1	10	0.34	66.6	3.06
L 4-4	18,000	1.89	65.6	4.52
L 3-1	46,360	4.68	58.8	14.4
L 3-2	60,000	7.21	59.6	13.2
L 4-3[1]	53,000	10 +	59.3	13.7
L 4-5	63,000	22.3	57.9	15.7
90° Specimens - cycled at 49 ksi, average regular strength 67.9 ksi				
L 1-1	10	0.53	64.5	5.01
L 1-2	20,000	1.47	60.2	11.4
L 1-3	60,000	4.48	59.9	11.7
L 1-4	150,660	6.68	58.7	13.5
L 1-5	186,000	11.6	57.3	15.6
L 1-6[2]	255,250	20 +		
L 1-7[3]	75,000			

[1] stiffness reading at 52,000 cycles indicated a 10% drop in stiffness. Rubber band holding extensometer broke at 52,600 cycles and was not replaced

[2] fatigue failure at 255,250 cycle -20% stiffness loss at 255,000 cycles: not included in figure 29

[3] unexpected early fatigue failure at 75,000 cycles: not included in figure 29

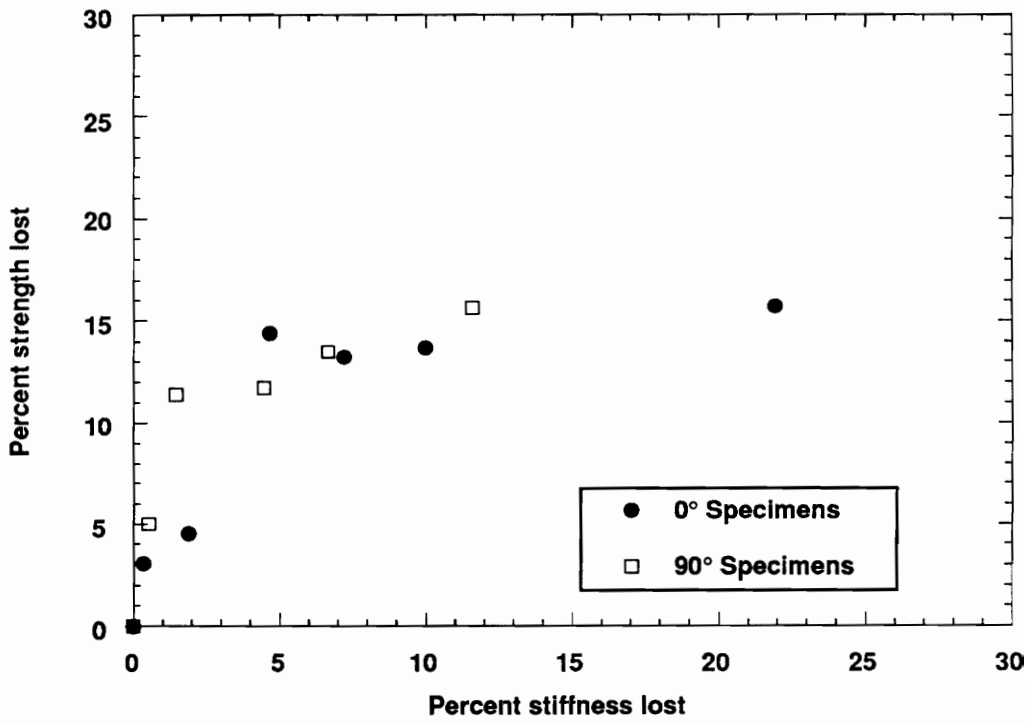

Figure 29. Residual Strength Curves

specimens available.

All residual strengths were below average regular static compressive strength. Plotted in figure 29 is percent of stiffness lost vs. percent of strength lost. At 0% stiffness lost there is 0% strength lost. If strength loss was linearly related to stiffness loss, figure 29 would be a straight line at a 45° angle. Instead, residual compressive strength seemed to follow a two stage pattern of sharp decline followed by a long levelling off period of no change in residual compressive strength. This two-stage pattern is similar to the pattern seen for woven composites [35], which because of the shape of the curve showed a superior performance to similar tape laminates in residual compression strength under low stress, long life fatigue loading. The shape of figure 29 indicates good compression damage tolerance for this material, one of the reasons it is being developed. However, many more data points are needed to finalize the shape of this curve, especially at the higher stiffness loss levels.

Edge History

The progress of damage along the edge of specimens was monitored using edge replications for 19 fatigue specimens, twelve 0° and seven 90°. These specimens and their loading histories are presented in table 13. There was at least one specimen from each plate in this testing group. Fatigue lives ranged from 1,690 cycles to 2,970,000 cycles, while cyclic stress levels ranged from 63 to 44.5 ksi. These edge damage histories were used to try to identify characteristic damage states - that is, did all specimens show similar degrees and patterns of damage at the same stage of life, regardless of applied cyclic stress level. The edge replicas themselves are not presented here - instead, schematic representations are presented to better illustrate the damage discussed below. The replicas are drawn in 1.67:1 scale, representing a specimen gage length of 1.5

Table 13. Edge replication specimen history

Specimen	Cyclic Stress Level, ksi	Cycles to Failure	Number of Replications Made
K 1-1	55.0	5,300	7
K 1-3	51.5	46,810	10
K 1-4	48.1	246,960	13
K 3-1	52.1	73,840	19
K 3-2	44.5	2,970,000	25
K 4-1	56.0	1,900	2
K 4-3	46.3	388,100	23
K 4-4	45.2	228,264	24
K 4-6	48.0	77,280	16
L 2-1	55.4	3,310	5
M 1-5	49.0	176,530	10
M 2-2	55.0	11,460	4
M 3-1	50.0	55,480	4
N 1-1	63.0	1,690	7
N 1-5	55.0	12,010	6
N 1-6	54.3	21,590	10
N 4-2	59.0	5,800	12
N 4-5	53.4	28,860	15
N 4-6	60.0	1,730	8

inches and a thickness of 0.30 inches. All are oriented so that the dome areas are up.

Represented in figure 30 are a series of edge replicas from a 0° specimen, N 4-5, which failed after 28,860 cycles at 53.4 ksi. This was a "good" specimen; that is, fairly straight stitches and no extensive manufacturing-induced microcracks or voids. Represented are six of the 15 sets of replicas of the right and left edges of the gage length portion of the specimen taken at different numbers of fatigue cycles. All replicas were taken while the specimen was experiencing mean load (slightly under half of the maximum compressive stress) in order to keep open any compression-induced damage while not causing any additional damage. Replicas **A** were initial replications taken before cycling began. These show the patterns of stitches, layers, and other features visible on the undamaged edges of the specimen. The left edge had a row of stitches buried less than 1 mm below the surface, which were faintly visible on the surface (represented by dashed lines), while the right edge coincided with a row of stitches. On the right edge there are 11 stitches visible; stitch #7 is slightly out of plane, causing some microcracks and voids near the back face edge. Replicas **B** were taken after 10 cycles, or 0.03% of the fatigue life. No damage is visible on the left edge. On the right edge, a few cracks and delaminations are visible near the front edge in the dome area, mostly between stitches 3 through 7. Replicas **C** were taken after 1,000 cycles, or 3.5% of life. Damage is now visible on the left edge in several places. There is an interstitial crack leading to a delamination on the front edge over the buried domes at stitch 7, and individual cracked plies occurring over buried stitch fibers 5 and 6. On the right side the dome cracks extend farther, and there is a large delamination between stitches 2 and 3. Replicas **D** were taken after 7,000 cycles, or 24.3% of life. Damage on the left edge has progressed much farther, both between and around buried stitches 3 and 4 and 7 through 9. Damage on the right side has not changed much. Replicas **E** were taken after 19,000 cycles, or 65.8% of life. The worst site of damage is on the left edge between buried stitches 7 and 8;

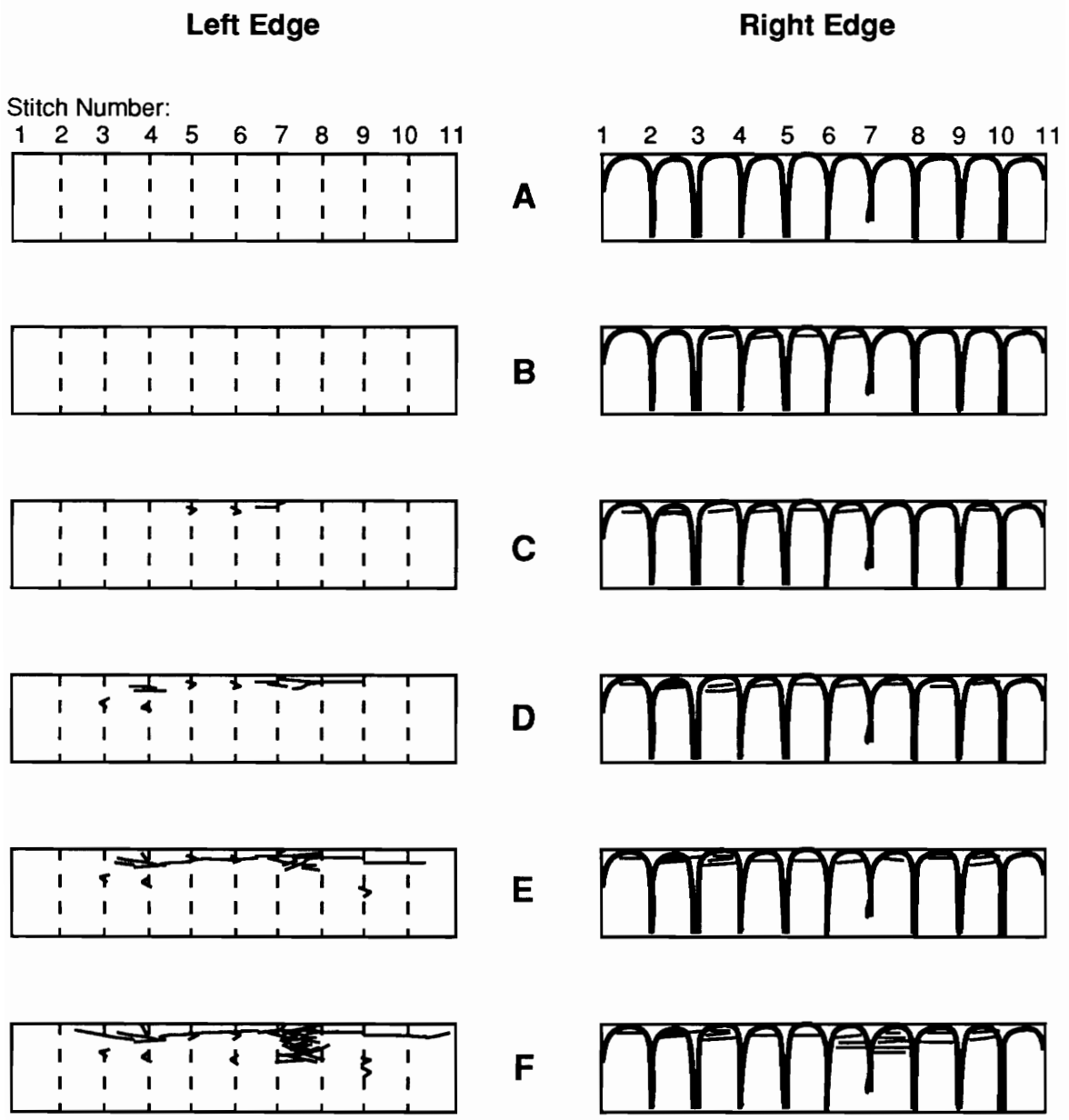

Figure 30. Edge Replicas of 0° Specimen N 4-5

damage extends along most of the length in the form of a long delamination between a 45° and a 90° layer. The through-the-thickness damage is up to 25% of the thickness at the worst site of damage. At this site, damage on the face of the specimen was visible. On the right side, damage did not progress much; there are a few more cracks through the thickness in some of the dome areas, but no face damage was visible growing from the right edge. Replicas **F** were taken after 28,000 cycles, or 97.0% of life. On the left edge, the delamination has spread even farther along the length, and the worst site (stitches 7-8) has even more extensive cracks and delaminations extending up to 50% of the thickness. Face damage extending from this site had now spread all the way across the width. This is visible in the right edge replica; suddenly, damage has concentrated at one site around and between stitches 7 and 8, and is already 25% through the thickness. Failure followed only 860 cycles after these replicas were taken. The failure pattern followed the visible front face damage and cut a 45° failure plane downward to the back face.

Shown in figure 31 are a series of edge replicas from another 0° specimen, K 4-3, which failed after 398,010 cycles at 46.3 ksi. This was a "bad" specimen, with inclined stitches and initial microcracks. From K 4-3 six of 25 sets of replicas were chosen to characterize the damage growth. Replicas **A** show the initial undamaged edge patterns of this specimen. The left edge was polished until the last trace of a cut-off row of stitches was removed; the next stitch row was buried approximately 0.1 inches below the surface. The right edge was polished to just above a stitch row; most of the stitches are still partially buried, but visible is the ≅11° inclination of the stitches. Microcracks were also visible around the buried stitches. Replicas **B** were taken after 41,000 cycles, or 10.3% of this specimen's fatigue life. No damage is visible on the left edge. On the right edge, all 10 stitches have cracks above the buried portions of the stitches. In addition, there are dome cracks between all stitches except stitches 8 through 10; the worst damage is between stitches 7 and 8. Replicas **C** were taken after 117,000 cycles, or 29.4% of life. The left

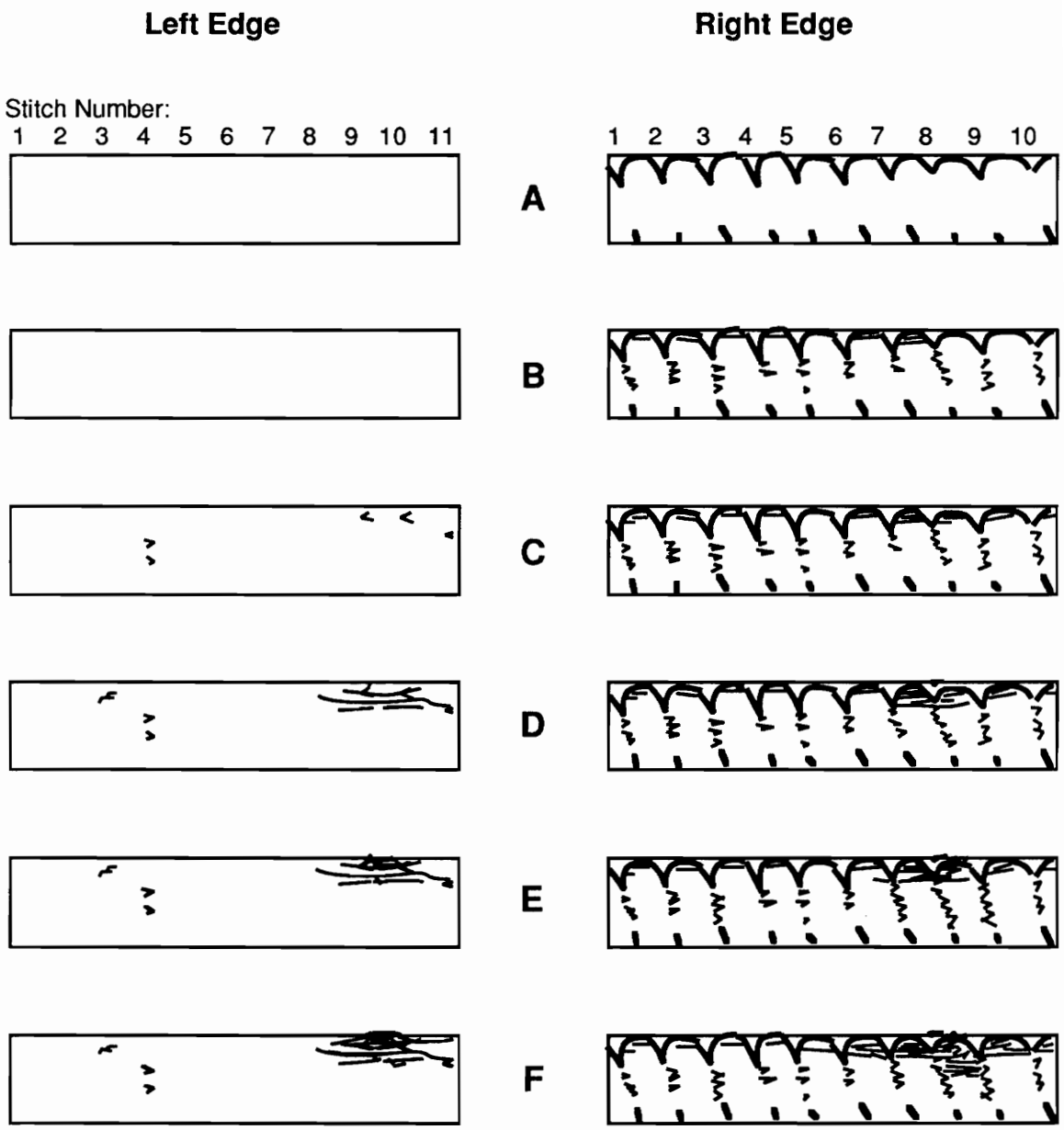

Figure 31. Edge Replicas of 0° Specimen K 4-3

edge now has damage consistent with damage observed on other specimens occurring above buried stitches; apparently, the depth a stitch is buried does not affect its ability to initiate damage. On the right side, the dome area damage has grown; the worst site seems to be between stitches 7 and 8, where delaminations extend to 25% of the thickness. Replicas **D** were taken after 240,000 cycles, or 60.3% of life. Damage on the left edge has spread along the length from the initial site and 25% of the thickness, and has also begun in another site. The worst damage on the right side has spread to include stitches 8-9 as well as stitches 7-8. Face damage was now observed to be growing from this site (stitch 8). Replicas **E** were taken after 326,000 cycles, or 81.9% of life. The worst site on the left side has spread a little along the length. Face damage was now visible growing from this site. The worst site on the right side was now 30% through the thickness of the specimen; the face damage growing from this site was half way across the width. Replicas **F** were taken after 380,000 cycles, or 98.0% of life. The damage on the left edge was causing that section of the face to bulge outward. The damage on the right edge had spread to 51% of the thickness at the worst site, stitches 8-9. Specimen failure followed 8,010 cycles later. The specimen experienced post-failure crushing which made it impossible to determine the fatigue failure pattern.

Shown in figure 32 are a series of edge replicas from a 90° specimen, N 1-6, which failed after 21,590 cycles at 54.3 ksi. All 90° specimens had similar edge damage histories, regardless of which plate they came from. From specimen N 1-6 six of 10 sets of replicas were chosen to characterize fatigue damage growth. Replicas **A** were the initial 0 cycle replicas showing the edge patterns. Twelve stitch rows are visible or buried under the surface. The loops visible are from the bottom needle thread looping with the upper bobbin thread; this occurs on the back surface opposite from the pinched layer zone due to the domes. A few microcracks are visible on both edges, mostly near the loops. Replicas **B** were taken after 650 cycles, or 3.0% of life.

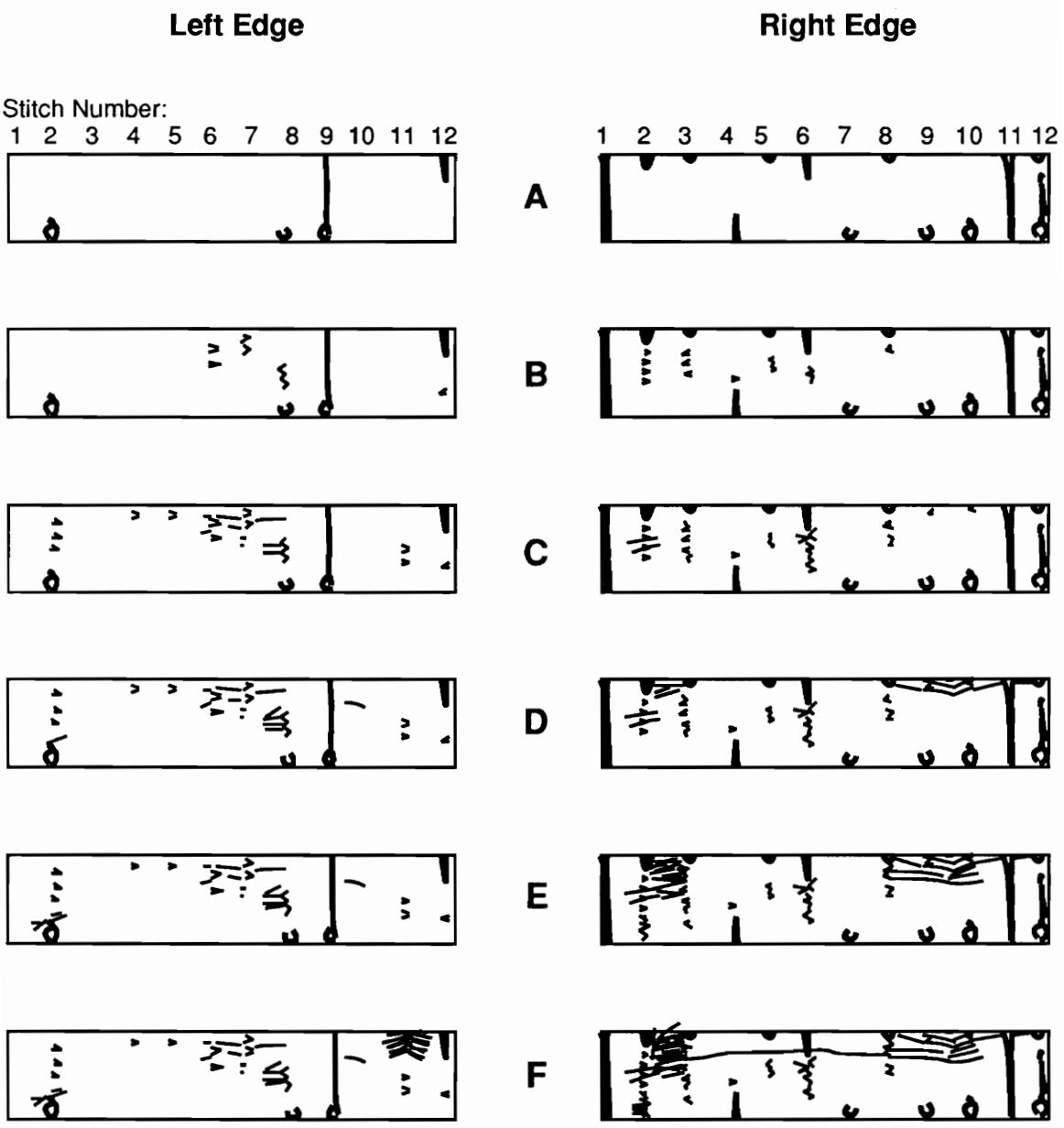

Figure 32. Edge Replicas of 90° Specimen N 1-6

Damage is visible on both edges in the form of cracked plies directly above a buried stitch fiber. This damage is visible over 4 stitches on the left side and over 6 stitches on the right side, with the worst-looking damage occurring on the right side over stitch #2. Replicas **C** were taken after 7,000 cycles, or 32.4% of life. There is more damage visible over stitches, and some of these cracks have extended lengthwise. The worst sites of damage appear to be between and around stitches 6 through 8 on the left side, and stitches 2 and 6 on the right side. Replicas **D** were taken after 17,000 cycles, or 78.7% of life. The left edge replica shows that the worst damage was still around stitches 6 through 8. The worst damage on the right edge was between stitches 2 and 3, with some between stitches 8 through 12. Replicas **E** were taken after 20,500 cycles, or 95.0% of life. The left edge had its worst damage centered over stitch 7, while the right edge was worst between stitches 2 and 3 and between stitches 9 and 10. Replicas **F** were taken after 21,000 cycles, or 97.3% of life. The left edge suddenly had the worst damage occurring near the grip around stitch 11. The right edge showed extensive damage along most of the length; a delamination 6 layers from the front face between 45° and 90° plies extended from stitch 2 to stitch 10. However, the worst site of damage was between stitches 2 and 3; this damage extended over 50% through the thickness, and was visible on the front face extending over 75% of the width. Impending failure was obvious, and occurred after only 590 more cycles. The failure pattern ran between stitches 2 and 3 on the front face, and cut a 45° failure plane through the thickness to a back face failure line which coincided with the lower grip.

Figures 30-32 are fairly typical examples of edge damage development. For 0° specimens, the first appearance of damage was always in the form of a delamination in the top layers pinched by the dome (for edges which had a stitch line visible on or near the surface). These dome cracks spread independently along the entire length of the specimen. Microcracks and voids did not generally initiate damage or propagate during cycling. However, if a stitch was buried below the

surface of the edge of a specimen, cracked plies appeared above this buried stitch and occasionally propagated, indicating that damage initiation is more due to the stitches than to edge effects. The specimens with inclined stitches (larger pinched layer zone due to domes) experienced earlier damage initiation and propagation than the specimens with straight stitches. Damage grew through the thickness to the end of the pinched layer zone in several places, but generally only continued past the zone in one place. Damage on the side of the edge opposite the domes occurred in some specimens, but was limited to the worst site of damage seen on the edge near the domes. This worst site of damage propagated both along the edge and through the thickness, and eventually became visible on the face as damage growing from the edge towards the center. This face damage site could occur either on one edge only and spread all the way across, or each edge could have its own independent worst damage site with accompanying face damage spreading inward from both edges. This generally only occurred in low-stress, long-life specimens, which had more time for damage to spread from both edges. Final failure was controlled by the observed face damage; either it spread all the way across from one edge, or it met somewhere in the middle if it spread from both edges.

The progression of damage in 90° specimens was slightly different because the pinched layer zones ran perpendicular to the edge, not parallel to it as in the 0° specimens. Again, manufacturing-induced voids and microcracks did not propagate. Initial damage in 90° specimens was observed to be in the form of cracked plies directly above a stitch fiber buried below the surface. Damage propagating from these cracks seemed to be superficial surface damage; the serious damage began in the form of delaminations on the edge nearest the front face of the specimen. These delaminations would then extend along most of the length of the specimen and also propagate inward through the thickness from the initial site accompanied by interstitial cracks right at or near the damage site. This damage site then became visible on the

face of the specimen and propagated across the face in between two rows of stitches. Damage on the edge away from the face damage site was limited or nonexistent once face damage began; just the main damage site continued to grow, both through the thickness and along the edge. Final failure occurred soon after face damage was observed to spread all the way across the face of the specimen, although how soon depended on the loading conditions (high stress-short life specimens failed fairly catastrophically after rapid damage propagation, while low stress-long life specimens continued to cycle for a little while after damage was observed to spread all the way across the face).

Since all of the specimens in table 13 were cycled to failure, the edge replications for different specimens could be compared on a percent of life basis. A schematic representation of edge damage history comparing these specimens is shown in figure 33. Listed vertically are different damage events. The horizontal axis is percent of life. Individual specimens are represented by a letter standing for which plate they came from (K, L, M, or N). Solid letters represent 0° specimens, and open letters represent 90° specimens. A line was drawn connecting the earliest observed occurrence of a damage event and the latest observed occurrence of that damage event. A specimen was only included on a line if that damage event occurred on at least one edge of that specimen, and if the replicas were taken close enough together to catch the event soon after it happened. If a particular damage event occurred on both edges of a specimen, only the earliest occurring one is recorded (no specimen is represented on one line more than once). Since damage was always concentrated in one area, the occurrence of events at this site was tracked. Specifically, the damage events tracked were when the through-the-thickness damage reached 1/8, 1/4, 1/2, and 3/4+ of the thickness of the specimen (which corresponds to six, twelve, 24, and 36+ layers of damage).

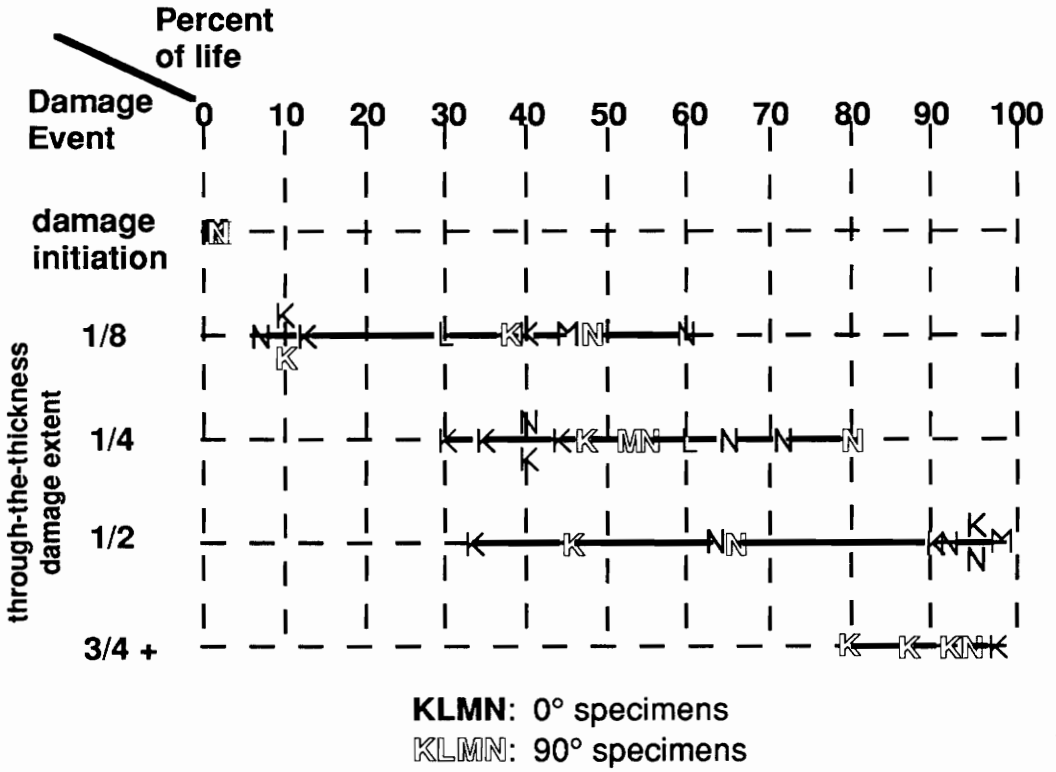

Figure 33. Edge Damage History Chart

Several things are indicated in figure 33. First, initial loading-induced damage (dome cracks or cracked plies above buried stitches) occurred very early, often in the first ten fatigue cycles or at latest before 2% of fatigue life had passed. However, other damage events occurred over a very large range of life fractions. Damage spreading one-eighth of the way through the thickness of a specimen at one site took anywhere from 5 to 60 percent of life. It took from 30 to 80 percent of life for damage to spread one-fourth through the thickness, 33-98 percent of life to spread one-half through the thickness, and 80-99.9 percent of life to spread three-fourths or more through the thickness. One difference was noted between 0° and 90° specimen performance; just before failure, 90° specimens tended to have damage that extended between 75 and 100 percent through the thickness, while 0° specimens were more likely to have only 50% through the thickness damage. This is probably due to the relation between stitch pattern and failure pattern discussed earlier. In addition, indicated in figure 33 is a dependence on stitch inclination; on all lines, specimens from plates K and L (inclined stitches) are generally concentrated toward the beginning of the line (earlier occurrence of that damage event), while specimens from plates M and N (straight stitches) are generally concentrated toward the ends of the lines. This indicates that stitch inclination caused damage to initiate earlier, and explains why under high stress-short life fatigue conditions specimens with inclined stitches performed worse than specimens with straight stitches (p. 60). This occurred because the inclined stitch specimens had damage initiating earlier and propagating faster. This effect was less noticeable under low stress-long life loading conditions because the propagation of damage was slower (failure was less catastrophic), making earlier damage initiation less of a factor.

Internal Damage

This section deals with the damage history of six specimens grouped into three pairs. These specimens are listed in table 14. During cyclic loading, the edge damage of these specimens was monitored using edge replicas. X-rays were taken while the specimen was under mean load in the grips, but these did not turn out well, due to the short penetrant soak time and the necessary folding of the photographic film (both discussed earlier). Therefore, the edge replicas were used to determine when to stop cycling the specimens. It was desired to compare 0° to 90° damage progression; therefore, the three pairs of 0° and 90° specimens were cycled at the same stress level to approximately the same number of cycles. Pair 1 was cycled at 54 ksi. The 90° specimen was cycled to 12,500 cycles, but the 0° specimen was stopped after 8,690 cycles due to catastrophic damage propagation and perceived impending failure. Pair 2 was cycled at 49 ksi. Both were cycled for 73,000 cycles. The 0° specimen was stopped at this point because it was determined to be near failure, and then the 90° specimen was stopped at this number of cycles regardless of its damage state for comparison purposes. Pair 3 was cycled at 45 ksi. The 90° specimen was run out to 2 million cycles, although damage did not seem to progress much in the last million cycles. The 0° specimen was stopped at 400,000 cycles because damage was progressing very slowly and had not yet concentrated in any one site. A final edge replication was made of each specimen before it was removed from the machine; these were used to compare with X-rays taken of the edge. Once removed from the machine, the specimens were soaked in penetrant overnight and both face and edge X-rays were taken. Compared in table 15 is the extent of damage observed: for face damage, visual observations are compared to X-ray results; for edge damage, edge replications are compared to X-ray results. After X-raying, the specimens were sectioned to examine internal damage. The results of these tests are summarized below.

Table 14. Internal damage specimen history

Pair	Specimen	Cyclic Stress Level, ksi	Cycles
1	M 1-6	54.0	12,500
	M 4-4	54.0	8,690
2	M 1-4	49.0	73,000
	M 4-2	49.0	73,000
3	M 1-2	45.0	2,000,000
	M 4-5	45.0	400,0[illegible]

Table 15. Damage extent observations

Pair	Specimen	Face Damage Extent: [1] Visual	X-Ray	Edge Damage Extent: [2] Replica	X-ray
1	M 1-6	1.0	.78	.30	.25
	M 4-4	.50	.60	.58	.50
2	M 1-4	.375	.35	.26	.18
	M 4-2	1.0	1.0	.51	.55
3	M 1-2	.25	.33	.18	.18
	M 4-5	-	-	.09	-

[1] Percent of width
[2] Percent of thickness

X-Rays

Shown in figure 34 are the magnified face X-rays of pair 1. The gage length is marked. M 4-4, the 0° specimen, is on the left, while M 1-6, the 90° specimen, is on the right. The dark circles are the stitch fibers: they are not in focus toward the ends of the specimens due to the X-ray head being centered over the gage length of the specimen. Also visible are some of the weave fibers, which appear as faint lines, and can be at either a 0°, 45°, -45°, or 90° angle. The damage in the two specimens is clearly visible, and, as noted in a previous section, concentrated at one site. Damage extends across 60% of the 0° specimen and 78% of the 90° specimen. These values are fairly close to visual observations made of the front face during the cyclic tests, as noted in table 15. This indicates that face damage begins on the surface at the front face and propagates towards the back face through the thickness. The darker damage areas on the X-rays indicate heavier damage (more extensive through the thickness damage). The X-ray of the 0° specimen shows heavier damage in the first 30% in from the edge. The third stitch row seems to have slowed the progression of the damage across the face; this was also visually observed in this and other specimens. In the 90° specimen, the damage seems fairly heavy for most of its length, and there is no obvious cut-off line between heavier and lighter damage, as the damage progresses in between two rows of stitches and does not encounter any stitch rows perpendicular to its path.

Figure 35 shows edge X-rays of the pair 1 specimens. Again, the 0° specimen is on the left, and the 90° specimen is on the right. This accounts for the different appearances of the X-rays; the 90° specimen has its stitch rows in line with the X-ray head, giving a crisp appearance of the rows directly underneath the X-ray head and a fuzzier image towards the edges; the 0° specimen has fuzzy stitches along the entire length because the stitches are not lined up in this direction. The small dark spots that are visible are the ends of weave fibers. In pair 1, the damage in the 0°

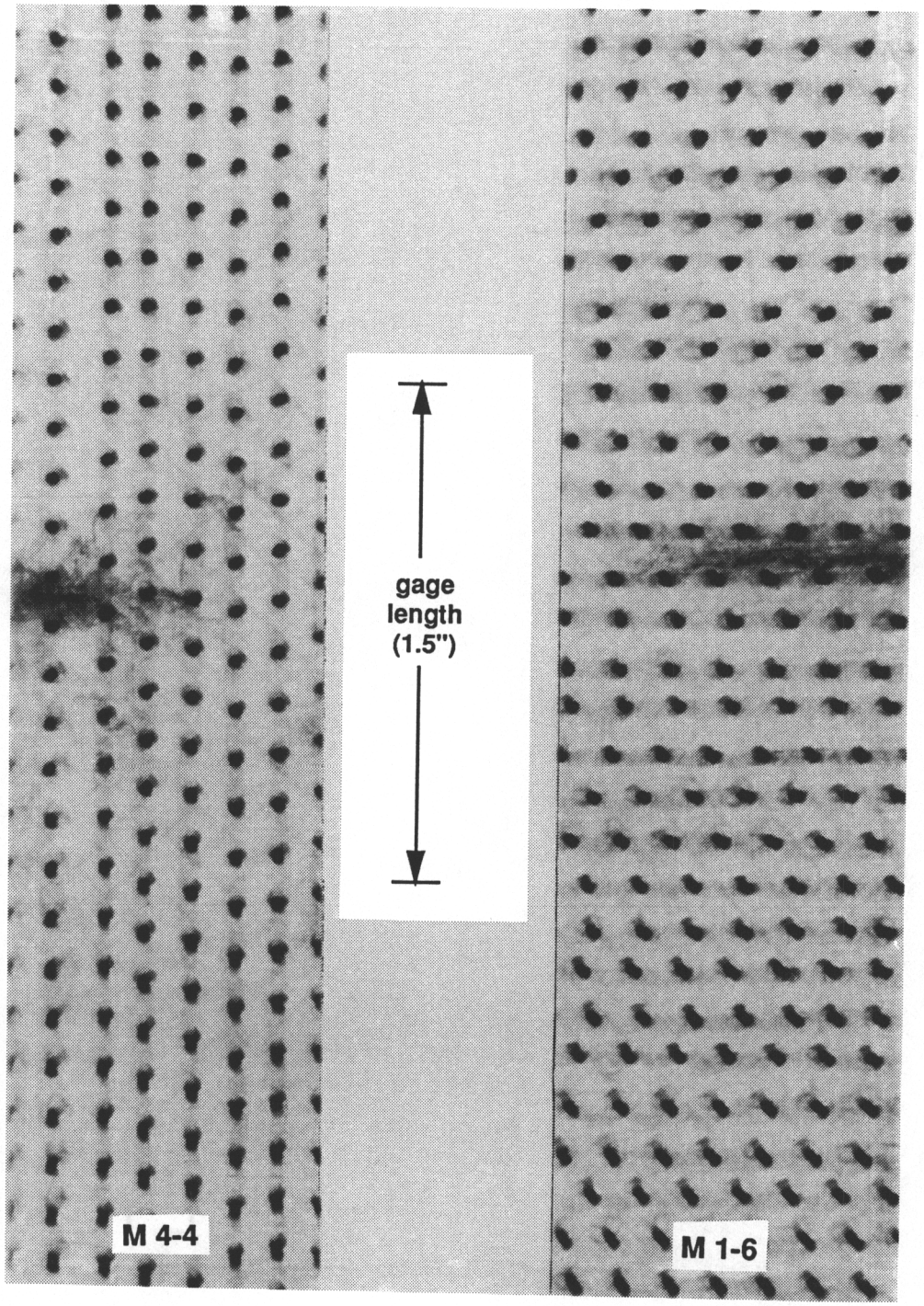

Figure 34. X-rays of Pair 1 Specimens: Face

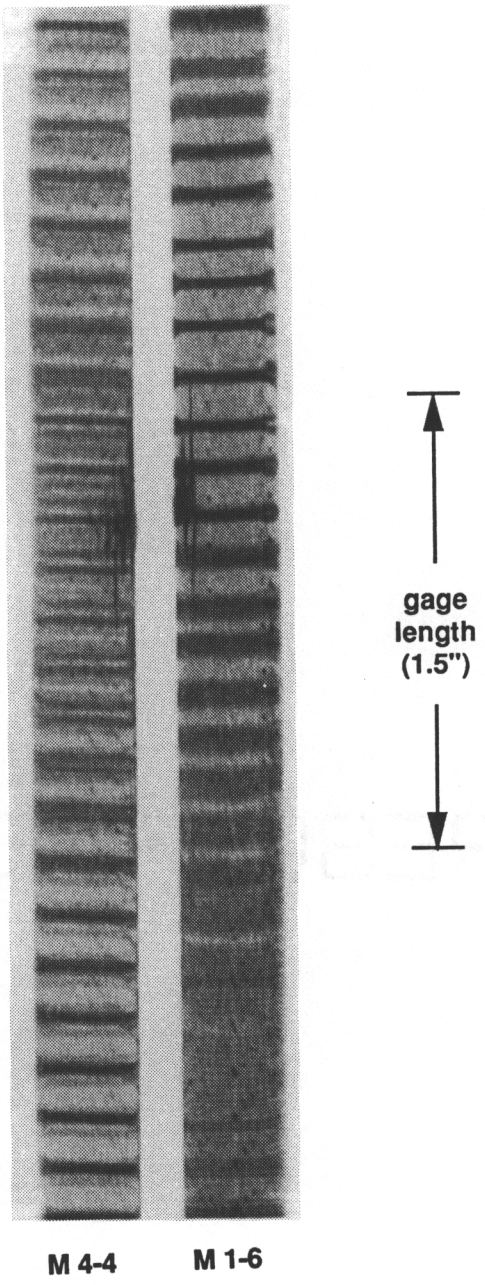

Figure 35. X-rays of Pair 1 Specimens: Edge

specimen is further advanced through the thickness than the damage in the 90° specimen; however, the 90° specimen has more extensive damage lengthwise. Since specimens always failed at one location, through-the-thickness damage is more serious than lengthwise damage; therefore, based on edge damage, in pair 1 the 0° specimen seems closer to failure than the 90° specimen, while based on face damage the 90° specimen seems closer to failure. While the 90° specimen had slightly more cycles on it than the 0° specimen did, the scatter in fatigue data (table 9) can account for a specimen with less cycles seeming to be nearer failure. The damage extent visible in the X-rays was similar to the extent of damage visible in the edge replicas, indicating that the worst damage occurred on the surface of the edge. In some cases the edge replicas showed more damage than the X-rays, probably indicating superficial surface damage.

Similarly, in pair 2 the 0° is much closer to failure than the 90° specimen, although both experienced the same number of fatigue cycles at the same cyclic stress level. Shown in figure 36 are the face X-rays of these two specimens. The 0° specimen, M 4-2, was cycled first and stopped when deemed to be near failure; subsequently, the 90° specimen, M 1-4, was run and stopped at the same number of cycles. Damage to the 0° specimen goes all the way across the face, but again is heaviest up to the third stitch row, and is lighter across the rest of the face. The 90° specimen only has damage for 35% of the width and is not very heavy yet, except right at the edge. These values for extent of face damage are very close to visually observed values, again indicating surface damage. The edge views for these specimens, figure 37, also indicate that the 0° specimen has a much further advanced damage state than the 90° specimen. The 0° specimen has damage over the entire gage length on the edge and over 50% through the thickness at its worst point, while the 90° specimen only has damage extending 18% of the thickness. Edge replica comparisons again indicate that the worst damage is on the surface.

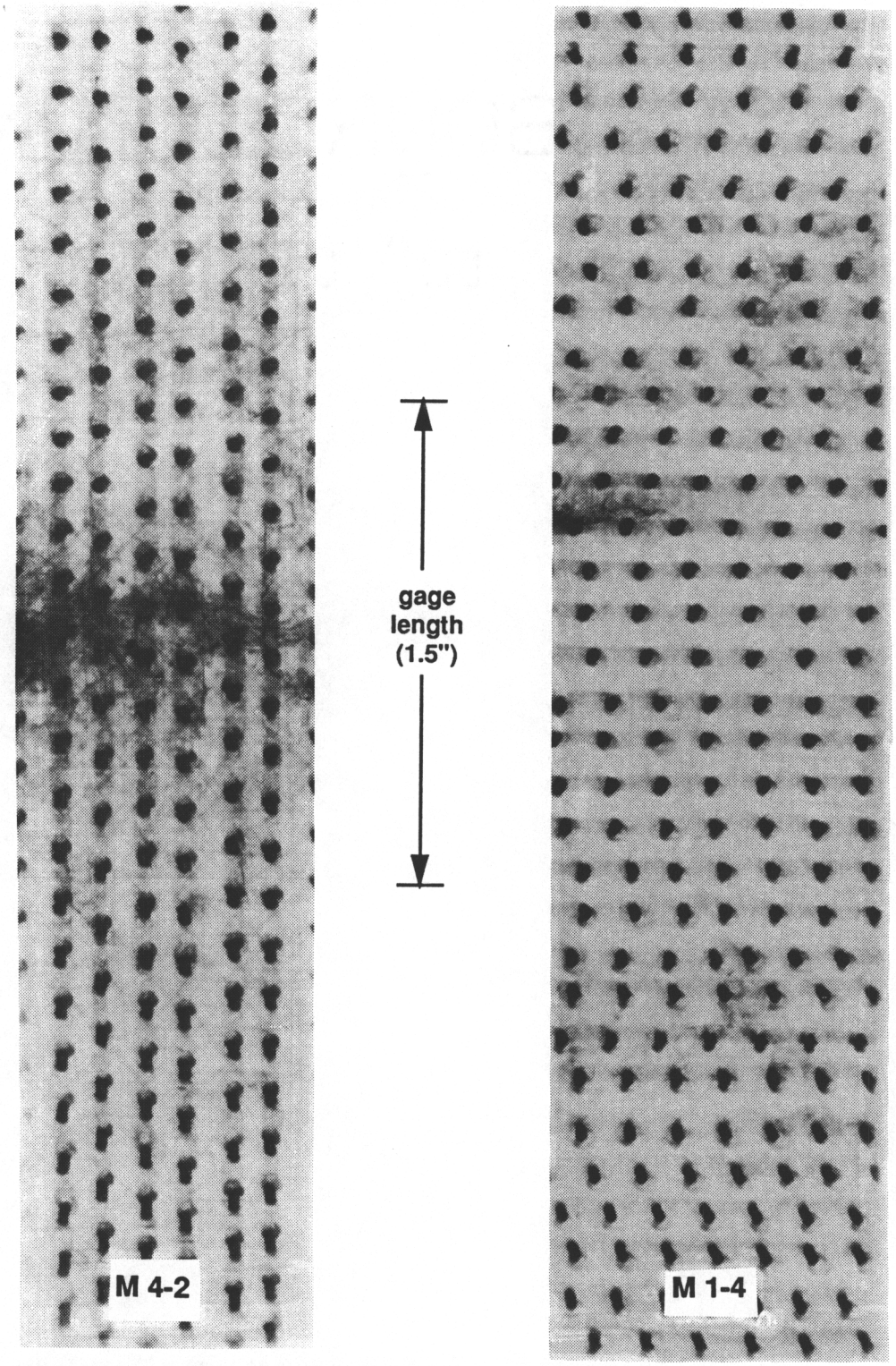

Figure 36. X-rays of Pair 2 Specimens: Face

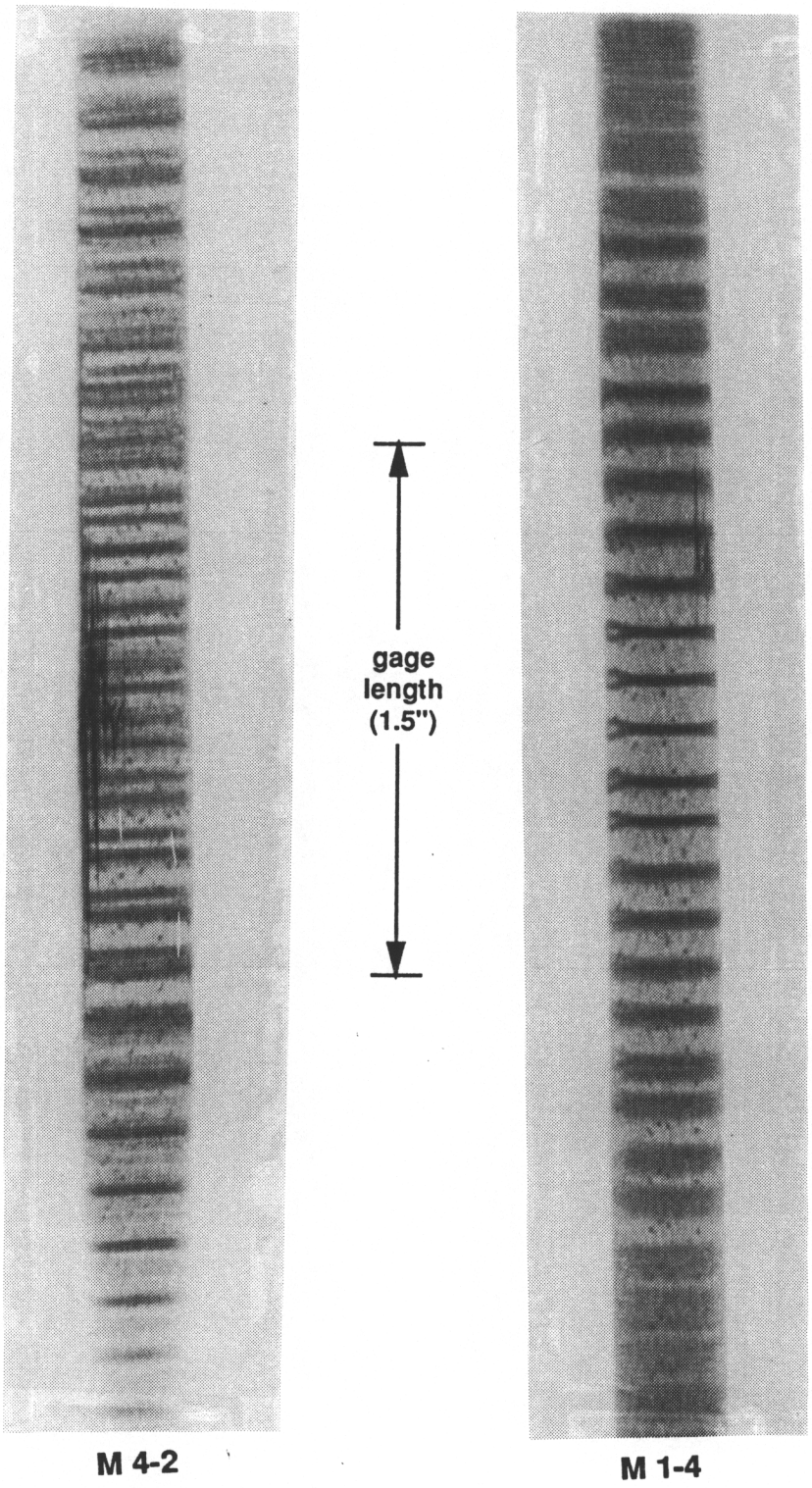

Figure 37. X-rays of Pair 2 Specimens: Edge

Shown in figure 38 are the X-rays of pair 3 specimens: the front X-ray of the 0° specimen, M 4-5, and the front and edge X-ray of the 90° specimen, M 1-2. The 90° specimen was run to 2 million cycles and then stopped, although its damage state did not change appreciably for the last 1 million cycles. This long-life specimen had time for damage to develop from more than one site, as visible in both the face and edge X-ray. Other areas were experiencing damage growth even after damage in the worst site had grown to 33% of the width and 18% of the thickness. The 0° specimen was stopped after 400,000 cycles, before damage had a chance to concentrate at any one site. Visible in the face X-ray is light (surface) damage in several areas; not much damage was visible in the edge X-ray, corresponding to the edge replica, in which only dome area damage was visible. This specimen was stopped at this point to examine the extent and depth of internal damage.

Laminate Sectioning

The three pairs of specimens were then sectioned down the middle, lengthwise. Each internal edge was then polished, examined in a light microscope, and replicated. Results correlated well with the X-ray results; if face damage on the X-ray did not pass through the middle of the specimen (M 1-4, M 1-2, M 4-5), no damage was visible on the internal edge; lighter face damage (M 4-2, M 4-4) corresponded to less through the thickness damage than heavier face damage (M 1-6). Observed through the thickness damage levels on the internal edge replicas were: M 1-4, M 1-2, and M 4-5, 0% ; M 4-2 and M 4-4, 15%; and M 1-6, 22%. These results indicate that surface observations (visual and edge replicas) are sufficient to assess the relative damage state of a specimen (how near it is to failing) without the necessity of using an internal damage evaluation technique.

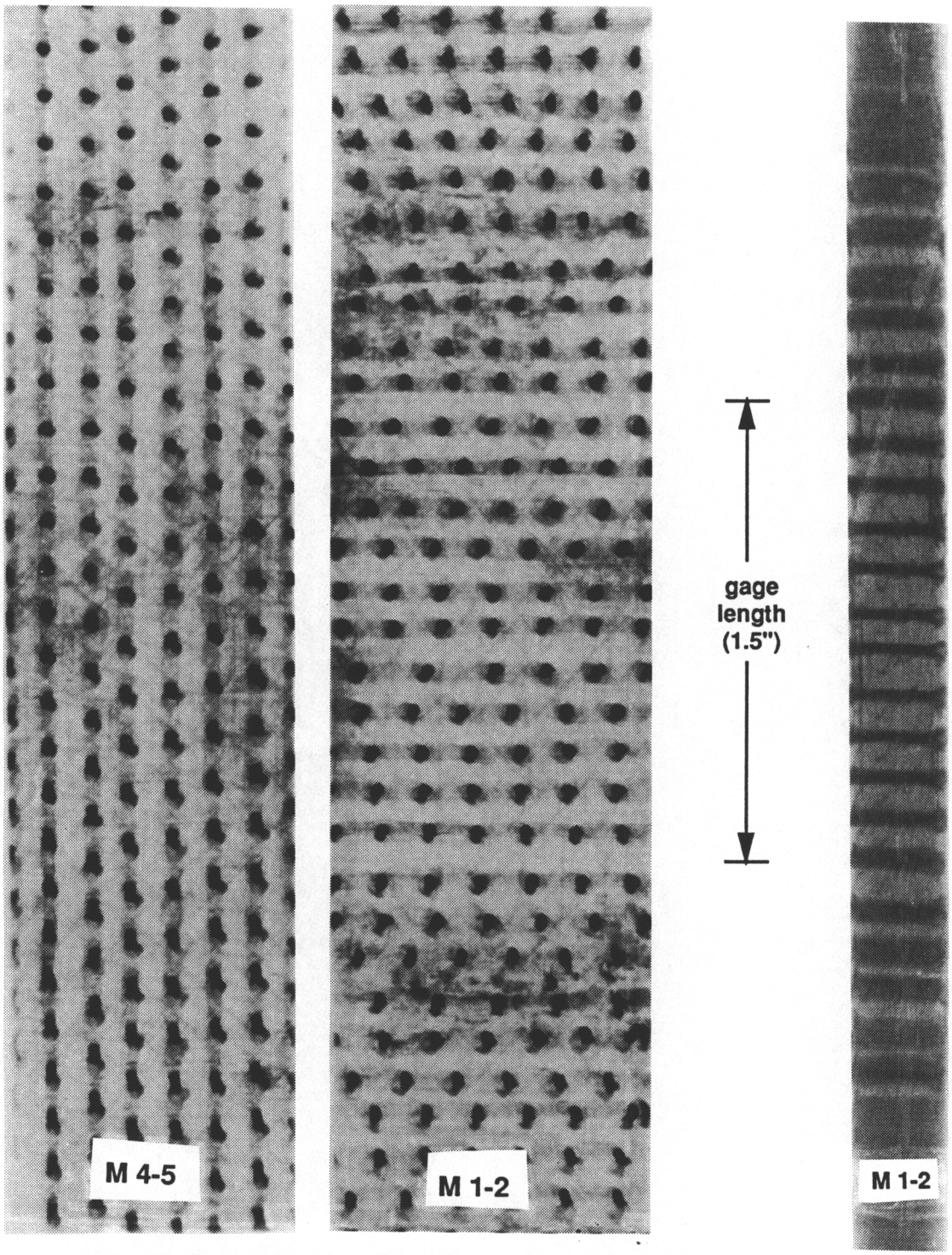

Figure 38. X-rays of Pair 3 Specimens: Front and edge

IV. OBSERVATIONS AND CONCLUSIONS

Experimental Procedures

Materials and Specimens

- This material is being examined for its delamination resistance, damage tolerance, and cost effectiveness; its proposed application suggests compression-compression fatigue cycling as the critical loading conditions.

- Of the four plates of material received, one had a lower fiber weight percentage, although ultrasonic C-scans indicated all four were of similar quality.

- Two of the four plates had inclined stitches, while two had straight stitches. This was attributed to transverse movement of the top and bottom surfaces during resin transfer molding.

- Other stitching-related manufacturing defects included uneven stitch and row spacing, microcracks and voids, a pinched layer zone at the top surface of each plate due to domes formed by the bobbin thread, and distortion of laminate plies in and out of plane in the vicinity of the stitch fibers.

Mechanical Tests

- All fatigue tests were run in the same mechanical fixure; this fixure was designed especially for compression-compression fatigue loading.

- The dimensions of full size specimens combined with the material's strength necessitated the use of a higher-capacity machine with a different type of grips (hydraulic) to run static compression tests on full size specimens.

- Short block compression tests were performed in order to compare the performance of this material to that of other materials tested at the NASA-Langley Research Center.

Damage Evaluation

- Ultrasonic C-scans were used to check the initial relative quality of the four plates; while these came out similar, acid digestion tests indicated one plate had a lower fiber weight percentage than the other plates..

- Edge replication was extensively employed to detect edge damage initiation and growth; it is a quick and easy method which gives a permanent record of a specimen's edge damage.

- X-rays were found to turn out best when the specimen was removed from the grips and left soaking in a zinc iodide penetrant for at least 12 hours. Settings for the X-ray machine were found by trial and error, and would be different for specimens of different thicknesses, widths, and materials.

Experimental Results

Static tests

- It was found that small width scraps left over from machining the plates could be statically compressed in the mechanical grips and give compression strengths similar to those obtained for tests done on full size specimens in the hydraulic grips. This result may not be valid for specimens of other widths and lengths.

- Compression strengths were similar for specimens with stitches in the 0° direction and specimens with stitches in the 90° direction relative to the axis of loading. This may not be true for non-quasi-isotropic layups, or for quasi-isotropic layups of different thicknesses.

- Compression strengths of specimens from the four different plates were similar, except for the plate with a lower fiber weight percentage; it had a correspondingly lower compressive strength. Stitch inclination did not affect static compressive strength.

- The short block compression tests performed on 1 3/4 inch tall specimens gave a 12.3% higher compression strength then the regular compression tests performed on 4 inch tall specimens.

- This material had a 10.9% higher compression strength than a similar stitched uniweave.

- The average elastic modulus of this material was 6.14 Msi. The elastic modulus of 90° specimens averaged 7.5% lower than that of 0° specimens.

- The experimental values for the compression strength and elastic modulus of this material were degraded 15.5% and 25.3%, respectively, from the theoretical values for an unstitched tape laminate of the same material, lay-up, and thickness.

- Failure patterns seen in full size static compression specimens were different for 0° and 90° specimens because of the orientation of the stitch rows. 90° specimens failed in between two rows of stitches, while 0° specimens failed in a zigzag fashion connecting stitch sites in adjacent rows. The failure mode for all specimens was transverse shear; the edge failure pattern was always a 45° failure plane through the thickness from the front surface to the back. Most specimens failed at the grips, probably because of the grip type (hydraulic).

Fatigue Tests

- As in static compression strength, 0° and 90° specimen performances were similar in fatigue (compression-compression loading).

- Using the short block compression strength, the fatigue data fit a logarithmic straight line curve with a correlation coefficient of 0.932; if the regular compression strength was used, the correlation coefficient was 0.969.

- Stitch inclination affected the fatigue performance of this material; under high stress-short life conditions, straight-stitch specimens performed superiorly to inclined-stitch specimens. This performance disparity ended at about 53 ksi, after which all specimens performed similarly.

- This material showed a much improved fatigue performance over a similar stitched uniweave, and it performed comparably to an unstitched version of that uniweave.

- Failure patterns for fatigue specimens were similar to those seen in static compression failures. However, there was a much lower percentage of grip failures, as these were all run in the specially-designed mechanical grips. Also, a lower percentage of 0° specimens failed at the grips than 90° specimens. This is presumably due to the relation between stitch patterns and failure patterns. While the failure mode was again transverse shear in all cases, some specimens (all with straight stitches, as opposed to inclined stitches) had a V-shaped edge failure pattern of two intersecting 45° failure planes.

Damage Development

- Stiffness loss under compression loading followed two different patterns. The first, seen in all 90° specimens and some 0° specimens, was a more or less two stage pattern of gradual linear decline followed by a sharp decline in the final 5-10% of life. The second pattern,

seen only in 0° specimens, showed nonlinear stiffness loss over the entire life of a specimen; this pattern appeared to correspond to surface damage occurring on the face of the specimen upon which the extensometer was mounted.

- Final stiffness loss just before failure averaged 26.1%, with a low of 5.4% and a high of 50.6%. No correspondence was seen between final stiffness loss and either applied maximum stress level or location of specimen failure (at grip vs. within gage length).

- Hysteresis was observed to increase during fatigue cycling; towards the end of life, permanent deformation occurred during a single loading cycle.

- Residual compressive strength did not decline linearly with stiffness loss; instead, it seemed to follow a two stage pattern of sharp decline followed by a levelling off. The long level period of no change in residual compressive strength (running from 5-20+% stiffness loss) indicates that this material has good compression damage tolerance.

- Damage initiated on or near the edge of a specimen at the stitch fibers, and occurred very early (in the first 2% of a specimen's fatigue life). Two forms of damage initiation were seen. For 0° specimens, delaminations appeared early in the pinched layer zone formed by the domes. For both 0° and 90° specimens, stitches which were buried below the surface of the edge caused cracked plies above the buried stitch, indicating that the stitches contributed more to damage initiation than edge effects did. Damage propagated from both types of initial damage sites for both 0° and 90° specimens.

- Damage continued to grow from the dome area damage sites both through the thickness and along the length of the edge. Eventually, it concentrated at one site, and damage became visible growing across the face of the specimen from this site.

- Because of the worst-site nature of the damage growth, the through the thickness damage was worse than the lengthwise damage. Face damage generally spread all the way across the face from the worst damage site before failure. Just before failure, 0° specimens tended to have 50% through the thickness damage, while 90° specimens had damage over 75% through the thickness at the worst site. The different extents of damage were again due to the orientation of the stitch rows.

- Specimens with inclined stitches experienced earlier damage initiation and faster damage growth than specimens with straight stitches; this explains why stitch inclination affected high stress-short life fatigue performance, because those types of specimens tended to fail more catastrophically than low stress-long life specimens, making earlier damage initiation contribute to earlier failure.

- The extent of face and edge damage estimated visually and with edge replicas correlated well with X-ray radiograph results, making the simpler techniques a reliable way to estimate the stage of life and closeness to failure of a specimen.

- X-rays also confirmed the visual observation that in 0° specimens, the stitch rows slowed damage propagation across the face of the specimen.

- While damage always initiated due to the stitch fibers (presumably earlier than it would have in an unstitched material), the stitches also helped to slow damage propagation.

- Sectioning specimens lengthwise down the middle and examining internal edge damage confirmed the visual and X-ray observations that damage is a surface phenomenon confined to a single site; once damage had concentrated in one site, it ceased to initiate or grow in other sites (except for very low stress-long life specimens).

Closure

Stitched uniweave materials were developed in response to damage tolerance problems found in traditional tape laminates. It was particularly desired to increase delamination resistance and compression after impact performance. Since compression performance often limits composite usage, compression-compression fatigue cycling was identified as the critical loading condition. Previous studies have found that this material system is a cost-effective method of improving composite performance under this type of loading. An effort by others is now under way to develop an analytical model of this material system so that full scale model parts do not need to be manufactured; the goal is to be able to predict the behavior of this material through an analytical process. In order to establish and verify the parameters of the analytical model, data was needed on the damage characteristics of this material under certain loading conditions. This study investigated damage initiation and growth in order to characterize it for the developers of the analytical model.

REFERENCES

1. Palmer, R. and Curzio, F. : **"Cost-Effective Damage Tolerant Composites Using Multi-Needle Stitching and RTM/VIM Processing,"** Fiber-Tex 1988 Conference Proceedings, NASA Conference Publication 3038, 1989, pp. 25-52

2. Funk, J.; Dexter, H. B.; and Lubowinski, S. J. : **"Experimental Evaluation of Stitched Graphite/Epoxy Composites,"** NASA Conference Publication 2420, 1985, pp. 185-205

3. Dexter, H. B. and Funk, J. : **"Impact Resistance and Interlaminar Fracture Toughness of Through-the-Thickness Reinforced Composites,"** 27th Structures, Structural Dynamics and Materials Conference, AIAA, 1986, pp. 700-709

4. Lubowinski, S. J. and Poe, C. C. : **"Fatigue Characterization of Stitched Graphite/Epoxy Composites,"** Fiber-Tex 1987 Conference Proceedings, NASA Conference Publication 3001, 1988, pp. 253-271

5. Dow, M. B. ; Smith, D. L. ; and Lubowinski, S. J. : **"An Evaluation of Stitching Concepts for Damage-Tolerant Composites,"** Fiber-Tex 1988 Conference Proceedings, NASA Conference Publication 3038, 1989, pp. 53-73

6. Dow, M. B. and Smith, D. L. : **"Damage-Tolerant Composite Materials Produced by Stitching Carbon Fabrics,"** SAMPE Conference Series, Vol. 21, 1989, pp. 595-605

7. Portanova, M. A. ; Poe, C. C. ; and Whitcomb, J. D. : **"Open Hole and Post-Impact Compression Fatigue of Stitched and Unstitched Carbon/Epoxy Composites,"** NASA Technical Memorandum 102676, June 1990

8. Simonds, R. A. ; Bakis, C. E. ; and Stinchcomb, W. W. : **"Effects of Matrix Toughness on Fatigue Response of Graphite Fiber Composite Laminates,"** ASTM STP 1012, P. A. Lagace, ed., 1989, pp. 5-18

9. Masters, J. E : **"Improved Impact and Delamination Resistance Through Interleafing,"** Key Engineering Materials, Vol. 37, 1989, pp. 317-348

10. Evans, D. A. and Boyce, J. S. : **"Transverse Reinforcement Methods for Improved Delamination Resistance,"** 34th International SAMPE Symposium, May 1989, pp. 271-282

11. Cholakara, M. T. ; Jang, B. Z. ; and Wang, C. Z. : **"Deformation and Failure Mechanisms**

in 3D Composites," 34th International SAMPE Symposium, May 1989, pp. 2153-2160

12. Chung, W. C. ; Jang, B. J. ; Chang, T. C. ; Hwang, L. R. ; and Wilcox, R. C. : **"Fracture Behavior in Stitched Multidirectional Composites,"** Materials Science and Engineering, A112, 1989, pp. 157-173

13. Du, X. ; Xue, F. ; and Gu, Z. : **"Experimental Study of the Effect of Stitching on Strength of a Composite Laminate,"** Proceedings of International Symposium on Composite Materials and Structures", June 1986, Loo, T. T., and Sun, C. T., ., pp. 912-918

14. Mignery, L. A. ; Tan, T. M. ; and Sun, C. T. : **"The Use of Stitching to Suppress Delamination in Laminated Composites,"** ASTM STP 876, W. S. Johnson, ed., 1985, pp. 371-385

15. Pelstring, R. M. and Madan, R. C. : **"Stitching to Improve Damage Tolerance of Composites,"** 34th International SAMPE Symposium, May 1989, pp. 1519-1528

16. Su, K. B. : **"Delamination Resistance of Stitched Thermoplastic Matrix Composite Laminates,"** ASTM STP 1044, G. M. Newaz, ed., 1989, pp. 279-300

17. Kennedy, J. M. : **"Damage Tolerance of Woven Graphite/Epoxy Buffer Strip Panels,"** NASA Technical Memorandum 102702, August 1990

18. Ogo, Y : **"The Effect of Stitching on In-Plane and Interlaminar Properties of Carbon/Epoxy Laminates,"** Master's thesis, University of Delaware, May 1987

19. Simonds, R. A. ; Stinchcomb, W. ; and Jones, R. M. : **"Mechanical Behavior of Braided Composite Materials,"** ASTM STP 972, J. D. Whitcomb, ed., 1988, pp. 438-453

20. Smith, D. L. and Dexter, H. B. : **"Woven Fabric Composites with Improved Fracture Toughness and Damage Tolerance,"** Fiber-Tex 1988, NASA Conference Publication 3038, 1989, pp. 75-90

21. Douglas Aircraft progress report to NASA-Langley, April 1990

22. Charewicz, A. and Daniel, I. M. : **"Damage Mechanisms and Accumulation in Graphite / Epoxy Composites,"** ASTM STP 907, H. T. Hahn, ed., 1986, pp. 274-297

23. Masters, J. E. : **"The Use of Surface Replication to Detect Matrix Cracks in Composite Laminates,"** Microstructural Science, Vol. 14, pp. 561-573

24. Stalnaker, D. O. and Stinchcomb, W. W. : **"Load History-Edge Damage Studies in Two Quasi-Isotropic Graphite Epoxy Laminates,"** ASTM STP 674, 1979, pp. 620-641

25. Schulte, K. and Stinchcomb, W. W. : **"Damage Development Near the Edges of a Composite Specimen During Quasi-static and Fatigue Loading,"** Composites Technology Review, Vol. 6, No. 1, 1984, pp. 3-9

26. Bakis, C. E.: **"Fatigue Response of Notched Composite Laminates Subjected to Tension-Compression Loading,"** Master's Thesis, Virginia Polytechnic Institute and State University, 1984

27. Wagnecz, L.: **"Mechanical Behavior and Damage Mechanisms of Woven Graphite Polymide Composite Materials,"** Master's Thesis, Virginia Polytechnic Institute and State University, 1987

28. Ryder, J. T. and Walker, E. K.: **"The Effect of Compressive Loading on the Fatigue Lifetime of Graphite/Epoxy Laminates,"** AFML-TR-79-4128, 1979

29. Ryder, J. T. and Walker, E. K.: **"Effect of Compression on Fatigue Properties of a Quasi-Isotropic Graphite/Epoxy Composite,"** ASTM STP 636, 1979, pp. 3-26

30. Robinson, C. T. and Francis, P. H. : **"Damage Initiation in a Three-Dimensional Carbon-Carbon Composite,"** ASTM STP 723, 1981, pp. 85-100

31. Communication with G. Farley at NASA-Langley, 30 November 1990

32. Communication with F. K. Ko at Virginia Tech, 22 March 1991

33. Gardner, M. R. : **"Continuous Linear Alignment Testing Grips,"** NASA TM LAR-13493, May 1980

34. Communication with M. A. Portanova at NASA-Langley, October 1990

35. Bishop, S. M. and Morton, J. : **Fatigue of Notched (0,+/- 45) CFRP with Woven and Nonwoven +/- 45° Layers",** Advances in Fracture Research, V. 4, 1984, pp. 3069-3078

36. **Magnamite@ AS4 / 3501-6 Graphite Prepreg and Tape Fabric Module**, Hercules Corporation

37. **CLASS: Composite Laminate Analysis Systems**, developed by Materials Science Corporation and Dr. John J. Kibler, copyright 1984,85,86,87 by Materials Science Corporation, release 3.50

38. Ralls, K. M.; Courtney, T. H.; and Wulff, J.: **Introduction to Materials Science and Engineering,** John Wiley and Sons, 1976

VITA

Nancy Vandermey was born on January 28, 1967, in the back room of Joseph F. and Dorothea A. Vandermey's home in Detroit, Michigan. She survived 12 years of Catholic schools, graduating as salutatorian in 1985 from Regina H. S., and earning a National Merit Scholarship. While studying mechanical engineering at Michigan Technological University (Go Huskies!), she worked at summer intern positions as a construction inspector and at SATURN Corporation. Ms. Vandermey graduated Magna Cum Laude with a B. S. M. E. in 1989. Turning down a job offer in San Diego, she came to Blacksburg to enroll in the NASA-Virginia Tech Composites Program as a GRA, also earning a Presidential Fellowship. While working on her Master's degree, she especially enjoyed her term at NASA-Langley and working as a volunteer at the Montgomery County Humane Society Animal Shelter. After completing this M. S. degree, she plans to tour Europe for 7 weeks, and then go to work in the Phillips Astronautics Laboratory at Edwards Air Force Base in California.

Nancy Vandermey